XBeach testbed report

status update 1241 (07/12/10 09:27:58)

Revision: 1241

July 12, 2010

XBeach testbed report

Contents

Chapter 1

Introduction

1.1 Introduction to the XBeach model

The devastating effects of hurricanes on low-lying sandy coasts, especially during the 2004 and 2005 seasons have pointed at an urgent need to be able to assess the vulnerability of coastal areas and (re-)design coastal protection for future events, and also to evaluate the performance of existing coastal protection projects compared to do-nothing scenarios. In view of this the Morphos-3D project was initiated by USACE-ERDC, bringing together models, modelers and data on hurricane winds, storm surges, wave generation and nearshore processes. As part of this initiative an open-source program, XBeach for eXtreme Beach behaviour, has been developed to model the nearshore response to hurricane impacts. The model includes wave breaking, surf and swash zone processes, dune erosion, overwashing and breaching.

Existing tools to assess dune erosion under extreme storm conditions assume alongshore uniform conditions and have been applied successfully along relatively undisturbed coasts (Vellinga, 1986, Steetzel, 1993, Nishi and Kraus, 1996, Larson et al., 2004), but are inadequate to assess the more complex situation where the coast has significant alongshore variability. This variability may result from anthropogenic causes, such as the presence of artificial inlets, sea walls, and revetments, but also from natural causes, such as the variation in dune height along the coast or the presence of rip channels and shoals on the shoreface (Thornton et al., 2007). A particularly complex situation is found when barrier islands protect storm impact on the main land coast. In that case the elevation, width and length of the barrier island, as well as the hydrodynamic conditions (surge level) of the back bay should be taken into account to assess the coastal response. Therefore, the assessment of storm impact in these more complex situations requires a two-dimensional process-based prediction tool, which contains the essential physics of dune erosion and overwash, avalanching, swash motions, infragravity waves and wave groups.

With regard to dune erosion, the development of a scarp andepisodic slumping after undercutting is a dominant process (van Gent et al., 2008). This supplies sand to the swash and surf zone that is transported seaward by the backwash motion and by the undertow; without it the upper beach scours down and the dune erosion process slows down considerably. One-dimensional (cross-shore) models such as DUROSTA (Steetzel, 1993) focus on the underwater offshore transport and obtain the supply of sand by extrapolating these transports to the dry dune. Overton and Fisher (1988), Nishi and Kraus (1996) focus on the supply of sand by the dune based on the concept of wave impact. Both approaches rely on heuristic estimates of the runup and are well suited for 1D application but difficult to apply in a horizontally 2D

setting. Hence, a more comprehensive modelling of the swash motions is called for.

Swash motions are up to a large degree a result from wave-group forcing of infragravity waves (Tucker, 1954). Depending on the beach configuration and directional properties of the incident wave spectrum both leaky and trapped infragravity waves contribute to the swash spectrum (Huntley et al., 1981). Raubenheimer and Guza (1996) show that incident band swash is saturated, infragravity swash is not, therefore infragravity swash is dominant in storm conditions. Models range from empirical formulations (e.g. Stockdon et al., 2006) through analytical approaches (Schaeffer, 1994, Erikson et al., 2005) to numerical models in 1D (e.g. List, 1992, Roelvink, 1993b) and 2DH (e.g. van Dongeren et al., 2003, Reniers et al., 2004a, 2006). 2DH wavegroup resolving models are well capable of describing low-frequency motions. However, for such a model to be applied for swash, a robust drying/flooding formulation is required.

1.2   Model approach and innovations

Our aim is to model processes in different regimes as described by Sallenger (2000). He defines an Impact Level to denote different regimes of impact on barrier islands by hurricanes, which are the 1) swash regime, 2) collision regime, 3) overwash regime and 4) inundation regime. The approach we follow to model the processes in these regimes is described below.

To resolve the swash dynamics the model employs a novel 2DH description of the wave groups and accompanying infragravity waves over an arbitrary bathymetry (thus including bound, free and refractively trapped infragravity waves). The wave-group forcing is derived from the time-varying wave-action balance e.g. Phillips (1977) with a dissipation model for use in combination with wave groups (Roelvink, 1993a). A roller model (Svendsen, 1984; Nairn et al., 1990; Stive and de Vriend, 1994) is used to represent momentum stored in surface rollers which leads to a shoreward shift in wave forcing.

The wave-group forcing drives infragravity motions and both longshore and cross-shore currents. Wave-current interaction within the wave boundary layer results in an increased wave-averaged bed shear stress acting on the infragravity waves and currents (e.g. Soulsby et al., 1993 and references therein). To account for the randomness of the incident waves the description by Feddersen et al. (2000) is applied which showed good skill for longshore current predictions using a constant drag coefficient (Ruessink et al., 2001).

During the swash and collision regime the mass flux carried by the waves and rollers returns offshore as a return flow or a rip-current. These offshore directed flows keep the erosion process going by removing sand from the slumping dune face. Various models have been proposed for the vertical profile of these currents (see Reniers et al., 2004b for a review). However, the vertical variation is not very strong during extreme conditions and has been neglected for the moment.

Surf and swash zone sediment transport processes are very complex, with sediment stirring by a combination of short-wave and long-wave orbital motion, currents and breaker-induced turbulence. However, intra-wave sediment transports due to wave asymmetry and wave skewness are expected to be relatively minor compared to long-wave and mean current contributions (van Thiel de Vries et al., 2008). This allows for a relatively simple and transparent formulation according to SoulsbyVan Rijn (Soulsby, 1997) in a shortwave averaged but wave-group resolving model of surf zone processes. This formulation has been applied successfully in describing the generation of rip channels (Damgaard et al., 2002 Reniers et al., 2004a) and barrier breaching (Roelvink et al., 2003).

In the collision regime, the transport of sediment from the dry dune face to the wet swash, i.e. slumping or avalanching, is modeled with an avalanching model accounting for the fact that saturated sand moves more easily than dry sand, by introducing both a critical wet slope and dry slope. As a result slumping is predominantly triggered by a combination of infragravity swash runup on the previously dry dune face and the (smaller) critical wet slope.

During the overwash regime the flow is dominated by lowfrequency motions on the time scale of wave groups, carrying water over the dunes. This onshore flux of water is an important landward transport process where dune sand is being deposited on the island and within the shallow inshore bay as overwash fans (e.g. Leatherman et al., 1977; Wang and Horwitz, 2007). To account for this landward transport some heuristic approaches exist in 1D, e.g. in the SBeach overwash module (Larson et al., 2004) which cannot be readily applied in 2D. Here, the overwash morphodynamics are taken into account with the wave-group forcing of low-frequency motions in combination with a robust momentum-conserving drying/flooding formulation (Stelling and Duinmeijer, 2003) and concurrent sediment transport and bed-elevation changes.

Breaching of barrier islands occurs during the inundation regime, where a new channel is formed cutting through the island. Visser (1998) presents a semi-empirical approach for breach evolution based on a schematic uniform cross-section. Here a generic description is used where the evolution of the channel is calculated from the sediment transports induced by the dynamic channel flow in combination with avalanche-triggered bank erosion.

1.3   XBeach testbed

The XBeach code and related functionalities develop fast. As a result there is a need from modelers and code developers to develop a tool that gives insight in the effect of code developments on model performnace. The XBeach testbed tries to fulfill this need by running a range of tests including analytical solutions, laboratory tests and practical field cases every week with the latest code.

Chapter 2

Release information

2.1   Release notes

We have been working on a lot of cool stuff that still needs to be described in more detail:

- hard structures

- multiple sediment fractions

- bed load and suspended load

- output options

- wave schemes

- non-hydrostatic model

- wave shap parameterization

- drifters

- river outflow

- boundary condition stuff

- ...

2.2   Change log

REVISION: 1239   AUTHOR: roelvin   DATE: 07/05/10 11:11:47
MESSAGE: Changed the README to state that XBeach is distributed under GNU Lesser GPL
, not GNU GPL, consistent with the headings in the code.
FILES: /trunk/README M

Chapter 3

Overview

In the table below the statuses of all tests found in the testbed are summarized. In case a test is ignored or has failed, the corresponding message is given in the column "Message". Please note that success or failure of the test runs are given in column "Run status", while the success or failure of the Matlab analyses are given in column "Matlab status". The last columns provide an overview of the main characteristics of each test.

Tests can be run multiple times using different settings. Different runs are identified by a run name, which follows after the test name and a dot sign. If a test is run once only, it is common use to name the run *default*.

Table 3.1: Status overview testbed tests

Test	Run status	Matlab status	Message	Configuration	Waves*	Water levels**	Fractions	Morphology	Hard layers	Groundwater flow
CarrierGreenspan.default	✓	✓		1D	ST	C	1			
CarrierGreenspan.mpi	✓	–		1D	ST	C	1			
long_wave_propagation.default	✓	✓		1D	ST	C	1			
long_wave_propagation.mpi	✓	–		1D	ST	C	1			
Boers_1C.default	✓	✓		1D	WG	C	1			
Boers_1C.mpi	✓	–		1D	WG	C	1			
Zelt_Case1.default	✓	✓		2D	WG	C	1			
Zelt_Case1.mpi	✓	–		2D	WG	C	1			
Delilah_199010131000.default	✓	✓		2D	WG	C	1			
Delilah_199010131000.mpi	✓	–		2D	WG	C	1			
Delilah_199010131000.meanvars	✓	–		2D	WG	C	1			
Deltaflume_M1263-3_Test-1.default	✓	✓		1D	WG	C	1	✓		
Deltaflume_M1263-3_Test-1.mpi	✓	–		1D	WG	C	1	✓		
Deltaflume_M1263-3_Test-2.default	✓	✓		1D	WG	C	1	✓		
Deltaflume_M1263-3_Test-2.mpi	✓	–		1D	WG	C	1	✓		
Deltaflume_M1263-3_Test-3.mpi	✓	–		1D	WG	V	1	✓		
Deltaflume_M1263-3_Test-3.default	✓	✓		1D	WG	V	1	✓		
Deltaflume_M1263-3_Test-4.mpi	✓	–		1D	WG	V	1	✓		

Table 3.1: Status overview testbed tests

Test	Run status	Matlab status	Message	Configuration	Waves*	Water levels**	Fractions	Morphology	Hard layers	Groundwater flow
Deltaflume_M1263-3_Test-4.default	✓	✓		1D	WG	V	1	✓		
Deltaflume_M1263-3_Test-5.default	✓	✓		1D	WG	C	1	✓		
Deltaflume_M1263-3_Test-5.mpi	✓	–		1D	WG	C	1	✓		
DeltaflumeH298_T1.mpi	✓	–		1D	WG	C	1	✓	✓	
DeltaflumeH298_T1.default	✓	✓		1D	WG	C	1	✓	✓	
DeltaflumeH298_T3.default	✓	✓		1D	WG	C	1	✓	✓	
DeltaflumeH298_T3.mpi	✓	–		1D	WG	C	1	✓	✓	
DeltaflumeLIP11D_1B	–	–	Disabled	1D	WG	C	1	✓		
DeltaflumeLIP11D_2E.mpi	✓	–		1D	WG	C	1	✓		
DeltaflumeLIP11D_2E.default	✓	✓		1D	WG	C	1	✓		
Deltaflume2006_T01.default	✓	✓		1D	WG	C	1	✓		
Deltaflume2006_T01.mpi	✓	–		1D	WG	C	1	✓		
Deltaflume2006_T01_zebra.mpi	✓	✓		1D	WG	C	2	✓		
Deltaflume2006_T01_zebra.default	✓	✓		1D	WG	C	2	✓		
Deltaflume2006_T02	–	–	Disabled	1D	WG	C	1	✓		
Deltaflume2006_T04.default	✓	✓		1D	WG	C	1	✓		
Deltaflume2006_T04.mpi	✓	–		1D	WG	C	1	✓		
Deltaflume2006_DP01	–	–	Disabled	1D	WG	C	1	✓		
1953_storm_surge	–	–	Disabled	1D	WG	V	1	✓		
Zwin_T01.default	✓	✓		2D	ST	V	1	✓		
Zwin_T01.mpi	✓	–		2D	ST	V	1	✓		
River_Outflow.default	✓	✓		2D	ST	C	1	✓		
River_Outflow.mpi	✓	–		2D	ST	C	1	✓		
Netcdf.mpi	–	–	No data	1D	ST	C	1			
Netcdf.default	✓	✓		1D	ST	C	1			
Assateague_Island.profB2	✓	–		1D	ST	C	1	✓		
Assateague_Island.profC	✓	–		1D	ST	C	1	✓		
Assateague_Island.profA	✓	✓		1D	ST	C	1	✓		
Assateague_Island.profB1_mpi	✓	–		1D	ST	C	1	✓		
Assateague_Island.profB1	✓	–		1D	ST	C	1	✓		

* ST = stationary, WG = wave groups, NH = non-hydrostatic
** C = constant, V = varying

Chapter 4

Test results

4.1 Carrier and Greenspan

Contact: Bas Hoonhout <bas.hoonhout@deltares.nl>

The purpose of this test is to check the ability of the model to represent runup and rundown of non-breaking long waves. To this end, a comparison was made with the analytical solution of the NSWE by Carrier and Greenspan (1958), which describes the motion of harmonic, non-breaking long waves on a plane sloping beach without friction.

A free long wave with a wave period of 32 seconds and wave amplitude of half the wave breaking amplitude ($a_{in} = 0.5 \cdot a_{br}$) propagates over a beach with constant slope equal to $1/25$. The wave breaking amplitude is computed as $a_{br} = 1/\sqrt{128} \cdot \pi^3 \cdot s^{2.5} \cdot T^{2.5} \cdot g^{1.25} \cdot h_0^{-0.25} = 0.0307 meter$, where s is the beach slope, T is the wave period and h_0 is the still water depth at the seaward boundary. The grid is non uniform and consists of 160 grid points. The grid size dx is decreasing in shoreward direction and is proportional to the (free) long wave celerity ($\sqrt{g \cdot h}$). The minimum grid size in shallow water was set at $dx = 0.1 meter$.

To compare XBeach output to the analytical solution of Carrier and Greenspan, the first are non-dimensionalized with the beach slope s, the acceleration of gravity g, the wave period T, a horizontal length scale L_x and the vertical excursion of the swash motion A. The horizontal length scale L_x is related to the wave period via $T = \sqrt{L_x/g \cdot s}$ and the vertical excursion of the swash motion A is expressed as: $A = a_{in} \cdot \pi/\sqrt{0.125 \cdot s \cdot T \cdot \sqrt{g/h_0}}$
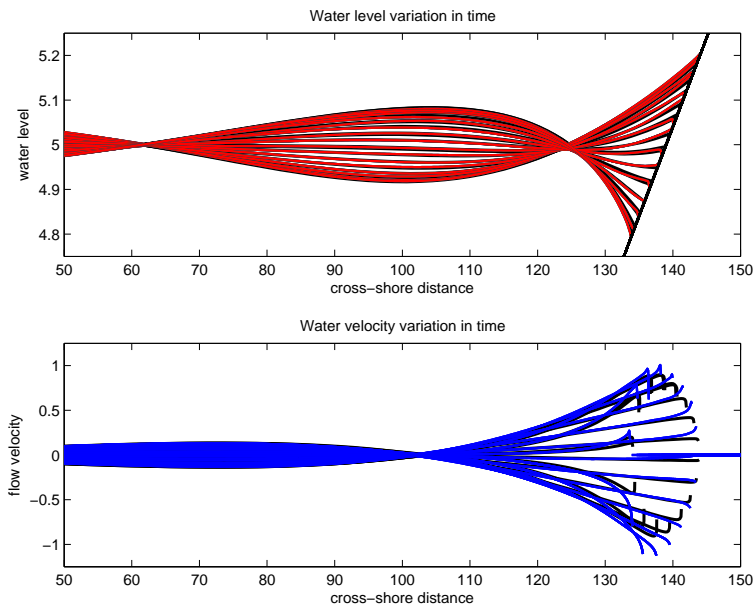
Water level variation in time

Figure 4.1

The two panels in Figure 4.1 compare the XBeach results with the analytical solution. The agreement should be reasonably well, though there are small deviations in the water level near the water line and the flow velocities seem to lag slightly on the analytical solution during the second part of the run down. Since the analytical solution is stationary, numerical output over multiple waves is shown in Figure 4.1, verifying that also the numerical solution is reasonably stationary.

Carrier, G.F., and Greenspan, H.P., *Water waves of finite amplitude on a sloping beach.* Journal of Fluid Mechanics, 1958, vol. 4, 97 - 109

4.2   Long wave propagation

Contact: Bas Hoonhout <bas.hoonhout@deltares.nl>

The purpose of the this test is to check if the NSWE numerical scheme is not too dissipative and that it does not create large errors in propagation speed.

A long wave with a small amplitude of $0.01m$ and period of $80s$ was sent into a domain of $5m$ depth, grid size of $5m$ and a length of $1km$. At the end, a fully reflecting wall is imposed. The wave length in this case should be $\sqrt{9.81 \cdot 5} \cdot 80 = 560m$. The velocity amplitude should be $\sqrt{g/h} \cdot A = \sqrt{9.81/5} \cdot 0.01 = 0.014m$. After the wave has reached the wall, a standing wave with double amplitude should be created.

Water level at t = 0 to 160s with 20s interval

Water velocity at t = 0 to 160s with 20s interval

Figure 4.2

Water level at t = 0 to 1200s with 20s interval

Water velocity at t = 0 to 1200s with 20s interval
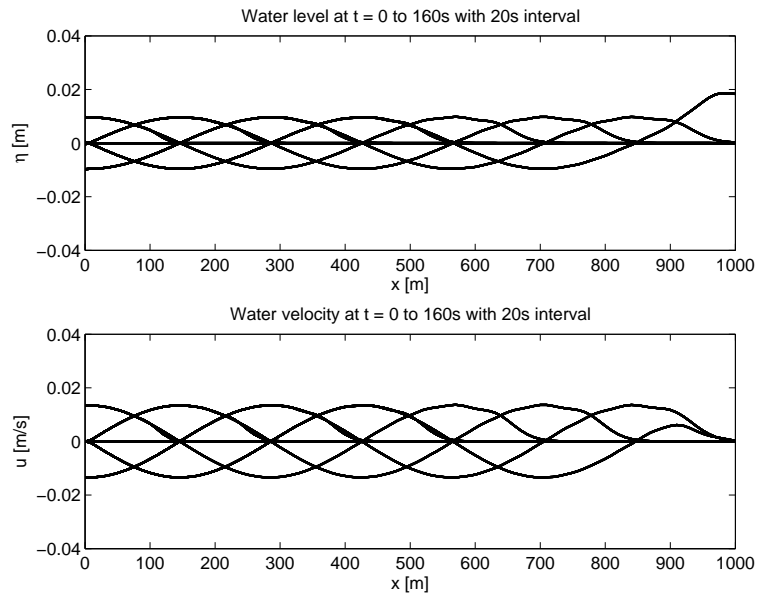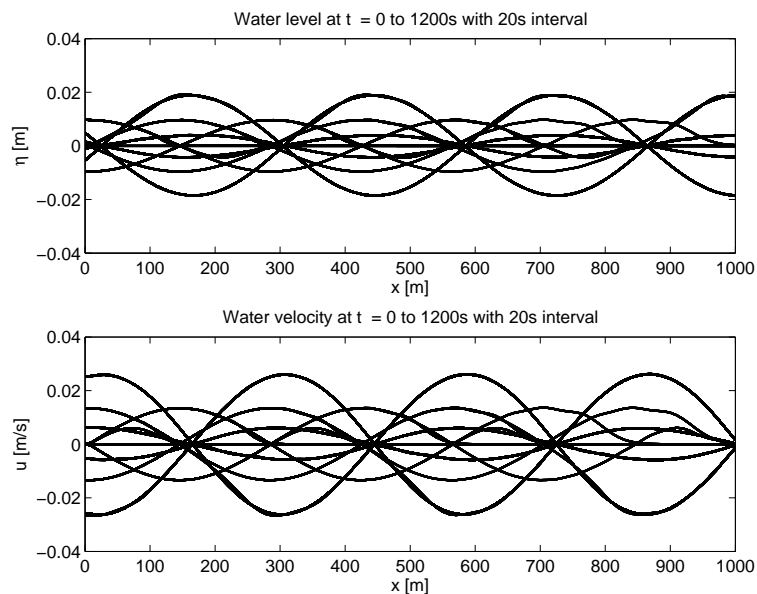
Figure 4.3

As Figure 4.2 and Figure 4.3 should show, the model accurately represents this situation. There is hardly any dissipation, the wave length is very close to what it should be and there is no reflection off the seaward boundary.

4.3 Boers 1C

Contact: Ap van Dongeren <ap.vandongeren@deltares.nl>

Boers (1996) performed experiments with irregular waves in the physical wave flume at Delft University of Technology with a length of 40 meters and a width of 0.8 m. The flume is

equipped with a hydraulically driven, piston type wave generator with second-order wave generation and Active Reflection Compensation. Boers ran waves over a concrete bar-trough beach, which was modelled after the Delta Flume experiments. He ran three different irregular wave conditions, but in this report we will focus on case 1C, a Jonswap spectrum with $H_{m,0} = 0.1m$ and $T_p = 3.3s$. The surface elevation was measured in 70 locations shown in Figure 4.4.
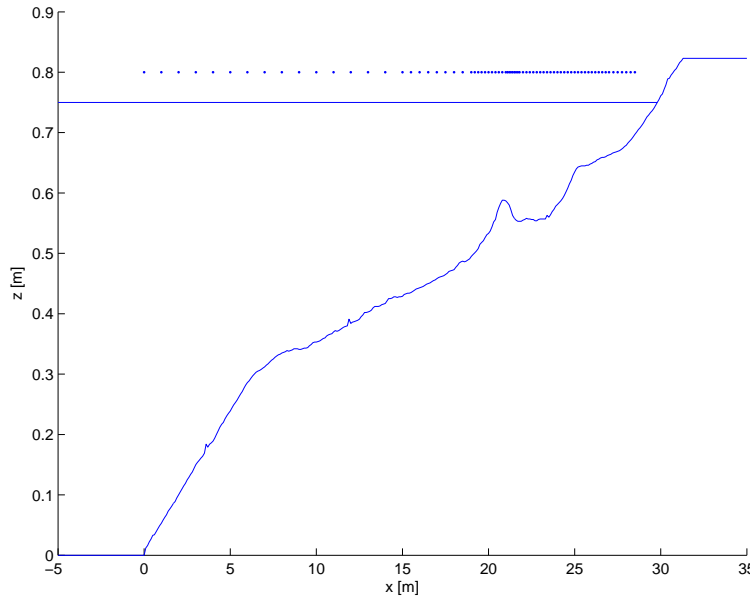

Figure 4.4

The comparison between the model and the data for the wave height transformation of the short waves and the long waves (defined as waves with a frequency greater than $f_p/2$ and less than $f_p/2$, respectively) is shown in Figure 4.5.

The top dark blue line indicates the short wave height transformation, which should compare well with the measurements, except for details around the breakpoint. The green line and stars indicate the mean (steady) set-up which should be well-predicted, except in the trough region (x=21-25 m). The red lines and stars indicate the total (incoming and reflected) low frequency wave, which is slightly overpredicted in the shoaling zone (up to the breakpoint) and stays too large after that.

The observational data is separated into incoming and reflected long wave components using an array of wave gauges (Bakkenes, 2002) and the numerical data has been separated into two components using co-located surface elevation and velocity information. The incoming long wave (cyan line) follows the observations (cyan stars) with a notable overprediction seaward of the breaking zone. The reflected long waves (black lines) match the observations (black stars) quite well.
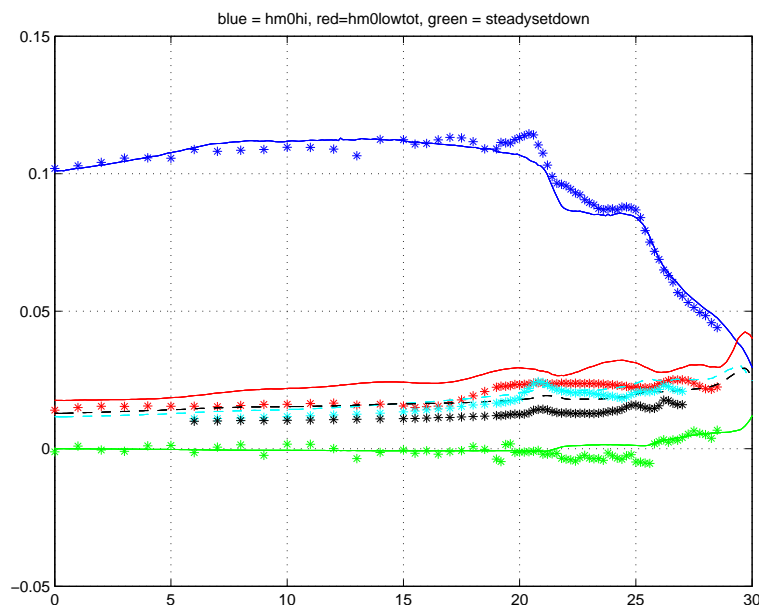
Figure 4.5

The model should perform reasonably well against the data for this well-measured but complex case.

Bakkenes, H.J., 2002. *Observation and seperation of bound and free low-frequency waves in the nearshore zone.* MSc Thesis, Delft University of Technology, Delft, The Netherlands.

Boers, M. (1996), *Simulation of a Surf Zone with a Barred Beach, Part 1: Wave heights and Wave breaking*, Communications on Hydraulic and Geotechnical Eng., Delft University of Technology, Civil Engineering, Report No. 96-5, 116 p.

4.4   Zelt case 1

Contact: Ap van Dongeren <ap.vandongeren@deltares.nl>

The verification cases so far considered solely the cross-shore dimension and assumed a long-shore uniform coast. In the following cases the potential of the model to predict coastal and dune erosion in situations that include the two horizontal dimensions is further examined. A first step towards a 2DH response is to verify that the 2DH forcing by surge run-up and run-down is accurately modelled by testing not against Zelt (1986), but actually Özkan-Haller & Kirby (1997). The reason is that Zelt modeled the NSW equations including some dispersive and dissipative terms, which the present model does not have. For that reason, we also compared our model to the results of Özkan-Haller & Kirby (1997) who modeled the NSW equations using a Fourier-Chebyshev Collocation method, which does not have any numerical dissipation or dispersion errors. They use a moving, adapting grid with a fixed Δy (which is equal to the present model's Δy in this comparison) but with a spatially and temporally varying Δx so that the grid spacing in x near the shoreline is very small. In the present model Δx is set equal to Δy, which means that we can expect to have less resolution at the shoreline than Özkan-Haller & Kirby (1997).
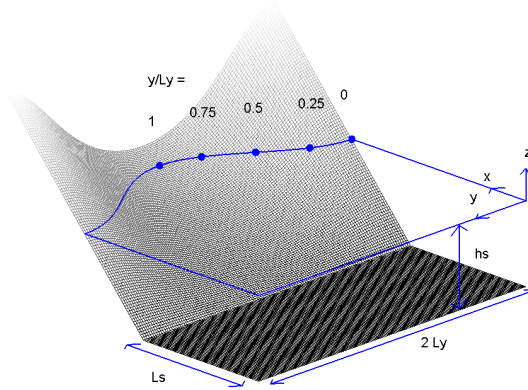
Figure 4.6

Figure 4.6 shows the definition sketch of the concave beach bathymetry in the present coordinate system, converted from the original system by Zelt (1986). The bathymetry consists of a flat bottom part and a beach part with a sinusoidally varying slope. For Zelt (1986)'s fixed parameter choice of $\sqrt{\beta} = \frac{h_s}{L_y} = \frac{4}{10\pi}$, the bathymetry is given by

$$h = \begin{cases} h_s & , \quad x \leq L_s \\ h_s - \frac{0.4\,(x - L_s)}{3 - \cos\left(\frac{\pi y}{L_y}\right)} & , \quad x > L_s \end{cases} \tag{4.1}$$

where h_s is the shelf depth, L_s is the length of the shelf in the modeled domain and L_y is the length scale of the longshore variation of the beach. This results in a beach slope of $h_x = \frac{1}{10}$ in the center of the bay and of $h_x = \frac{1}{5}$ normal to the "headlands". In the following we chose $L_y = 8\,m$, which determines $h_s = 1.0182\,m$. We set $L_s = L_y$. Different values for L_s only cause phase shifts in the results, but no qualitative difference, so this parameter is not important in this problem. Also indicated in the figure are the five stations where the vertical run-up (the surface elevation at the shoreline) will be measured.

At the offshore ($x = 0$) boundary we specify an incoming solitary wave, which in dimensional form reads

$$\zeta_i\,(t) = \alpha\,h_s\,\mathrm{sech}^2\left(\sqrt{\frac{3\,g}{4\,h_s}\,\alpha\,(1 + \alpha)}\ \ (t - t_o)\right) \tag{4.2}$$

which is similar to Zelt (1986)'s Eq. (5.3.7). The phase shift t_o is chosen such that the surface elevation of the solitary wave at $t = 0$ is 1% of the maximum amplitude. The only parameter yet to be chosen is α. We will compare our model to Zelt's case of $\alpha = \frac{H}{h_s} = 0.02$, where H is the offshore wave height. Zelt found that the wave broke for a value of $\alpha = 0.03$, so the present test should involve no breaking, but has a large enough nonlinearity to exhibit a pronounced two-dimensional run-up.

Any outgoing waves will be absorbed at the offshore boundary by the absorbing-generating boundary condition. At the lateral boundaries $y = 0$ and $y = 2 L_y$ we specify a no-flux (wall) boundary condition following Zelt. The model equations used in this test are the nonlinear shallow water equations without forcing or friction. The numerical parameters are $\Delta x = \Delta y = \frac{1}{8} m$ with a Courant number $\nu = 0.7$.
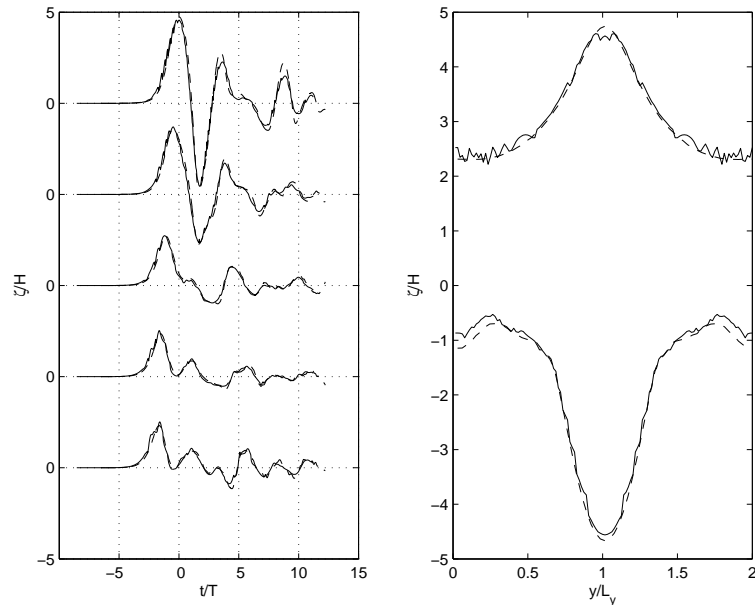

Figure 4.7

The first panel in Figure 4.7 shows the vertical runup normalized with the offshore wave height H as a function of time, which is normalized by $\sqrt{g\,h_s}/L_y$ at the 5 cross-sections indicated in Figure 4.6. The solid lines represent the present model results, while the dashed lines denotes Ozkan & Kirby (1997)'s numerical results. We should see that the agreement is generally good, except that the present model does not capture the second peak in the time series at $y/Ly = 1$ very well. This secondary peak or "ringing" is due to the wave energy that is trapped along the coast and propagates towards the midpoint of the bay (Zelt, 1986). It is suspected that this focusing mechanism is not properly captured, because the present method approximates the shoreline as a staircase pattern, which in effect lengthens the shoreline. Also, the spatial derivatives are not evaluated parallel and perpendicular to the actual shoreline but in the fixed x and y directions. The agreement at the locations $y/Ly = 0.25$, $y/Ly = 0.5$ and $y/Ly = 0.75$ is generally good despite the large gradient of the local shoreline relative to our grid.

The second panel in Figure 4.7 shows the maximum vertical run-up and run-down, normalized by H, versus the alongshore coordinate y. The maximum runup should agree well with Ozkan & Kirby (1997), but that the maximum rundown is not represented well in the center of the domain. The wiggles in the solid line are evidence of the staircasing of the shoreline: since the shoreline is not treated as a continuous but rather as a discrete function, so is the runup in the individual nodes.

Table 4.1: Error statistics Zelt Case 1

	R^2	Sci	Rel. bias	BSS
Timeseries (min)	0.07	0.16	-0.15	-5.09
Timeseries (max)	0.99	2.24	0.03	0.97
Max. runup	0.98	0.03	0.02	0.99

In conclusion, the shoreline boundary condition agrees well with the analytical solutions for the longshore uniform case but shows some discrepancies for the case of a concave beach, which can be attributed to the "staircase" discretization of the shoreline. The above results are consistent with the results obtained with the SHORECIRC model which is based on similar hydrodynamic equations, see Van Dongeren and Svendsen (1997), and show that also the current model is capable of representing run-up and run-down.

Özkan-Haller, H.T. and J.T. Kirby (1997). *A Fourier-Chebyshev collocation method for the shallow water equations including shoreline runup.* Applied Ocean Research, 19, pp. 21-34.

Zelt, J.A. (1986). *Tsunamis: the response of harbours with sloping boundaries to long wave excitation.* Doctoral dissertation, Rep. No. KH-R-47, W.M. Keck Laboratory of Hydraulics and Water Resources, Division of Engineering and Applied Science, California Institute of Technology, Pasadena, CA, 318 p.

4.5   Delilah

Contact: Robert McCall <robert.mccall@deltares.nl>

In order to verify the 2DH hydrodynamics of XBeach when forced by directionally-spread short waves, a simulation is set up to compare model results to field measurements. In this case the DELILAH field experiment at Duck, North Carolina is selected as a suitable test location. The period that is modeled is October 13th 1990, which was a stormy day, between 16:00 and 17:00 hours. The significant wave height at 8 m water depth was 1.81 m, with a peak period of 10.8 s and a mean angle of incidence of -16 relative to the shoreward normal. This period is selected because the wave conditions are energetic enough to generate a significant infragravity wave component and the incident wave spectrum is sufficiently narrow-banded to justify the assumptions in the model boundary conditions. The model is forced with the wave spectrum measured at 8 m water depth (Birkemeier et al., 1997). A measured tidal signal is imposed on the model boundaries of which the mean level is 0.69 m above datum. The slope of the wave front in the roller model is set to 0.05, which is found to be a slight improvement over the value of 0.10 used in the previous sections. A constant grid size of 5 m in cross shore and 10 m in longshore direction is used. The resolution of the wave model in directional space is 15. The model is set to generate output at the location of the primary cross shore measurement array, gauge numbers 10, 20, 30, 40, 50, 60, 70, 80 and 90 (Figure 4.8).
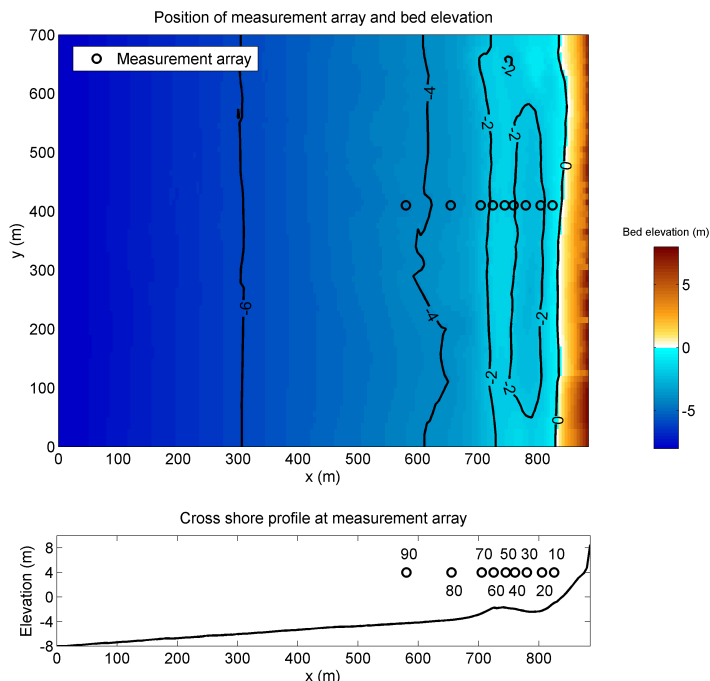
Figure 4.8: DELILAH field experiment 1990. Top panel: Plan view of the model location and measurement gauge array (circles). Bottom panel: Cross shore profile at the location of the measurement gauge array (circles) and measurement gauge names.

The modeled time-averaged wave heights of the short waves are compared to the time-averaged wave heights measured at the gauges. These results are shown in the first panel of Figure 4.9. Unfortunately, no data exist for gauge number 60.

The infragravity wave height is calculated as follows (van Dongeren et al., 2003):

$$H_{rms,low} = \sqrt{8 \int_{0.005Hz}^{0.05Hz} S df}$$

The second panel of Figure 4.9 should show that the XBeach model overestimates the infragravity wave height, but does follow the measured cross shore trend well.

The measured and modelled time-averaged longshore current are shown in the third panel of Figure 4.9. It can be seen that the model strongly under predicts the longshore current in the trench between measurement gauge 60 and the shore. Further calibration of the short wave and roller parameters is required in order to improve the simulated longshore current in this trough. The correlation coefficient, scatter index, relative bias and Brier Skill Score for the simulation are shown in Table 4.2.
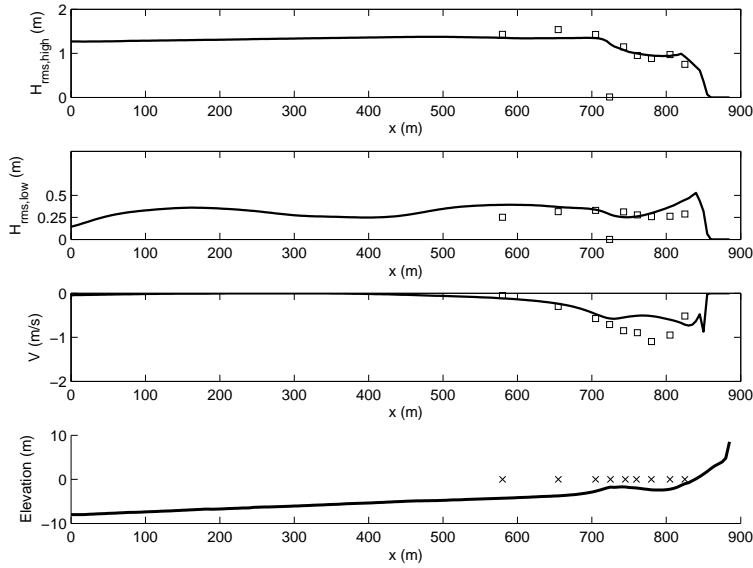
Figure 4.9: DELILAH field experiment 1990. First panel: Time-averaged measured (squares) and modelled (line) RMS-wave height of the short waves. Second panel: Time-averaged measured (squares) and modeled (line) RMS-wave height of the infragravity waves. Third panel: Time-averaged measured (squares) and modeled (line) longshore velocity. Fourth panel: Cross shore profile at the location of the measurement gauge array with the positions of the gauges (crosses).

Table 4.2: Error statistics Delilah

	R^2	Sci	Rel. bias	BSS
$H_{rms,HI}$	0.85	0.09	-0.02	0.85
$H_{rms,LO}$	-0.14	0.31	0.19	-5.94
v	0.37	0.40	0.28	0.17

The modeled and measured sea surface elevation spectra at all nine gauge locations are shown in Figure 4.10. Note that the modeled surface elevation spectra only contain low frequency components associated with wave groups. The figure shows a migration of energy from high to low frequencies in shoreward direction in the measured spectra. The simulated spectra reproduce well the trend of increasing energy in the low frequency band in shoreward direction, but the amount of energy in the simulated low frequency band is less than in the measurements. In conclusion it can be stated that the model reproduces to a high degree of accuracy the short wave transformation in the shoaling and breaker zone. The transfer of energy from high to low frequencies in the model has qualitative skill. The longshore velocity in the nearshore requires additional calibration of the short wave and roller parameters.
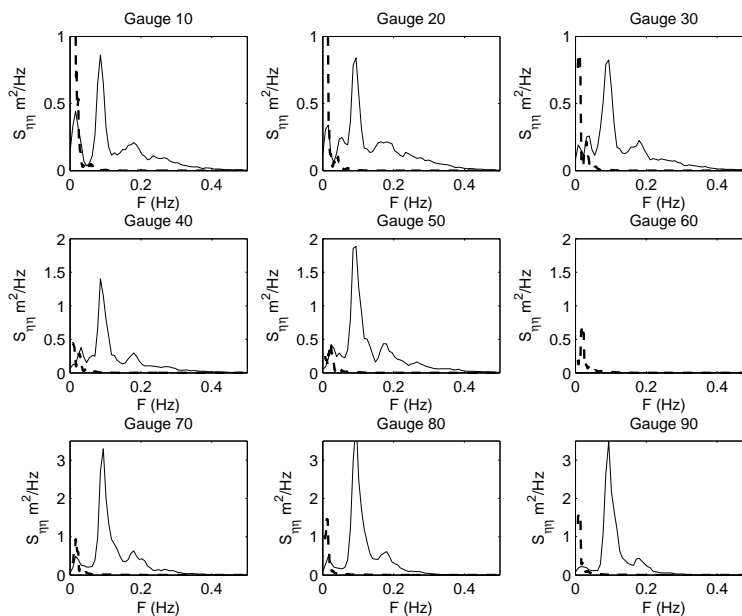
Figure 4.10: DELILAH field experiment 1990: Measured (solid line) and modelled (dashed line) surface elevation spectra for nine locations in the primary cross shore array. Gauge 90 is the most seaward.

Birkemeier, W.A., C. Donoghue, C. E. Long, K. K. Hathaway, and C. F. Baron (1997) *1990 DELILAH Nearshore Experiment: Summary report*, Tech. Rep. CHL-97-4-24, Field Res. Facil., U.S. Army Corps of Eng., Waterways Exper. Stn., Vicksburg., Miss.

Van Dongeren, A., A. Reniers, J. Battjes, and I. Svendsen (2003), *Numerical modeling of infragravity wave response during DELILAH*, J. Geophys. Res., 108(C9), 3288, doi:10.1029/2002JC001332.

4.6   Deltaflume M1263 part III test 1

Contact: Kees den Heijer <Kees.denHeijer@Deltares.nl>

4.6.1   Introduction

The M1263 dune erosion experiments were carried out in the large wave flume of Delft Hydraulics (now Deltares).

The dimensions of the so-called Deltaflume are as follows:

length	233 m
depth	7 m (locally 9 m)
width	5 m

The facility is equipped with a flap-type programmable wave generator,

maximum wave height random waves:	$H_s = 2$ m
maximum wave height periodic waves:	$H = 3$ m
wave period range:	$T = 2$ s to $T = 10$ s.

This experiment was carried out to verify the scale relations as developed by Vellinga (1986). Within the XBeach testbed, this test gives insight in the performance of the model with

respect to one of the major experiments where DUROS (Vellinga, 1986) is based on.

4.6.2 Conditions

The cross-shore profile is based on a simplified profile which is considered as more or less representative for most of the Dutch coast. This profile is often referred to as *reference profile*. It has been scaled according to:

$n_d = 5$

$n_l = n_d(n_d/n_w^2)^{0.28} = 5(5/1)^{0.28} = 5^{1.28} = 7.85$

Sand from prototype with $D_{50} = 225$ μm was used as a bed material.

This experiment was carried out with constant hydraulic conditions:

wave height	1.5 m
wave period	5.4 s

4.6.3 Results

Figure 4.11 shows the profile development in time, simulated compared to measured. Table 4.3 shows the Brier Skill Scores at the moments in time which are comparable to profile measurements.

Table 4.3: Brier skill scores (time)

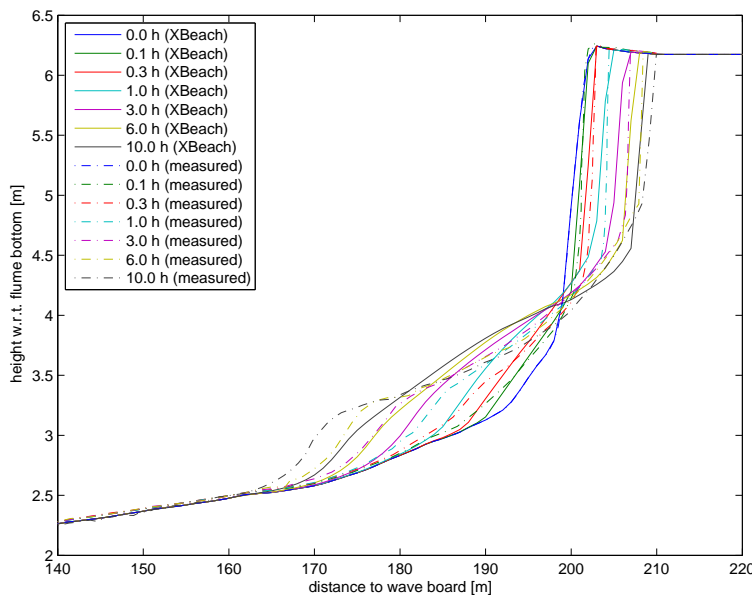| t [s]	BSS
360	0.71
1080	0.88
3600	0.87
10800	0.82
21600	0.87
36000	0.88
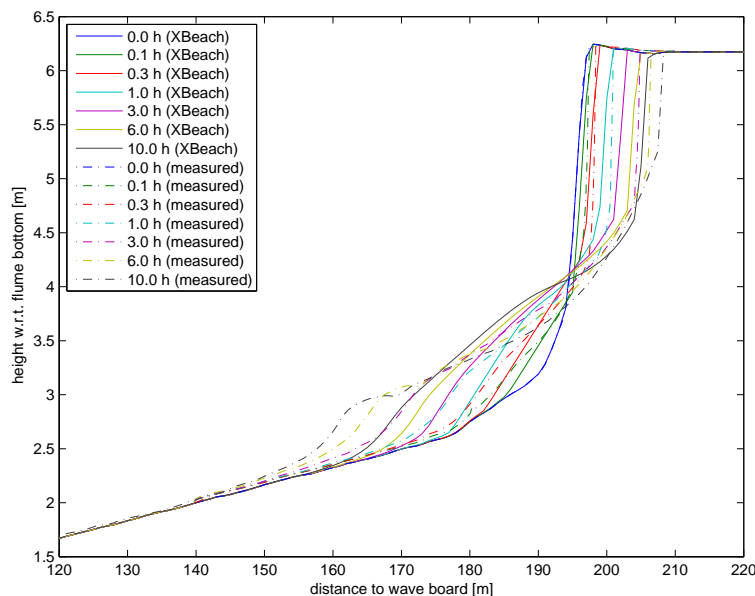
Figure 4.11: Comparison between measured and modelled profiles

4.6.4   References

Vellinga, P. (1986). Beach and Dune Erosion during Storm Surges. PhD thesis, Delft University of Technology. Also published as: Delft Hydraulics communications, no. 372, 1986.

4.7   Deltaflume M1263 part III test 2

Contact: Kees den Heijer <Kees.denHeijer@Deltares.nl>

4.7.1   Introduction

Similar to the previous one, this experiment was carried out to verify the scale relations as developed by Vellinga (1986). Within the XBeach testbed, this test gives again insight in the performance of the model with respect to one of the major experiments where DUROS (Vellinga, 1986) is based on.

4.7.2   Conditions

In this experiment, the same cross-shore profile as in Test 1 (subsection 4.6.2).

Sand from prototype with $D_{50} = 225$ μm was used as a bed material.

This experiment was carried out with constant hydraulic conditions:

wave height	1.5 m
wave period	5.4 s

4.7.3 Results

Figure 4.12 shows the profile development in time, simulated compared to measured. Table 4.4 shows the Brier Skill Scores at the moments in time which are comparable to profile measurements.

Table 4.4: Brier skill scores (time)

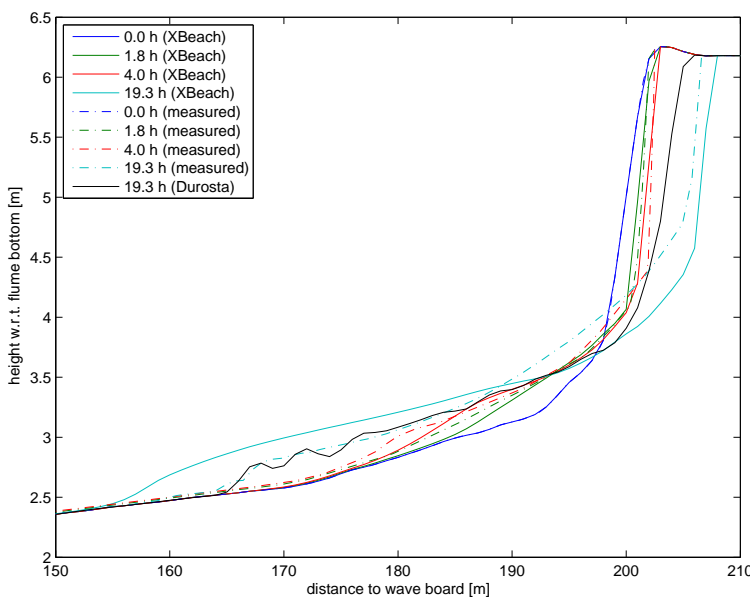| t [s]	BSS
360	0.83
1080	0.88
3600	0.90
10800	0.90
21600	0.91
36000	0.93

Figure 4.12: Comparison between measured and modelled profiles

4.7.4 References

Vellinga, P. (1986). Beach and Dune Erosion during Storm Surges. PhD thesis, Delft University of Technology. Also published as: Delft Hydraulics communications, no. 372, 1986.

4.8 Deltaflume M1263 part III test 3

Contact: Kees den Heijer <Kees.denHeijer@Deltares.nl>

4.8.1   Introduction

The aim of this experiment was to get more insight in the so far applied schematisation concerning the hydraulic conditions (WL | Delft Hydraulics, 1984). In this test the conditions are varying in time, whereas most other tests have constant conditions at the maximum level (storm surge level = NAP + 5m) with a shorter duration. Constant conditions were applied since the time scale of the dune erosion process was not yet known. It was more or less assumed that the erosion after 5 hours of constant conditions at the maximum storm surge level was comparable to a full storm surge with varying conditions.

Within the XBeach testbed, this test focusses on dune erosion under time varying conditions, which are very important for real cases.

4.8.2   Conditions

In this experiment, the same cross-shore profile as in Test 1 and 2 (subsection 4.6.2).

Sand from prototype with $D_{50} = 225$ μm was used as a bed material.

This experiment was carried out with time varying hydraulic conditions (Figure 4.15), of which the maximum values were:

wave height	1.5 m
wave period	5.4 s

4.8.3   Results

Figure 4.14 shows the profile development in time, simulated compared to measured. Table 4.5 shows the Brier Skill Scores at the moments in time which are comparable to profile measurements.

Table 4.5: Brier skill scores (time)

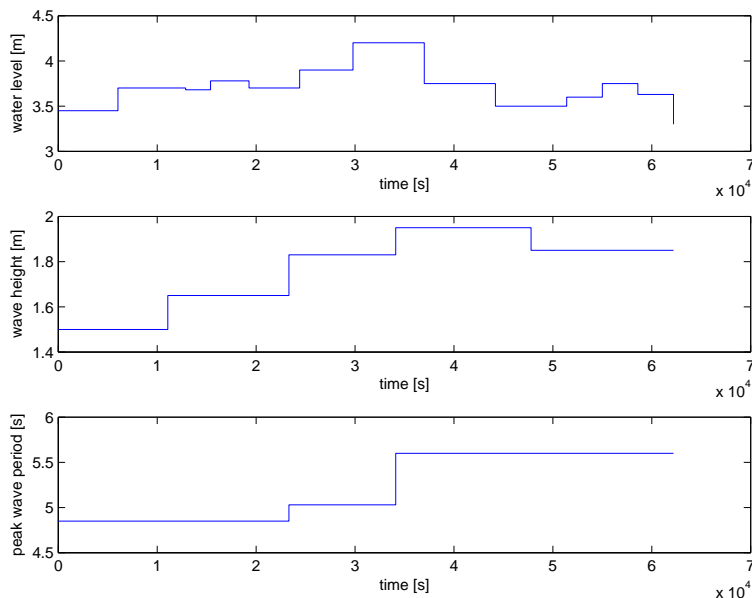| t [s]	BSS
6480	0.90
14400	0.91
69480	0.79
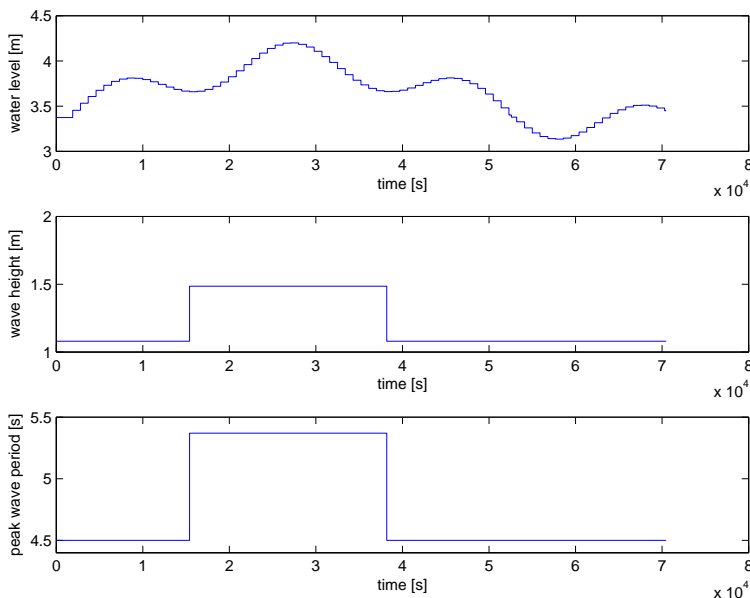
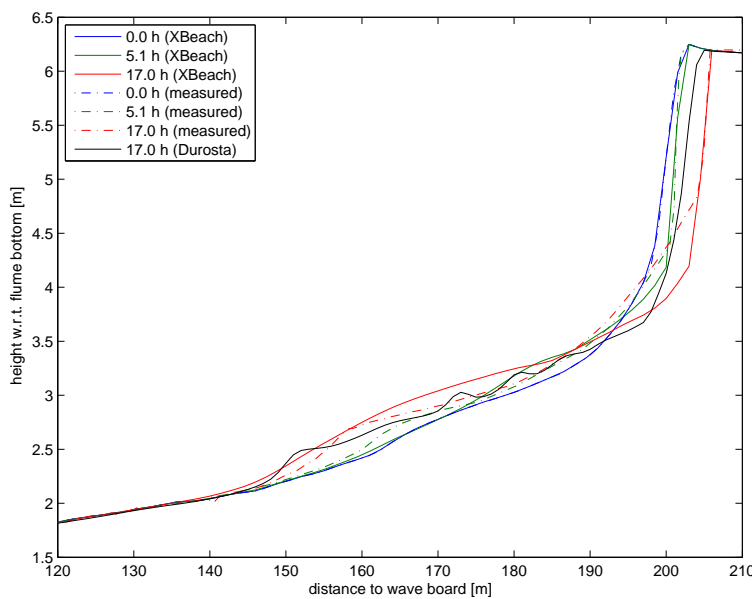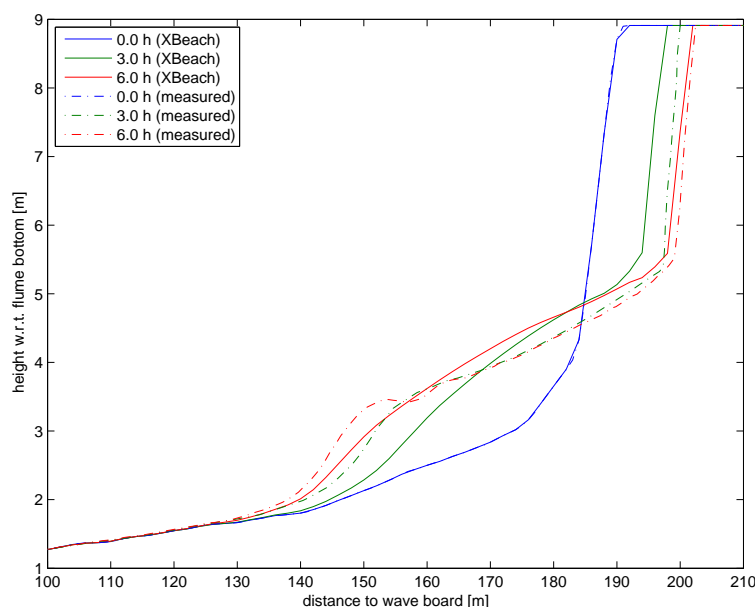Figure 4.13: Hydraulic boundary conditions as function of time

Figure 4.14: Comparison between measured and modelled profiles

4.8.4   References

Vellinga, P. (1986). Beach and Dune Erosion during Storm Surges. PhD thesis, Delft University of Technology. Also published as: Delft Hydraulics communications, no. 372, 1986.

4.9   Deltaflume M1263 part III test 4

Contact: Kees den Heijer <Kees.denHeijer@Deltares.nl>

4.9.1 Introduction

This experiment was meant as a large scale reproduction of the 1953 storm for a profile at the Delfland coast (The Netherlands). This also includes time varying conditions.

4.9.2 Conditions

The cross-shore profile in this experiment is a representation of a profile at the Delfland coast. It has been scaled according to:

$n_d = n_H = n_L = n_T{}^2 = 3.27$

$n_l = (3.27)^{1.28} = 4.56$

$n_t = (n_d)^{0.5} = (3.27)^{0.5} = 1.81$

Sand from prototype with $D_{50} = 225$ μm was used as a bed material.

This experiment was carried out with time varying hydraulic conditions (Figure 4.15), of which the maximum values were:

wave height	1.85 m
wave period	5.0 s

4.9.3 Results

Figure 4.16 shows the profile development in time, simulated compared to measured.

Table 4.6 shows the Brier Skill Scores at the moments in time which are comparable to profile measurements.

Table 4.6: Brier skill scores (time)

t [s]	BSS
18360	0.76
61200	0.80

Figure 4.15: Hydraulic boundary conditions as function of time

Figure 4.16: Comparison between measured and modelled profiles

4.9.4 References

Vellinga, P. (1986). Beach and Dune Erosion during Storm Surges. PhD thesis, Delft University of Technology. Also published as: Delft Hydraulics communications, no. 372, 1986.

4.10 Deltaflume M1263 part III test 5

Contact: Kees den Heijer <Kees.denHeijer@Deltares.nl>

4.10.1 Introduction

This experiment was set up as a full scale replica of a moderate storm surge in nature. Albeit that the conditions were constant.

4.10.2 Conditions

The cross-shore profile in this experiment was derived from the reference profile (subsection 4.6.2).

4.10.3 Results

Figure 4.17 shows the profile development in time, simulated compared to measured. Table 4.7 shows the Brier Skill Scores at the moments in time which are comparable to profile measurements.

Table 4.7: Brier skill scores (time)

t [s]	BSS
10800	0.83
21600	0.97

Figure 4.17: Comparison between measured and modelled profiles

4.10.4 References

Vellinga, P. (1986). Beach and Dune Erosion during Storm Surges. PhD thesis, Delft University of Technology. Also published as: Delft Hydraulics communications, no. 372, 1986.
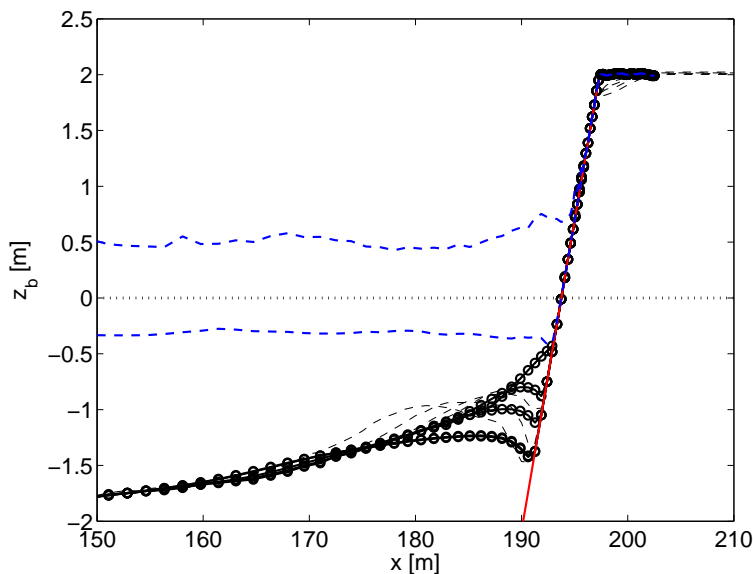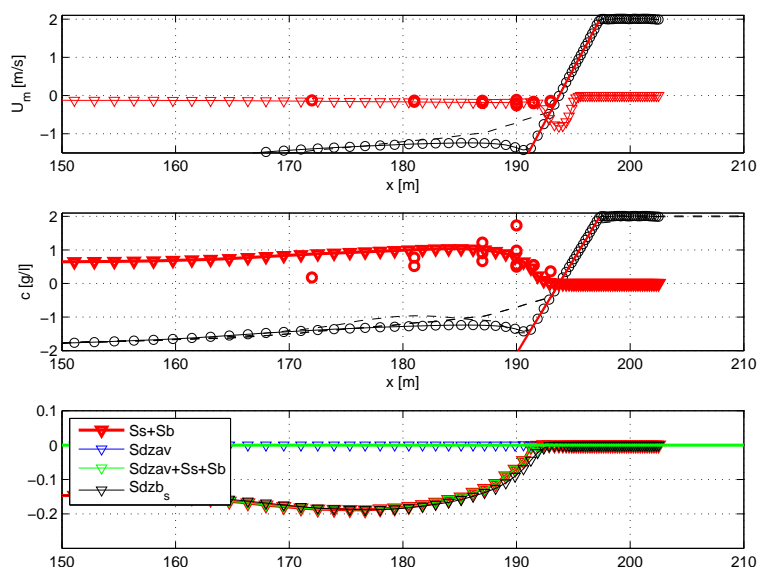
4.11   DeltaflumeH298 T1

Contact: Jaap van Thiel de Vries <jaap.vanthieldevries@deltares.nl>

In test T1 of the Deltflume H298 series (Steetzel,1987) scour hole development in front of a dune revetment is ivestigated. The test was carried out at a depth scale nd = 5 (Vellinga, 1986) and the initial profile in the flume correponds to the reference profile for the Dutch Holland coast. At the dune foot (located at x = 193 m from the wave board and z = 3.80 m above the flumes floor) a concrete revetment is applied that covers almost the whole dune face (slope of 1:1.8). The lower end of the revetment is located at z = 2.5 m and the top end at z = 6.2 m. The test was conducted with a constant water level (set at z = 4.2 m) and wave conditions that correpsond to a Pierson Moskowitz spectrum with Hm0 = 1.52 m and Tp = 5.37s. The sand applied in the test has a median grain diameter (D_{50}) of approximately 210 um.

4.11.1   Results

Simulated and measured profile development are compared in (Figure 4.18). In the physical experiment the scour hole devlops till a depth of z = 2.59 m above after seven hours simulation (is 1.21 meter below the dune foot). Computed bedlevel changes for sources and sinks (sourcesink=1) versus sediment transport gradients (sourcesink=0) are comparable. Without any relevant model improvements it is concluded that XBeach underestimates the erosion depth at the toe of the revetment. It seems an explaination may be found in simulated sediment suspensions in the proximity of the revtment, which are underestimated with a factor two (Figure 4.19). The simulated mean flow is supposed to be in reasonable agreement with measurements.

Steetzel, H.J., 1987. Systematic reserach on the effectiveness of dune toe revetments, Large scale model investigation (in Dutch), Report H298-I, Delft Hydraulics, Delft, The Netherlands.

Table 4.8

	R^2	SCI	Rel. Bias	BSS
sedero	0.8156	0.6131	-0.2111	0.6653

Figure 4.18

Figure 4.19

4.12   DeltaflumeH298 T3

Contact: Jaap van Thiel de Vries <jaap.vanthieldevries@deltares.nl>

In test T3 of the Deltflume H298 series (Steetzel,1987) erosion above medium height dune revetment is ivestigated. The test was carried out at a depth scale nd = 5 (Vellinga, 1986) and the initial profile in the flume correponds to the reference profile for the Dutch Holland coast. At the dune foot (located at x = 193 m from the wave board and z = 3.80 m above the flumes floor) a concrete revetment is applied that partly covers the dune face (slope of 1:1.8). The lower end of the revetment is located at z = 2.5 m and the top end at z = 4.8 m. The test was conducted with a constant water level (set at z = 4.2 m) and wave conditions that correpsond to a Pierson Moskowitz spectrum with Hm0 = 1.52 m and Tp = 5.37s. The

sand applied in the test has a median grain diameter (D_{50}) of approximately 210 um.

4.12.1 Results

Simulated and measured profile development are compared in (Figure 4.20). In the physical experiment the eroded volume above the revetment is $10.37 m^3$ and at the toe of the revtment a scour hole devlops till a depth of z = 0.92 m above after seven hours simulation (is 1.21 meter below the dune foot). Without any relevant model improvements it is concluded that XBeach underestimates the erosion volume above the revetment and the erosion depth at the toe of the revetment. Considering the limited erosion volume above the revetment it is hypothesized that in addition to long wave run-up also short wave runup should be included in the avalanching algorithm (which is the main mechanism to release sand from the dunes). As mentioned before in test T1 a reasonable explaination for the underestimation of the scour depth at the toe of the revetment may be found in simulated sediment suspensions in the proximity of the revtment, which are underestimated with a factor two ((Figure 4.21)). The simulated mean flow is supposed to be in reasonable agreement with measurements.

Steetzel, H.J., 1987. Systematic reserach on the effectiveness of dune toe revetments, Large scale model investigation (in Dutch), Report H298-I, Delft Hydraulics, Delft, The Netherlands.

Table 4.9

	R^2	SCI	Rel. Bias	BSS
sedero	0.5211	0.8872	0.0208	0.2110
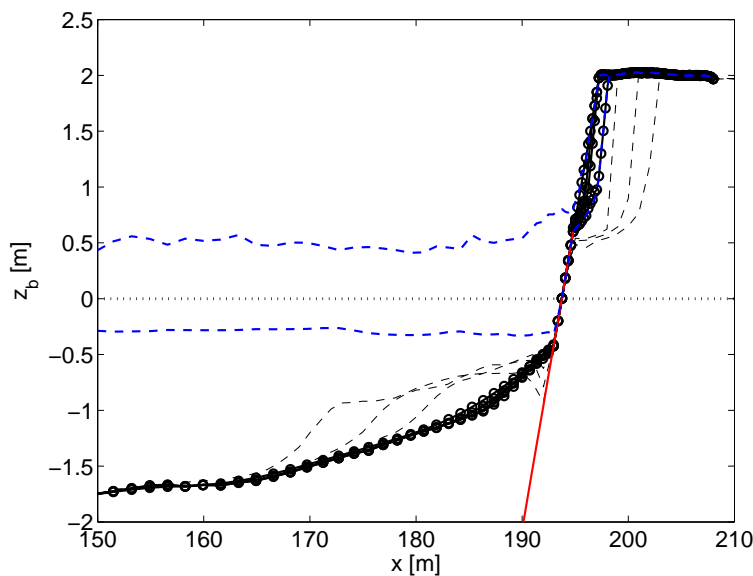
Figure 4.20
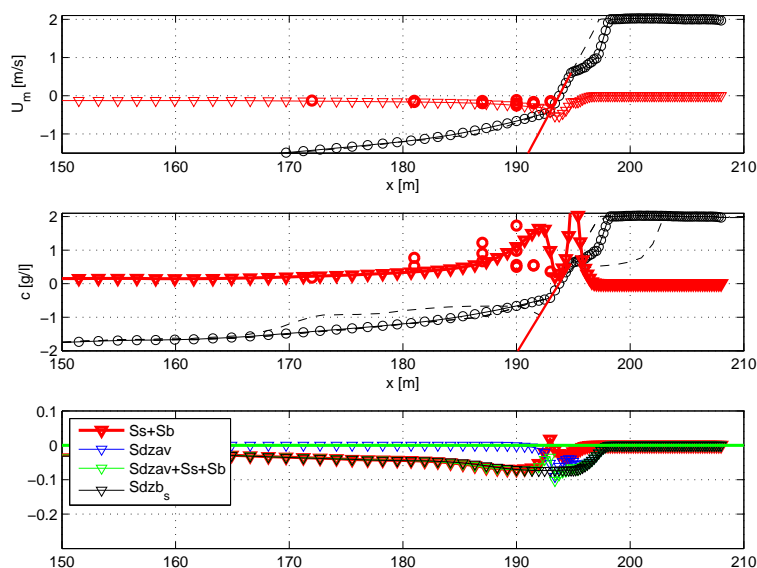
Figure 4.21

4.13   Deltaflume LIP 11D 2E

Contact: Bas Hoonhout <bas.hoonhout@deltares.nl>

This model test, described in Arcilla et al. (1994), concerns extreme conditions with a raised water level at 4.58 m above the flume bottom, a significant wave height, H_{m0}, of 1.4 m and peak period, T_p, of 5 s. Bed material consisted of sand with a D_{50} of approximately 0.2 mm. During the test substantial dune erosion took place.

Based on the integral wave parameters H_{m0} and T_p and a standard Jonswap spectral shape, time series of wave energy were generated and imposed as boundary condition. Since the flume tests were carried out with first-order wave generation (no imposed super-harmonics and sub-harmonics), the hindcast runs were carried out with the incoming bound long waves set to zero ('first order wave generation'). Active wave reflection compensation was applied in the physical model, which has a result similar to the weakly reflective boundary condition in XBeach, namely to prevent re-reflecting of outgoing waves at the wave paddle (offshore boundary).

A grid resolution of 1 m was applied and the sediment transport settings were set at default values. For the morphodynamic testing the model was run for 0.8 hours of hydrodynamic time with a morphological factor of 10, effectively representing a morphological simulation time of 8 hours.

Test results are given for the root mean square wave height, H_{rms}, and the root mean square orbital velocity, U_{rms}, separated in high-frequency (frequencies above $f_p/2$ corresponding to incident waves) and low-frequency parts (corresponding to infragravity waves). In XBeach model terms, these parameters are defined as follows:

$$H_{rms,HI} = \sqrt{<H^2>} \tag{4.3}$$

$$u_{rms,HI} = \sqrt{<u_{rms}^2>} \quad , \quad u_{rms} = \frac{1}{\sqrt{2}}\frac{\pi H}{T_p sinh(kh)} \tag{4.4}$$

$$H_{rms,LO} = \sqrt{8<(\eta-<\eta>)^2>} \tag{4.5}$$

$$u_{rms,LO} = \sqrt{<(u^L-<u^L>)^2>} \tag{4.6}$$

$$\tag{4.7}$$

In Figure 4.22 the results are shown for first order wave generation (as in the flume tests). The model is clearly capable of capturing both the HF and LF wave heights and orbital velocities. For this test, the agreement is better if incoming bound long waves are omitted from the flow boundary condition (as they were in the laboratory test).
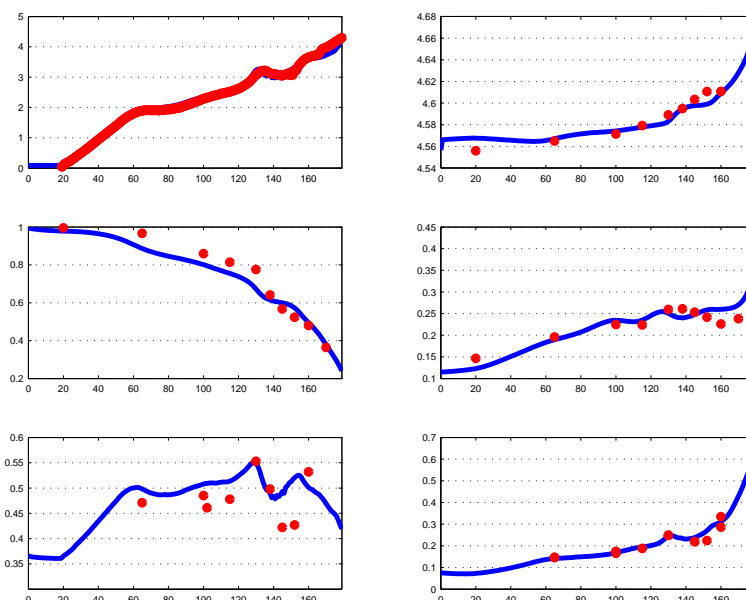
Figure 4.22: Computed and observed hydrodynamic parameters for test 2E of the LIP11D experiment. Top left: bed level and mean water level. Top right: measured (dots) and computed mean water level with first-order steering (drawn line) as function of the cross-shore distance. Middle left: same for HF wave height; middle right: same for LF wave height; bottom left: same for HF orbital velocity; bottom right: same for LF orbital velocity.

In Figure 4.23 the horizontal distribution of sedimentation and erosion after 8 hours is shown, and the evolution in time of the erosion volume and the dune retreat. We see a good agreement for all three parameters. Noteworthy is the episodic behaviour of the dune erosion, both in measurements and model, although the almost exact (deterministic) reproduction of the (stochastic) dune retreat must be a coincidence. An important conclusion for physical model tests is that for dune erosion it does make a difference whether first-order or second-order wave steering is applied.
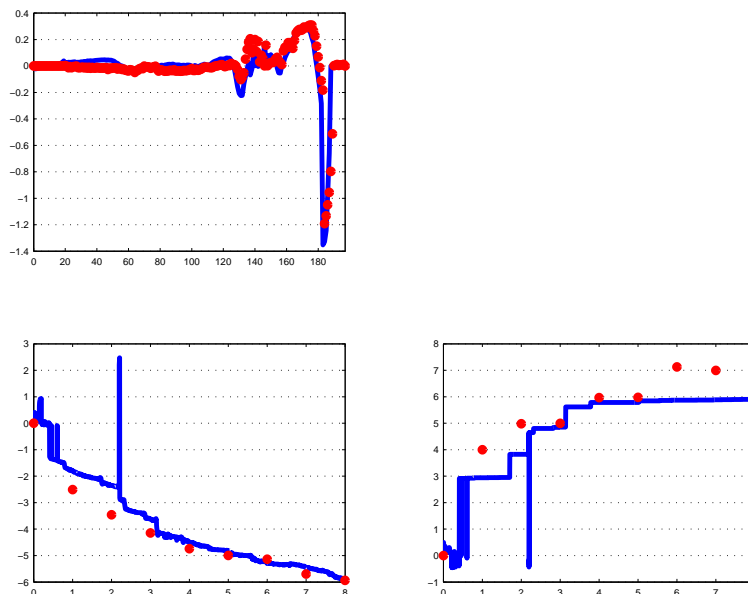
Figure 4.23: Computed and observed sedimentation and erosion after 8 hrs (top panel); erosion volume as function of time (bottom left) and dune retreat (bottom right) as function of time for test 2E of the LIP11D experiment, (Arcilla et al, 1993). All results with first-order steering.

A key element in the modelling is the avalanching algorithm; even though surfbeat waves running up and down the upper beach are fully resolved by the model, without a mechanism to transport sand from the dry dune face to the beach the dune face erosion rate is substantially underestimated. The relatively simple avalanching algorithm described above, whereby an underwater critical slope of 0.3 and a critical slope above water of 1.0 are applied, proves to be quite successful in representing the retreat of the upper beach and dune face. In Figure 4.24 the measured and modelled bed evolution are shown, which looks quite good in the upper region.
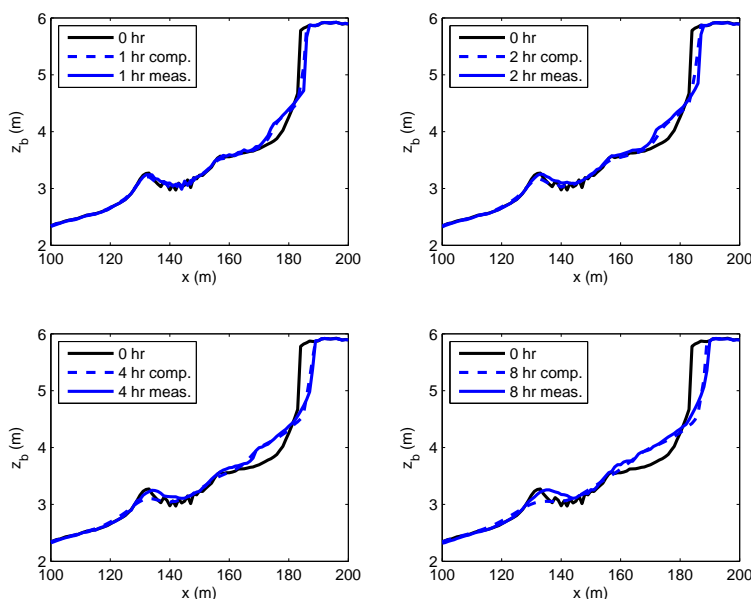
Figure 4.24: Measured and modelled bed level after 1, 2, 4 and 8 hours of wave action, for a water level of 4.56 m above the flume bottom.

Error statistics for the standard run are collected in Table 4.10, and generally show a scatter index and relative bias of less than 10% for the hydrodynamic parameters and overall erosion volumes and dune retreat. An exception is the mean velocity, for which the higher scatter and bias can be attributed to the (neglected) 3D structure of this parameter. The horizontal distribution of the sedimentation and erosion at the end of the test shows a higher scatter, determined in part by the areas with small changes; the Brier Skill Score shows a value of 0.72, which for morphodynamic models is considered good (Van Rijn et al., 2003).

Table 4.10: Error statistics Deltaflume LIP 11D 2E

	R^2	Sci	Rel. bias	BSS
$SEDERO$	0.80	0.63	-0.14	0.63
ETA	0.86	0.00	-0.00	0.89
VOL	0.86	0.11	0.08	0.88
R	0.79	0.15	-0.13	0.81
$URMS$	0.37	0.10	0.06	0.17
$URMS_{LO}$	0.87	0.08	0.03	0.89

Arcilla, A. S., J. A. Roelvink, B. A. OConnor, A. Reniers, and J. A.Jimenez (1994), *The Delta flume 93 experiment*, in Coastal Dynamics '94, edited by A. S. Arcilla, N. C. Kraus, and S. J. F. Marcel, pp. 488-502, Am. Soc. of Civ. Eng., Reston, Va.

Van Rijn, L.C., D. J. R. Walstra, B. Grasmeijer, J. Sutherland, S. Pan, J. P. Sierra, *The predictability of cross-shore bed evolution of sandy beaches at the time scale of storms and seasons using process-based Profile models*, Coastal Engineering, Volume 47, Issue 3, January 2003, Pages 295-327, ISSN 0378-3839, DOI: 10.1016/S0378-3839(02)00120-5.

4.14   Deltaflume 2006 T01

Contact: Jaap van Thiel de Vries <jaap.vanthieldevries@deltares.nl>

The aim of this test is to make a detailed comparison between simulated physics over an evolving bathymetry and the measurements obtained during the Deltaflume experiment in 2006 (Van Gent et al, 2008). For brevity this comparison is performed only for test T01 (this test corresponds best to the Dutch normative conditions). The simulation is performed on a regular grid with dx = 1 m and input to the model are time series of short wave varying energy (low pass filtered on the wave group time scale) and incoming (bound) long waves. The time series are constructed from pressure and flow measurements at x = 41 m from the wave board. The short wave group velocity (associated with advection of wave action) is based on the Tm-1,0 wave period. Other model settings can be found in Van Thiel de Vries (2009)

4.14.1   Results

Wave height transformation and wave setup (Figure 4.25) are favourably reproduced with the model. The long wave height is slightly underestimated whereas the wave setup is slightly overestimated. The correlation between measured short wave variance and long wave water surface elevations (Figure 4.26) corresponds reasonably well with the measurements. Towards the shoreline this correlation increases (Abdelrahman and Thornton, 1987; Roelvink and

Stive, 1989) meaning the highest short waves travel on top of long waves, which likely causes that more short wave energy gets closer to the dune face.

Short wave skewness and asymmetry are reasonably predicted with the extended Rienecker Fenton model (Figure 4.27). However, in the inner surf zone both wave skewness and asymmetry are overestimated. Possible explanations are wave breaking, which limits the steepness and height of waves and the presence of free harmonics in the flume. Both these effects are not included in the wave shape model but indeed are present in the flume test (see Van Thiel de Vries, 2009). From simulated skewness and asymmetry it follows that the total nonlinearity of a short wave is overestimated close to the dune face (Figure 4.28). The phase Beta is favourably simulated with the model but is underestimated further offshore.
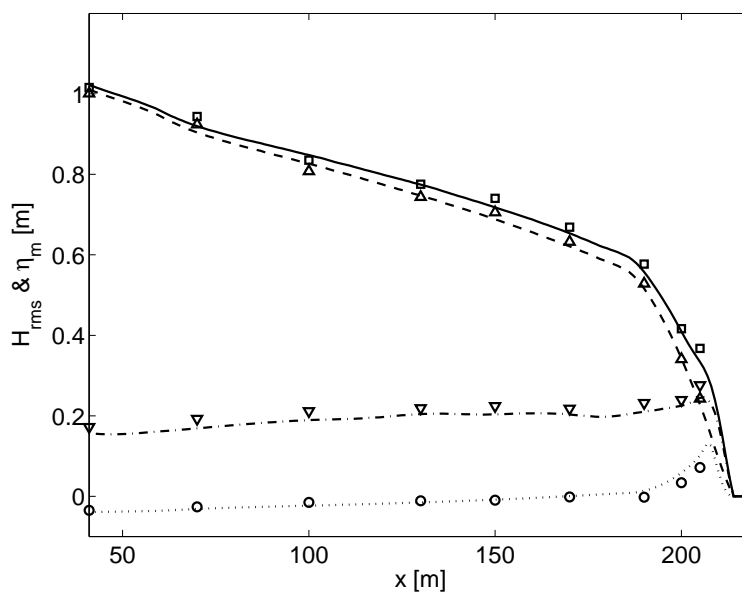
Figure 4.25: *Simulated wave setup (dotted line) and transformation of the total (solid line), short (dashed line) and long (dashed-dotted line) wave height compared with measurements of the wave setup (circles) and the total (squares), short (upward triangles) and long (downward triangles) wave height.*
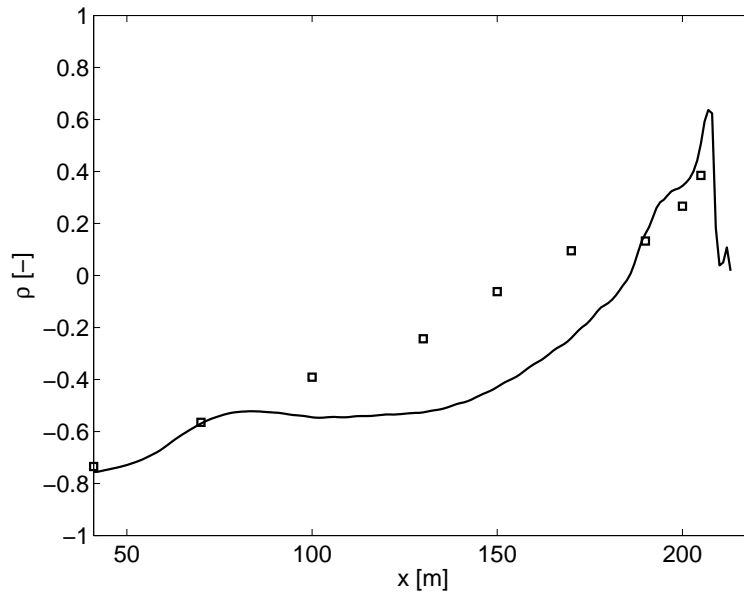
Figure 4.26: Simulated correlation ρ between the short wave variance and long wave water surface elevations (solid line) compared with the measured correlation (squares) as function of cross-shore position.
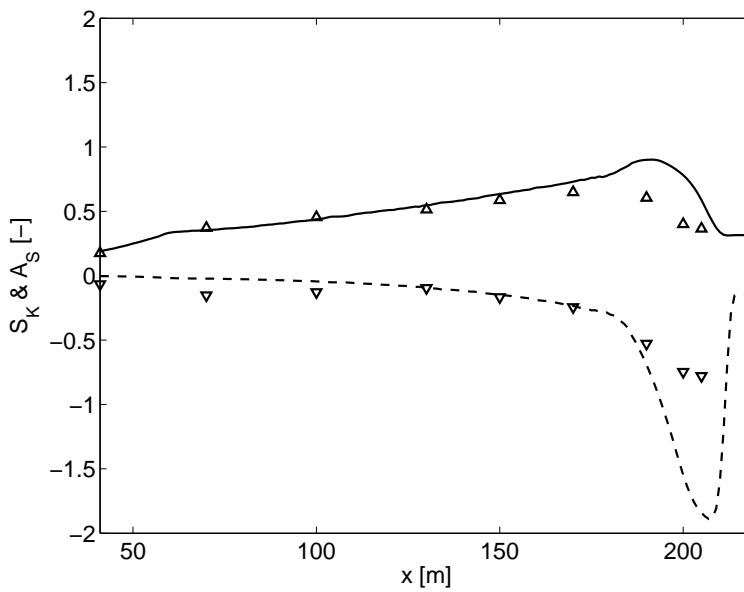
Figure 4.27: Simulated wave skewness S_K (solid line) and asymmetry A_S (dashed line) compared with measured skewness (upward triangles) and asymmetry (downward triangles) as function of cross-shore position.
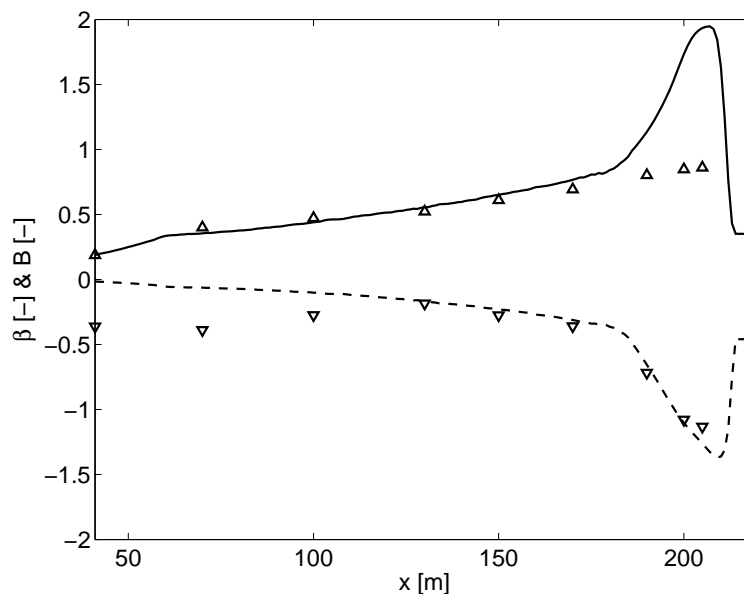
Figure 4.28: Simulated wave nonlinearity B (solid line) and phase β (dashed line) compared with measured nonlinearity (upward triangles) and phase (down-ward triangles) as function of cross-shore position.

The simulated test and depth averaged flow velocity shows the same trend as in the measurements and increases towards the shoreline (Figure 4.29). However, in the simulation the cross-shore range with a higher offshore mean flow is smaller and extends less far seaward than in the measurements. This is possibly explained by differences in measured and simulated profile development (Figure 4.35) or inaccurate measurements. In addition, another explanation may be found in the incorrect modelling of the roller energy dissipation. Simulations (not shown) with a smaller roller dissipation rate revealed that roller energy in the inner surf increases, leading to higher return flow over a broader cross-shore range.

Long waves contribute to the time and depth averaged flow close to the shoreline. The contribution of long waves to the mean flow is explained by on average larger water depths during the interval associated with shoreward flow velocities in relation to the interval with offshore flow velocities. Considering continuity and a uniform vertical structure of the long wave flow this means a time and depth averaged offshore directed flow should be present.

Nonlinear waves may cause onshore sediment transport presuming non-uniform sediment stirring over the wave cycle and a positive correlation between sediment suspension and the intra wave flow. In order to include the wave averaged effect of nonlinear waves on the sediment transport a mean flow u_A is computed, which is added to the mean (Eulerian) flow U_m (see Van Thiel de Vries et al., 2009 for more details). The simulated time averaged flow associated with nonlinear waves shows a comparable evolution as in the measurements but is overestimated especially closer to the dune face. Near the shoreline the wave skewness related sediment transport vanishes (Figure 4.27) since waves develop towards fully saw tooth shaped bores that have negligible skewness.

The orbital flow velocity (Figure 4.30) is favourably predicted by the model. The short wave orbital flow velocity is slightly overestimated whereas the long wave orbital flow is underestimated. The underestimation of the simulated long wave orbital flow corresponds well to the slight underestimation of the observed long wave water surface variance.
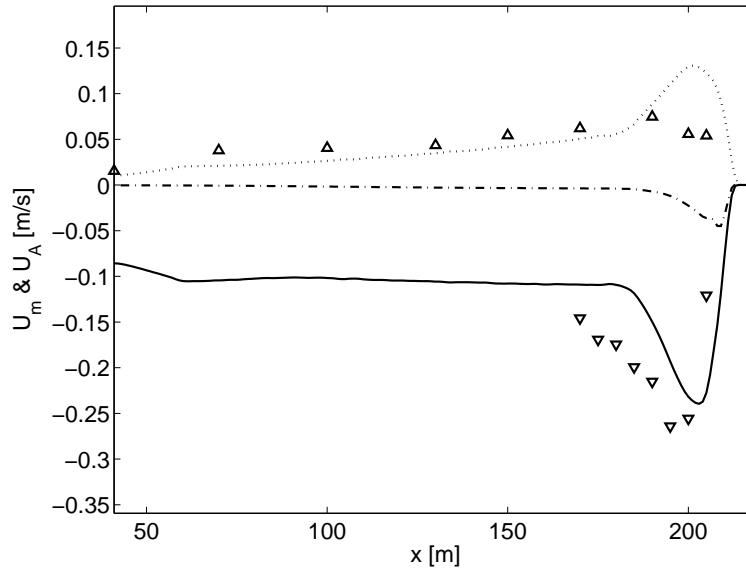
Figure 4.29: Simulated test and depth averaged flow Um due to short and long waves (solid line) and long waves only (dashed line) as function of the cross-shore position. The dotted line corresponds to the wave averaged sediment advection velocity u_A due to nonlinear short waves. Markers correspond to measured undertow flow velocities due to short and long waves (downward triangles) and the sediment advection velocity due to nonlinear waves (upward triangles).
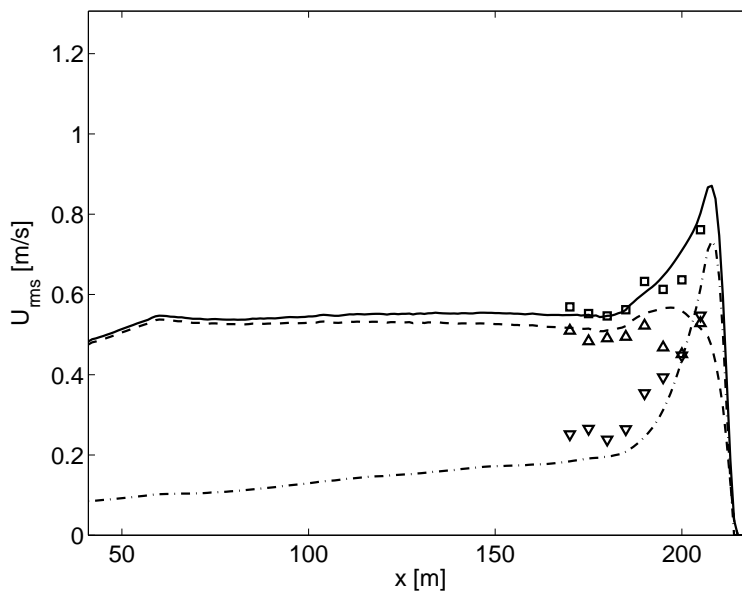

Figure 4.30: Transformation of the simulated total (solid line), short (dashed line) and long (dashed-dotted line) wave orbital flow compared with the meas-ured total (squares), short (upward triangles) and long (downward triangles) wave orbital flow as function of cross-shore position.

The simulated test and depth averaged sediment concentration increases towards the shoreline but is underestimated, especially in deeper water where the modelled sediment concentration is smaller (Figure 4.31 and Figure 4.32). In the proximity of the dune face the simulated mean sediment concentration is within a factor two with the measurements. Further offshore the discrepancy between simulations and measurements is larger. The sharp rise in the near dune

sediment concentration compares well with the bore averaged near-bed turbulence intensity (Figure 4.33) that also increases towards the shoreline. This increase in turbulence intensity through the inner surf is explained by more intensive wave breaking (turbulence production at the water surface increases) and by decreasing water depth (generated turbulence at the water surface is more effective in reaching the bed).

The simulated time averaged sediment transport compares well with the measured sediment transport computed from profile changes (Figure 4.34). Sediment is eroded from the dune face via avalanching and as a result the sediment transport associated with avalanching is dominant over the dune face and in the swash zone. From the swash zone seaward, the flow based sediment transport becomes more important. At 205 m from the wave board, in a water depth that varies between 0.1 m and 0.2 m, the flow related sediment transport is dominant.

The simulated flow related sediment transport is separated in sediment transports associated with nonlinear waves (SW), long waves (SL) and the short wave driven under-tow (SR) (Figure 4.35):

$$S_W = u_A ch$$

$$S_L = u^L ch$$

$$S_R = (u^E - u^L)ch$$

The offshore sediment transport results from the short wave and roller driven under-tow (SR) combined with the transport associated with the long waves (SL). The transport that follows from the short wave undertow is dominant in the present simu-lation but the long wave related sediment transport cannot be neglected (about 30

Profile evolution and dune erosion volumes are favourably predicted with the model during test T01 (Figure 4.36 and Figure 4.37). Between t = 2.04 and 6.0 hours (interval E) the dune erosion rate is slightly underestimated. At the offshore edge of the developing foreshore, the model seems not capable to reproduce the steep transition from the original (unaffected) profile towards the newly developed foreshore. A bar type feature is observed at this transition that is hypothesized to be related to (partly) plunging breakers that generate a water jet, which penetrates in the water column and causes additional sediment stirring when it reaches the bed. Though the effect of wave breaking induced turbulence on sediment suspension is included in the simulation, the applied model only considers spilling breakers, which are expected to be less efficient than plunging breakers in stirring up sand.
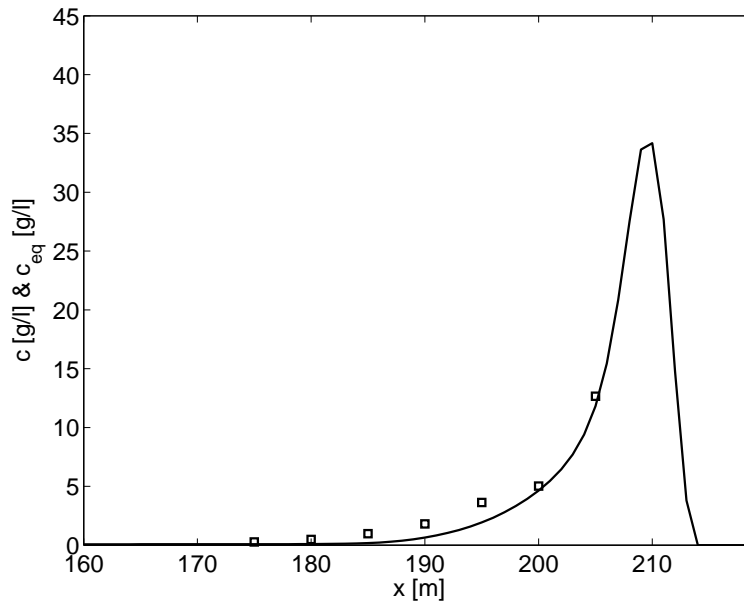
Figure 4.31: Simulated test and depth averaged sediment concentration (solid line) compared with the sediment concentrations obtained from suction tubes (squares).
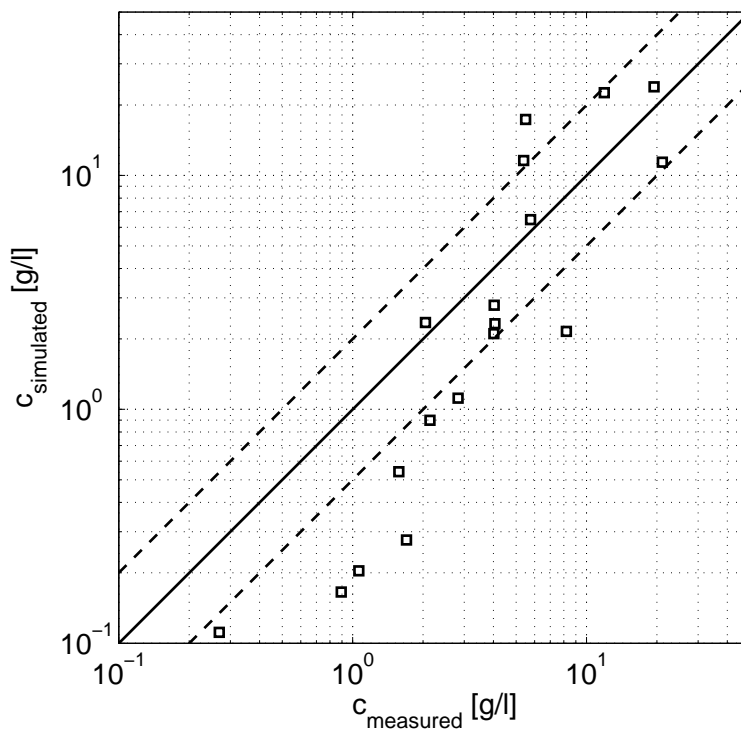

Figure 4.32: Scatter plot of simulated time and depth averaged sediment concentrations compared with vertically integrated suction tube measurements. The solid line corresponds to a perfect match between measurements and simulations whereas simulation results between the dashed lines are within a factor two with the measurements.
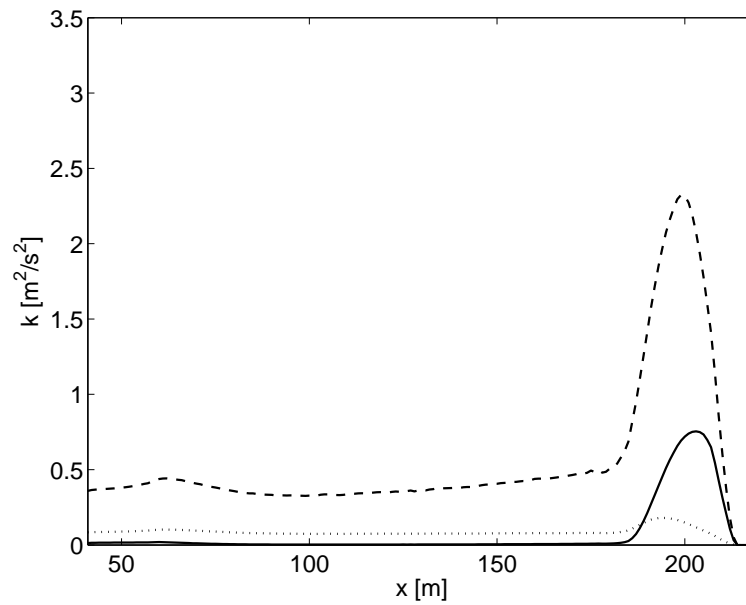
Figure 4.33: *Simulated wave averaged turbulence energy (dotted line), bore averaged turbulence energy (dashed line) and near-bed bore averaged turbulence energy (solid line) as function of cross-shore position.*
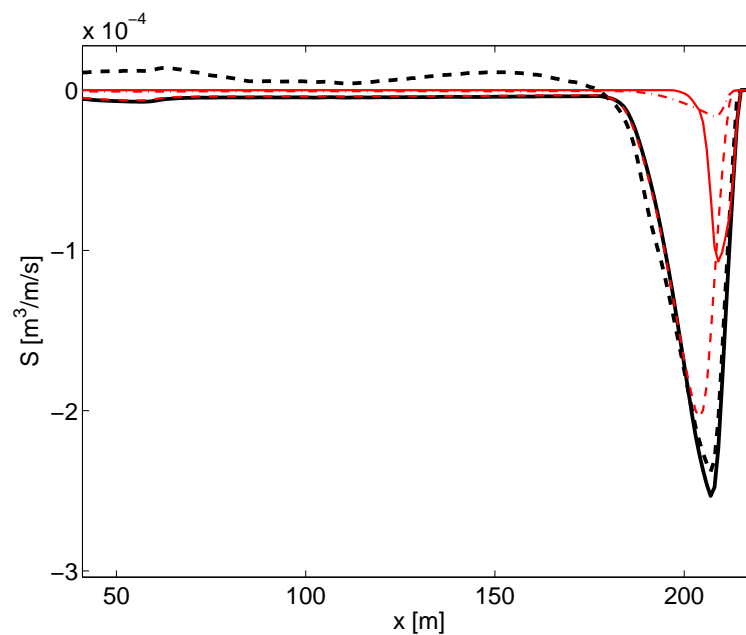
Figure 4.34: *Measured (thick dashed line) and simulated (thick solid line) test av-eraged sediment transport from bed level changes. The simulated transport is separated in a transport due to avalanching (dashed-dotted line) and a transport related to the hydrody-namics (dotted line).*
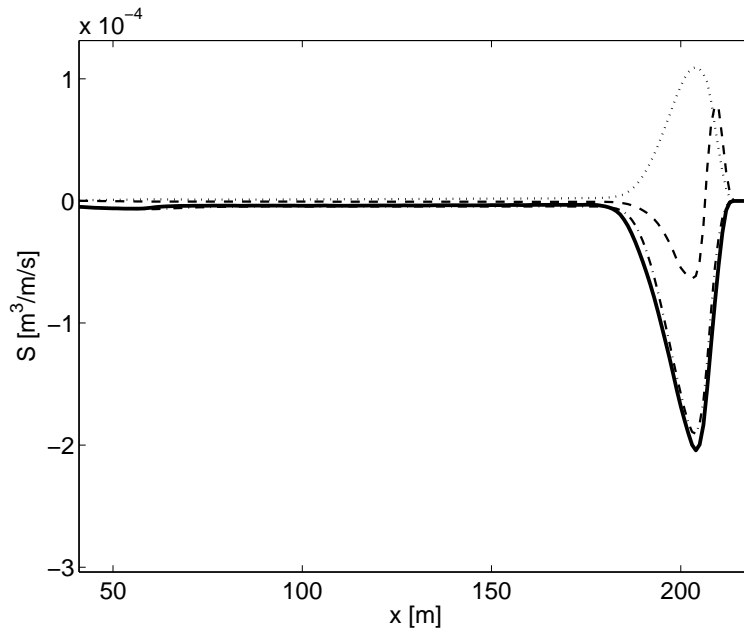
Figure 4.35: *Simulated test averaged sediment transport related to the hydrodynamics (solid line) divided into wave asymmetry related sediment transport (dotted line), long wave related sediment transport (dashed line) and sediment transport associated with the short wave undertow (dashed-dotted line).*
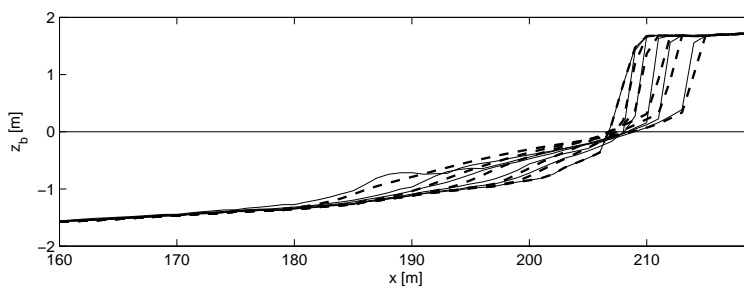
Figure 4.36: *Simulated profile evolution (dashed lines) compared with measured profile evolu-tion (solid lines) after t = 0.0, 0.1, 0.3, 1.0, 2.04 and 6.0 hours.*
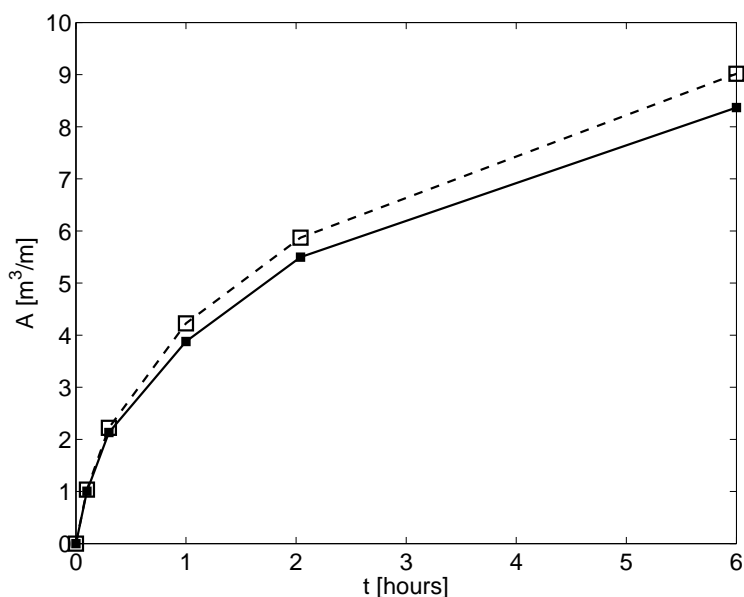
Figure 4.37: Simulated dune erosion volume above still water level (dashed line with open squares) compared with the measured dune erosion volume (solid lines with closed squares) as function of time.

It is concluded that profile evolution and dune erosion during test T01 are favourably simulated. Also simulated wave heights, flows, sediment concentrations and sediment transports compare reasonably well with measurements. However, looking at the results in more detail some discrepancies are found:

1. The long wave height and especially associated long wave orbital flows are underestimated.

2. The test and depth averaged flow between x = 170 m and x = 200 m is underestimated. Close to the shoreline no reliable measurements are available to verify the model results.

3. The simulated sediment concentration compares well with measurements close to the dune face. However, for smaller sediment concentrations in deeper water the simulated concentration is underestimated.

4. The offshore sediment transport is mainly driven by the short wave and roller induced undertow whereas the offshore directed long wave related sediment transport cancels out with the onshore sediment transport due to nonlinear short waves.

It is remarked that shoreward of the maximum offshore sediment transport, the importance of the long wave related transport increases and eventually becomes dominant in relation to the transport associated with short wave and roller driven undertow. Considering the mainly long wave associated sediment transport in proximity of the dune face and the importance of long wave run-up for avalanching it is expected that long waves are mainly responsible for the swash zone sediment transport.

Abdelrahman, S.M. and Thornton, E.B., 1987. Changes in the short wave amplitude and wavenumber due to presence of infragravity waves, Proceedings of Specialty Conference on Coastal Hydrodynamics, pp. 458-478.

Roelvink, J.A. and Stive, M.J.F., 1989. Bar-generating cross-shore flow mechanisms on a beach. Journal of Geophysical Research, 94(C4): 4785-4800.

Van Gent, M.R.A., Van Thiel de Vries, J.S.M., Coeveld, E.M., De Vroeg, J.H. and Van

de Graaff, J., 2008. Large-scale dune erosion tests to study the influence of wave periods. Coastal Engineering, 55(12): 1041-1051.

Van Thiel de Vries, J.S.M., 2009. Dune erosion during storm surges. PhD Thesis, Delft University of Technology, Delft, The Netherlands.

Table 4.11

	R^2	SCI	Rel. Bias	BSS
$H_{rms,hf}$	0.9987	0.0193	-0.0070	0.9972
$H_{rms,lf}$	0.9821	0.0927	-0.0893	0.9605
ρ	0.9147	0.5319	-0.2717	0.7664
S_k	0.7559	0.3756	0.2408	0.0303
A_s	0.9751	1.0740	-0.4556	-1.3220
β	0.9599	0.2820	0.1527	0.8050
B	0.8938	0.7510	0.4119	-2.4984
$U_{rms,hf}$	-0.4834	0.1114	0.0775	-1.5743
$U_{rms,lf}$	0.9660	0.1914	-0.1294	0.7623
U_m	0.3175	0.3422	0.1864	-0.4566
C_m	0.9950	0.9997	-0.7562	0.0008
sedero	0.9836	0.1894	-0.0182	0.9645
A	0.9999	0.0756	0.0607	0.9927

4.15   T01 Zebra

Contact: Robert McCall <robert.mccall@deltares.nl>

The purpose of this simulation is to ensure the multiple sediment fractions model in XBeach performs as expected. In this test, the Deltaflume 2006 T01 test is recreated with two types of sand with different colours, red and blue. The sand is initially placed in a zebra-stripe pattern in the profile. The properties of both types of sand such as the grain size and mobility are the same as the sand used in the Deltaflume experiment. For the test to be successful, the following conditions should be met:

- The simulated final profile should be the same as the final profile in the original Deltaflume 2006 T01 test.

- The two sediment types should mix and form layers over each other.
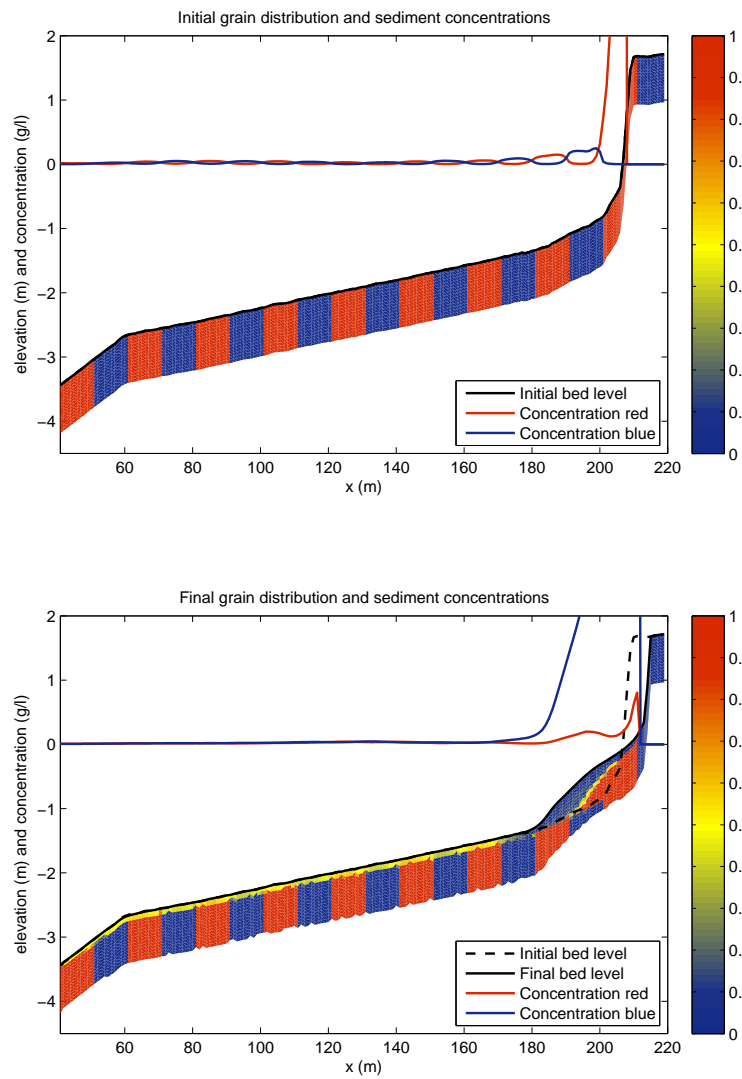
Figure 4.38
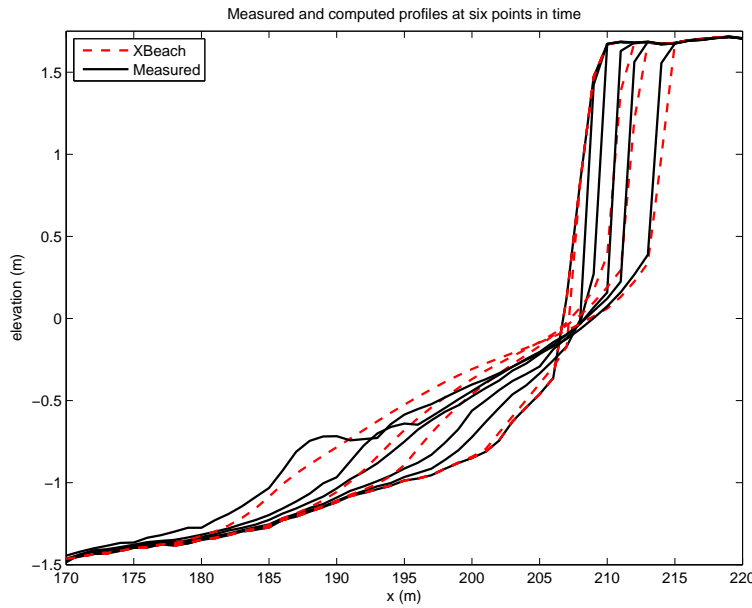
Figure 4.39

The two panels in Figure 4.40 show the initial and final distribution of red and blue sediment in the profile near the dune face. The red and blue lines in the same figure show the sediment concentration of each sediment type in the water column. If the simulation is successful, the red and blue sediment will be well mixed on the foreshore and fresh blue sediment will be deposited over the red sediment at the dune foot as the dune face retreats. The concentration of blue sediment in the water column should be higher than the concentration of red sediment in the water in areas where only blue sediment is available in the top layer of the bed.

The red lines in Figure 4.39 show the predicted dune face retreat and bed level change in the XBeach multiple-sediment model. The black lines in the same figure are the corresponding measured profiles. If the simulation has been successful, the red and black lines will align reasonably well. The results of this simulation should be compared to the Deltaflume 2006 T01 test described earlier in this report.

Table 4.12

	R	SCI	Rel. Bias	BSS (S)	BSS (ME)	α	β	γ
$t = 360s$	0.9972	0.0754	-0.0255	0.9942	0.9943	0.9945	0.0003	0.0007
$t = 1080s$	0.9780	0.2105	-0.0331	0.9500	0.9555	0.9565	0.0065	0.0012
$t = 3600s$	0.9965	0.0826	-0.0269	0.9928	0.9932	0.9931	0.0003	0.0008
$t = 7344s$	0.9945	0.0977	-0.0214	0.9888	0.9904	0.9890	0.0002	0.0005
$t = 21600s$	0.9821	0.1584	-0.0131	0.9641	0.9747	0.9644	0.0003	0.0002

Table 4.12 shows the error statistics of the predicted bed level of the multiple-sediment model of the Deltaflume 2006 T01 test. These statistics should be compared quantitatively with the error statistics of the original Deltaflume 2006 T01 model, described earlier in this report (Table 4.11).

4.15.1 MPI

Two processes are used in the MPI-version of this simulation. The results of this simulation should compare well with the results of the serial version. If the simulation is successful, **??** will be similar to Figure 4.40, and Figure 4.41 will be similar to Figure 4.39.
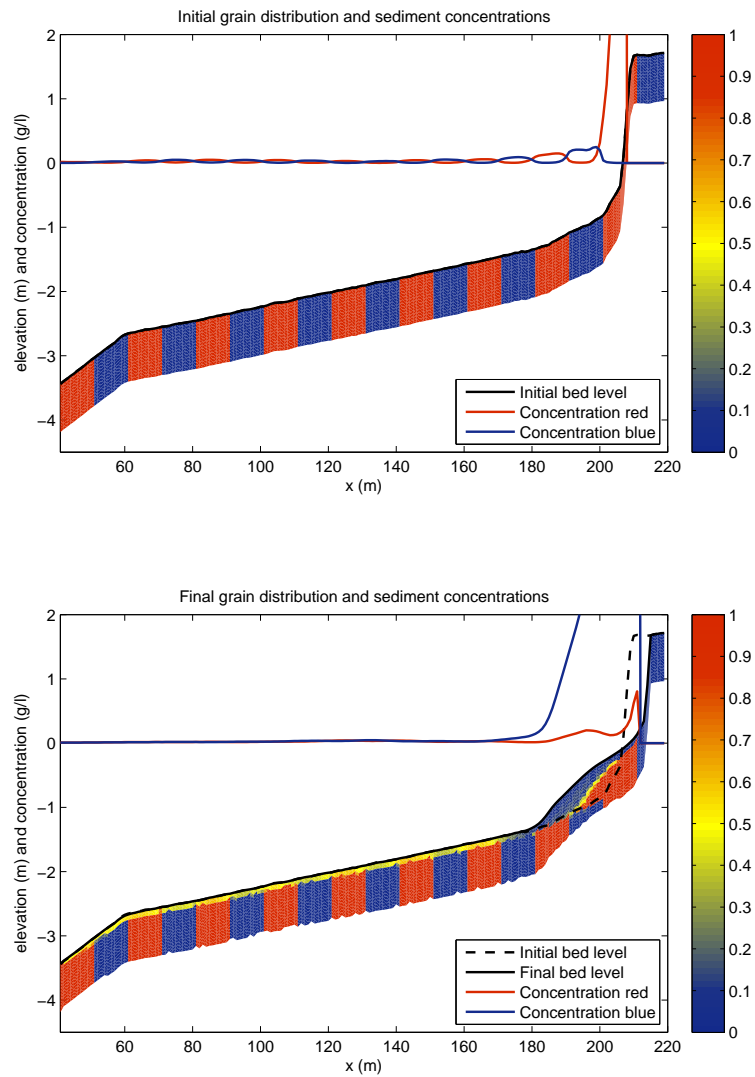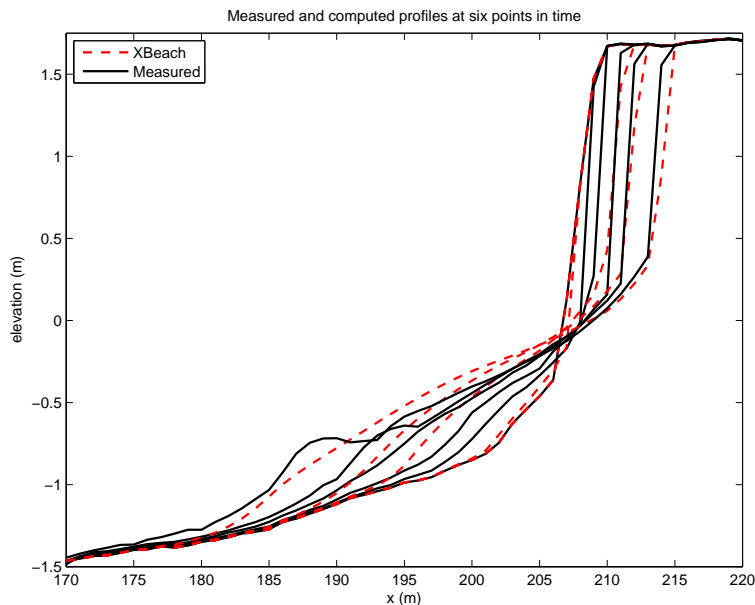

Figure 4.40

Figure 4.41

4.16   Deltaflume 2006 T04

Contact: Bas Hoonhout <bas.hoonhout@deltares.nl>

We continue with a more recent test of a more complex profile (van Gent et al., 2008, test T4) in which a small dune in front of a large volume dune is breached (Figure 4.42). This test is the best controlled case with dune overwash known to us. The test duration is six hours and profile measurements were obtained after 0.1, 0.3, 1.0, 2.0 and 6.0 hours. Also detailed measurements of wave transformation, near dune flows and sediment concentrations are available for comparing with model results. In the physical model test the still water level was set at 4.5 m above the flumes floor and imposed wave conditions correpsond to a Pierson-Moskowitz spectrum with $H_{m0} = 1.5$ m and $T_p = 4.90$ s. The wave paddle was operated with active wave reflection and second order steering. Further details may be found in Van Gent et al., 2008 and Van Thiel de Vries et al., 2008.

The simulation is performed for 6 hours on a uniform grid in which the grid size δ x is set at 1 m. In order to make a detailed comparison between measured and simulated hydrodynamics over the developing profile, the simulation is carried out with a morphological factor of 1. The offshore model boundary is located at 41 m from the wave board and we use measured water surface elevations and flow velocities at this location to obtain time series of the incident wave energy and the incoming bound long wave water surface elevations. Other model settings are the same as for test 2E of the LIP11D experiment and are listed in Appendix I.

Figure 4.42 compares the modelled and observed profile evolution. Both model and data first show a scarping of the profile, a brief period of overwashing followed by a smoothing out of the remainder of the berm and a renewed attack on the actual dune face, which is slow as most of the wave energy dissipates on the shallow upper profile left by the berm. The modelled profile evolution appears to be slightly slower than observed and also at the end of the test the modelled upper profile is slightly too low, which could be due to lack of onshore sediment transports.
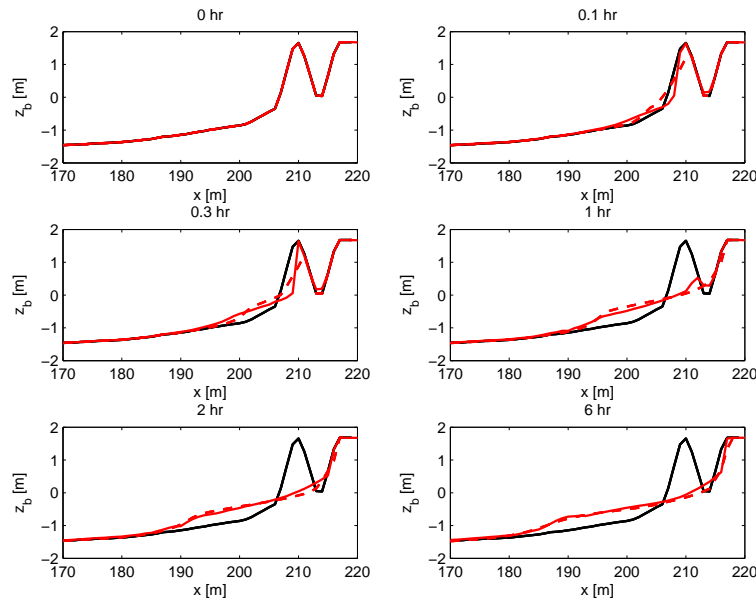
Figure 4.42: *Deltaflume 2006 test T04. Measured (drawn lines) and modelled (dashed lines) profile after 0, 0.1, 0.3, 1, 2 and 6 hours of wave action.*

Test averaged hydrodynamic parameters are compared in Figure 4.43 and reveal a good agreement between measured and simulated wave height transformation for both incident and long waves (upper left panel), the wave orbital flows for both incident and long waves (upper right panel) and the time and depth averaged return flow (lower right panel). It is remarked that the measured time and depth averaged flows just in front of the dune (at x = 205 m) should be interpreted with care since in the physical model only limited observation points over depth are available (Van Thiel de Vries et al., 2008).
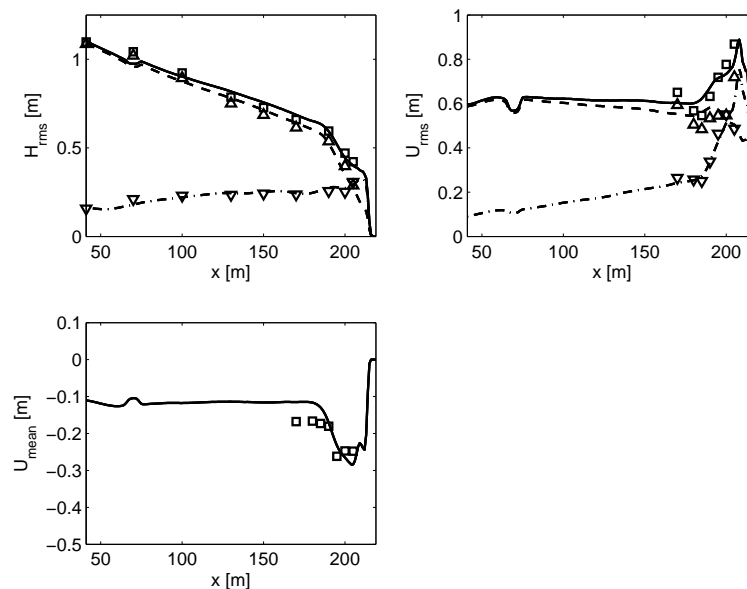
Figure 4.43: *Deltaflume 2006 test T04. Upper left panel: Measured (markers) and simulated (lines) LF (downward triangles / dashed-dotted line), HF (upward triangles / dashed line) and total (squares / solid line) wave height. Upper right panel: Measured (markers) and simulated (lines) orbital flow velocity. Lower left panel: Measured (squares) and simulated (solid line) time and depth averaged flow velocity.*

A more detailed analysis of the hydrodynamics is given in Figure 4.44 and Figure 4.45 which compare measured and simulated wave spectra and water surface elevation time series respectively. It is remarked that the measured wave spectra and water surface elevations include both the incident waves and long waves whereas the simulation results are associated with (wave group generated) long waves only. Considering the wave spectra first, it is seen that the measured wave spectra show a shift in variance towards lower frequencies as the waves propagate to the dune face. At the offshore model boundary most of the measured wave variance is associated with incident waves and the simulated long wave spectrum explains a marginal part of the measured wave spectrum. However, getting close to the dune face the incident wave variance reduces due to depth induced breaking whereas the long wave variance increases due to shoaling (Battjes, 2004). At the most shoreward pressure sensor (about 10 meter from the dune face) most of the measured wave variance is associated with long waves and is favorably simulated with the surfbeat model. The same phenomenon can be observed in Figure 4.45, which shows a reasonably good correlation ($R^2 = 0.32$) between measured and simulated water surface elevations close to the dune face (lower right panel). Also the time series show steep long wave fronts indicating breaking as was shown in the bichromatic wave case by Van Dongeren et al. (2007).
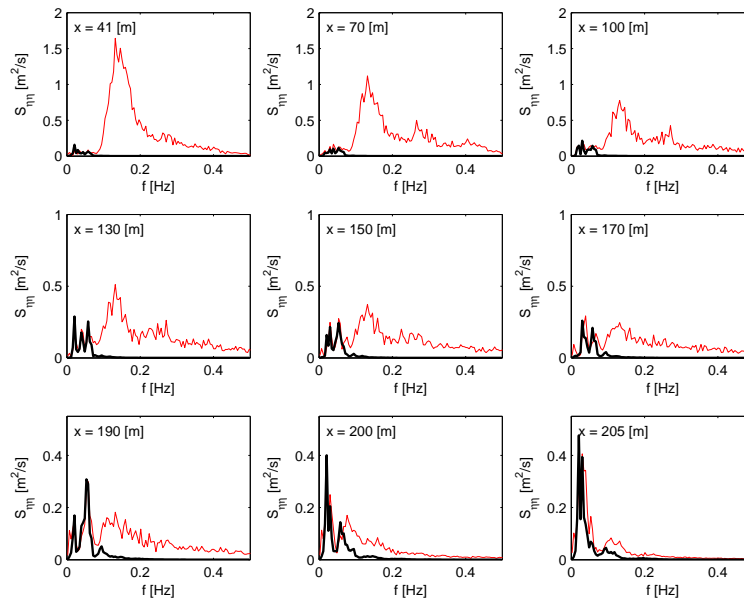
Figure 4.44: Measured wave spectra including both incident waves and long waves (thin line) compared with simulated long wave spectra (thick line) at different cross-shore positions (see upper left corner of sub-panels). Measured and simulated spectra are computed over the whole test duration.
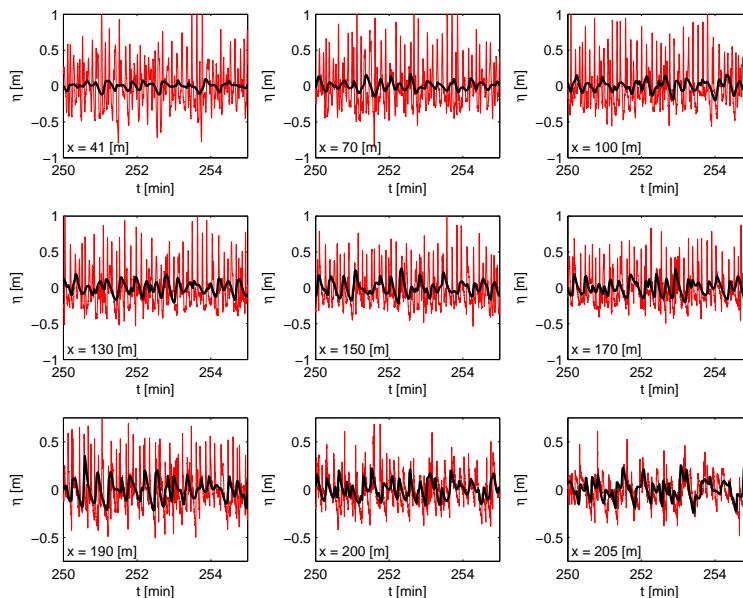
Figure 4.45: Measured water surface elevations including both incident and long waves (thin line) compared with simulated long wave water surface elevations (thick line) at different cross shore positions (see lower left corner of sub-panels) after 4.17 wave hours.

A comparison is given between the observed and modelled sediment concentrations and sediment transports (Figure 4.46) shows that the model clearly underestimates the concentration near the dune face, whereas the sediment transport is somewhat overestimated. The explanation for this could be found in an overestimation of the near dune time and depth averaged undertow which compensates for underestimating the near dune sediment concentrations. Throughout the flume, the sediment transport is too much seaward, as no onshore processes are included yet; work to improve this is currently underway but beyond the scope of this paper.
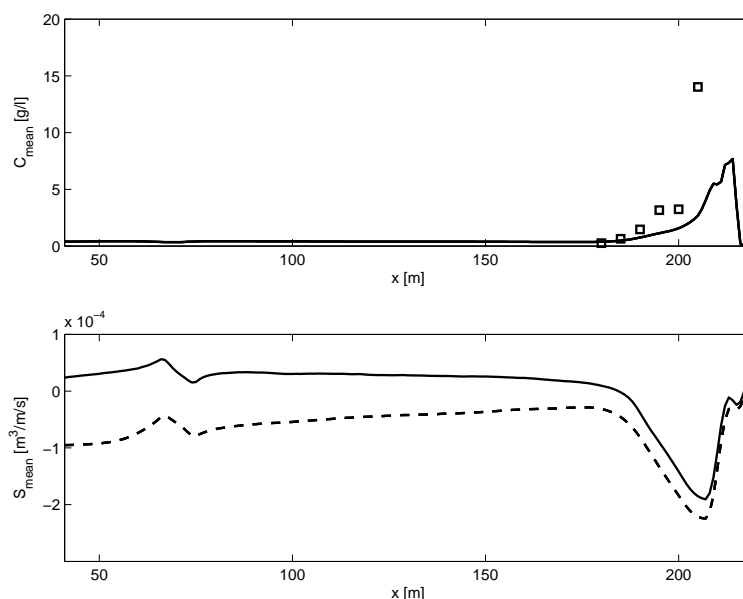
Figure 4.46: Deltaflume 2006. Test T04. Top panel: observed depth-averaged concentrations (squares) vs. model result. Bottom panel: total sediment transport observed from profile evolution (drawn line) vs. model result (dashed line).

Error statistics are collected in Table 4.13, and generally show a scatter index and relative bias of less than 10% for the hydrodynamic parameters and overall erosion volumes and dune retreat. An exception is the mean velocity, for which the higher scatter and bias can be attributed to the (neglected) 3D structure of this parameter. The horizontal distribution of the sedimentation and erosion at the end of the test shows a bit higher scatter, determined in part by the areas with small changes; the Brier Skill Score shows a value of 0.98.

Table 4.13: Error statistics Deltaflume 2006 T04

	R^2	Sci	Rel. bias	BSS
H_{rms}	0.88	0.04	-0.01	0.98
$H_{rms,HI}$	0.88	0.04	-0.01	0.99
$H_{rms,LO}$	0.82	0.07	0.01	0.82
U_{rms}	0.79	0.08	-0.00	0.77
$U_{rms,HI}$	-0.57	0.16	-0.02	-0.58
$U_{rms,LO}$	0.79	0.13	0.02	0.81
U_m	0.80	0.18	0.09	0.36
Sed/Ero	0.97	0.14	-0.07	0.98

Battjes, J.A., H.J. Bakkenes, T.T. Janssen and A.R. Van Dongeren (2004). *Shoaling of subharmonic gravity waves.* J. Geoph. Res. , 109, C2, C02009, 10.1029/2003JC001863.

Van Dongeren, A., J. Battjes, T. Janssen, J van Noorloos, K. Steenhauer, G. Steenbergen, and A. Reniers (2007), *Shoaling and shoreline dissipation of low-frequency waves*, J. Geophys. Res., 112, C02011, doi:10.1029/2006JC003701.

Van Gent, M.R.A., Van Thiel de Vries, J.S.M., Coeveld, E.M., De Vroeg, J.H. and Van de Graaff, J., 2008. *Large scale dune erosion tests to study the influence of the wave periods.* Coastal Engineering, 55(12): 1041-1051.

Van Thiel de Vries, J.S.M., M.R.A. van Gent, D.J.R. Walstra and A.J.H.M. Reniers, 2008. *Analysis of dune erosion processes in large-scale flume experiments*, Coastal Eng., 55(12).

4.17 Zwin T01

Contact: Dano Roelvink <d.roelvink@unesco-ihe.org>

Having examined two-dimensional hydrodynamics, we move to 2D morphodynamics. The next test carried out is that on the Zwin breach growth experiment, as reported by Visser (1998). In the mouth of the Zwin, a tidal inlet located at the border between the Netherlands and Belgium, an artificial dam was constructed with a crest height of 3.3 m +N.A.P. (Dutch datum, approx. MSL), crest width 8 m, inner slope 1:3 outer slope 1:1.6 and length 250 m. An initial depression of 0.8 m was made in the middle of the dam having a width of 1 m and a side slope of 1:1.6 to ensure that the breach initiated at this location. The level of the surrounding sea bed was about 0.7 m + N.A.P. The mean tidal prism of the Zwin is about 350,000 m3. The polder area A_p as a function of the water level behind the dam is given by:

$$A_p = (170.000m)z_s - 100.000m^2, 0.6m < zs < 2.3m + NAP$$

$$A_p = (2.100.000m)z_s - 4.540.000m^2, zs > 2.3m + NAP$$

At t = 0, about 10 minutes prior to high water, the water level at the seaside was NAP + 2.72 m. At t = 10 minutes a water level of 2.75 m + N.A.P. was reached. For the remainder

of the test, which had a total duration of 1 hour, the water level marginally decreased. After 1 the breach growth became nil, as the water level of the polder area behind the breached equaled the sea level. The wave height near the dam was negligible during the experiment. The wind speed was about 2 m/s.

Until t = 6.5 minutes the breach depth grew whereas the breach width remained constant. At t = 6.5 minutes the original dike structure had nearly completely disappeared over the initial depression width of 1 m. Near t = 6.5 minutes the onset of lateral breach growth was observed. The scour hole developed further down to a depth of 1.6 m -N.A.P. (4.9 m below the original dam crest level). The rate of lateral breach growth was about 2 cm/s. After approximately 40 minutes the process slowed down considerably and after approximately one hour the water levels at both sides were equal.

A schematized representation of the Zwin test was created in XBeach, with at the sea side a uniform bed level at 0.7 m +NAP, and inside the basin a prismatic profile with the deepest point at 0.7 m + NAP and sloping sides, such that the polder area as a function of the water level was in accordance with the equations above. The grid is non-equidistant with grid sizes gradually varying from 0.5 m near the breach to approx. 50 m far away from it. The median grain diameter D50 of the bed material was set to 0.3 mm in accordance with the prototype test conditions for the artificial dam. The applied critical slopes for avalanching are the same as in other tests and standard settings were applied for the transport formulations. Waves were negligible in the test and were set to zero. The model was run with a CFL of 0.5 and remained smooth and stable despite the steep slopes and supercritical flows.

4.17.1   Results

In Figure 4.47 a sequence of 3D images is shown depicting the various stages in the breaching process: the initial overflowing, the cutting back of the breach, the deepening and finally the widening of the breach. Qualitatively and quantitatively the results are in agreement with the experiment by Visser (1998), although details may be different due to the schematized initial bathymetry.
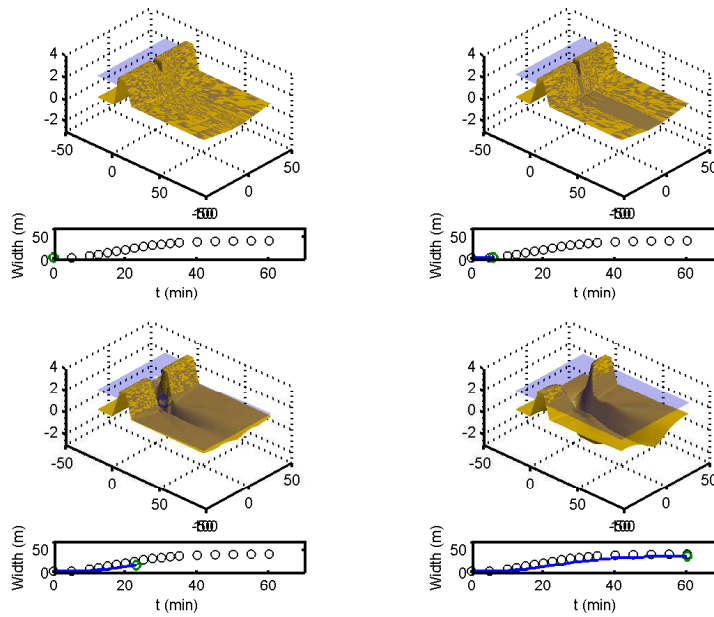
Figure 4.47: Sequence of 3D visualizations of the breach during the Zwin test (Visser, 1998). Bed level, water level and development of breach width (dots: observation, line: model).

In Figure 4.48 a comparison is given between measured and simulated water levels, flow velocities and development of the breach width in time. Observation point MS2 is 30 m upstream of the centre point of the breach and MS4 is 30 m downstream of it. In MS4 there was some ambiguity in the measured initial water level, which explains the initial discrepancy between measurements and simulations. The slight reduction in water level at the end of the measurement in MS2 is due to a rather narrow channel that was present in reality but not in the model, which causes higher velocities than in our model and a reduction of the mean water surface. In spite of these differences, the overall agreement for the development of the velocity in MS4 and for the breach widening is quite satisfactory. Measured and simulated flow velocities compare reasonably well in MS4.
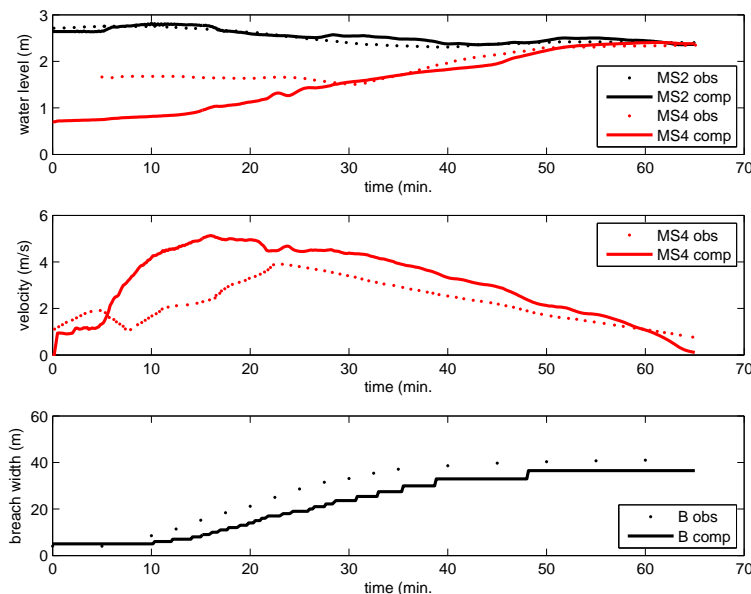
Figure 4.48: Zwin test (Visser, 1998). Observed (drawn lines) and modelled (dashed lines) time series of water level (top panel and velocity (middle panel). Bottom panel: development of breach width, observations (dots) vs. model (drawn line).

Visser, P.J. 1998. *Breach growth in sand dikes.* Ph.D.-thesis Delft University of Technology, the Netherlands.

4.18   River Outflow

Contact: Dano Roelvink <d.roelvink@unesco-ihe.org>

The river outflow case is meant to test the models for the combined effects of a river outflow and a steady wave-driven longshore current on the sediment transport and the morphological evolution. Though purely hypothetical, this case contains many salient features of real-life applications, such as longshore currents through open side-boundaries and exchange of water and sand through a gap in a closed boundary. Thus, the formulation of open boundary conditions is also tested here.

The initial topography consists of a plane beach (slope 1: 50), which is interrupted by a 75 m wide river mouth with a water outflow of 150 m3/s. The bottom contours are straight and parallel to the shoreline, except for a shallow submerged channel in line with the river.

The computational grid is rectangular, with 56 nodes in the x-direction (cross-shore) and 111 nodes in the y-direction (longshore), with a uniform grid spacing of 15 m. The waves are irregular and long-crested, with a root-mean-square height of 2m at a water depth of 13.5 m. The direction of wave incidence is 30 with respect to the shore-normal. The peak wave period is 8 s. The bed material is uniform sand of 250 am, with a settling velocity of 0.031 m/s.
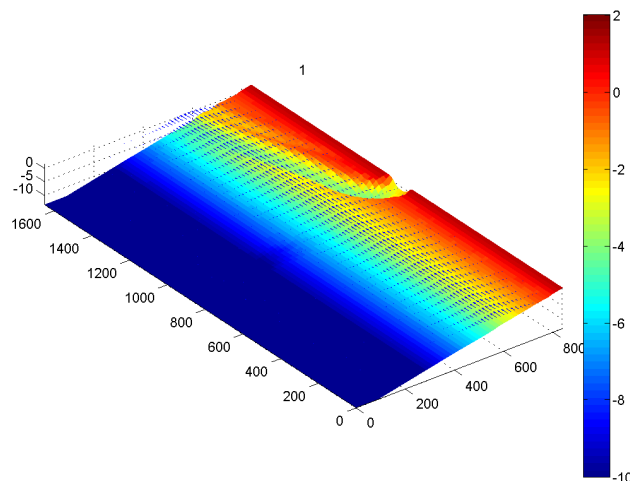
Figure 4.49

In this figure the bathymetry is shown after approx. 4 days; arrows indicate the sediment transport vectors. plotted for every cross-shore cell and every third longshore cell. When functioning correctly, we see a channel that has turned towards the north and striasght contour lines downstream of the channel.

4.19   Assateague Island

Contact: Bas Hoonhout <bas.hoonhout@deltares.nl>

Besides well-controlled laboratory cases, the model is also applied to the field. The first example concerns the morphodynamic response of sandy dunes to extreme storm impacts at Assateague Island, Maryland, USA, which was analyzed before by Jimnez et al (2006). Two consecutive northeasters attacked the barrier island during late January and early February, 1998. The bathymetry was measured using LIDAR in September 1997 and again February 9th and 10th, 1998 after the two storms had subsided.

Three types of dunes were identified by Jimnez et al (2006), shown in Figure 4.50. Profile A (upper left panel) is initially characterized by a steep faced dune, where the maximum run-up exceeded the dune crest height and the mildly sloped back of the dune. The morphological response is characterised by profile lowering, decrease of the beach face slope and landward barrier displacement, while retaining barrier width.

Profile type B is a double-peaked dune profile and has two different shapes. Profile B1 (upper right panel) is initially characterized by a primary and secondary dune, both of which are lower than the maximum run-up height and which are separated by a valley. Profile B2 (bottom left panel) initially has two peaks of which the seaward one is lower. The backside of the barrier of either type is therefore either characterized by a secondary dune line (profile B1) or a taller crest of the dune (profile B2) which prevents the eroded sand from being transported to the backside of the dune. The main morphological response for these profile types is a decrease of the beach face slope, outer shoreline retreat and narrowing of the barrier.

The height of the dune crest of profile C (lower right panel) exceeds the maximum run-up height and so little overwash is observed. The morphological response of this type of profile is crest lowering due to slumping, decrease of the beach face slope and retreat of the outer shoreline. The width of the barrier is seen to decrease.

The storm impact of the two North Easters on Assateague Island were modelled with XBeach for the four profiles described by Jimnez et al. (2006). The profiles were extended with a shallow foreshore and a 1:100 slope in seaward direction till a water depth of 9 m below NAVD88. As XBeach has not been shown to accurately simulate morphological change during very long storm durations, the simulations were run for a total of 20 hours. The measured wave and surge conditions were parameterized for each storm by a constant surge level and a constant wave spectrum (Pierson-Moskowitz) (see Table 4.14). This approach assumes that two 72 hour storms with varying surge and wave conditions can be approximated by two 10 hour simulations with constant maximum surge and wave conditions following a similar approach as Vellinga (1986). This approach also facilitates further sensitivity studies into the effect of varying hydraulic forcing conditions. The calculation grid size varies from 18 m at the offshore boundary to 2 m on the islands. A morphological acceleration factor of 5 is applied. The final simulated bed profiles are shown in Figure 4.50.

Table 4.14: *Hydrodynamic boundary conditions XBeach simulations*

	Storm 1	Storm 2
Surge level [m +NAVD]	0.8	1.0
H_s [m]	4.1	3.9
T_p [s]	8.5	8.5
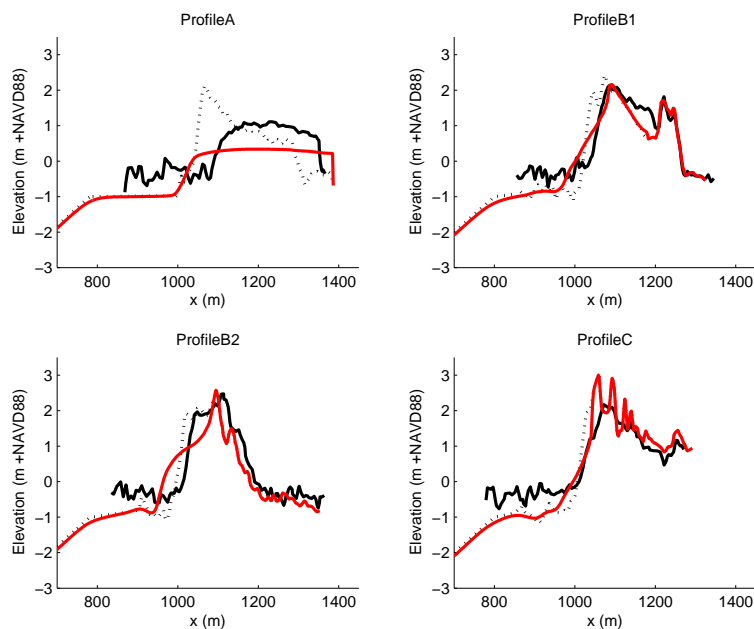
Figure 4.50: *Pre-storm profiles (black dotted line), measured post-storm profiles (black solid line) and modelled post-storm profiles (red solid line). Upper left panel: profile A. Upper right panel: profile B1. Lower left panel: profile B2. Lower right panel: profile C. The seaward side is on the left in all panels. Note that the measured post-storm profiles contain only the sea surface and emerged topography and no submerged topography.*

The profile changes calculated by XBeach are largely consistent with the description of dune

evolution given by Jimnez et al (2006). Jimnez et al observed that profile A became flatter, with large quantities of eroded sediment deposited on the back side of the barrier island, due to the consistent wave over-topping. The model replicates this behaviour, except that the island is lowered more than in the measurements and that the seaward face of the island does not roll back as it does in the measurements.

The observed response of profile B1 was dune face retreat, overwash deposition in the dune valley between the primary and secondary dunes and narrowing of the island, Jimnez et al (2006) also noted decrease of the beach face slope. It can be seen in Figure 4.50 that the morphological development of the island is well represented by the model. The simulated dune crest retreat corresponds closely to the measured retreat. Overwash takes place in the model and sediment is deposited in the valley between the primary and secondary dunes, although the magnitude of deposition is less than in the measurements.

The XBeach model of profile B2 shows a slope reduction on the seaward side and lowering of the seaward dune. The second dune crest retains its crest level as described in the work of Jimnez et al (2006). The beach slope decrease in the XBeach model is in line with the description given by Jimnez et al (2006), but differs from their measured profile. It is unclear why the measured profile shows almost no erosion of the beach face.

Jimenez et al. (2006) observed, in general, profile C to lower in height, the seaward dune slope to become smaller, and seaside retreat of the shoreline resulting in barrier narrowing. The XBeach model shows retreat of the upper dune face and a reduction of the seaward dune slope. The model over predicts the sedimentation at the base of the dune and under predicts the crest lowering.

Jimnez, J.A., Sallenger, A.H. and Fauver, L., 2006. *Sediment transport and barrier island changes during massive overwash events*, ICCE 2006, San Diego.

Vellinga, P., 1986. *Beach and dune erosion during storm surges.* PhD Thesis, Delft University of Technology.

4.20 NetCDF output

Contact: Bas Hoonhout <bas.hoonhout@deltares.nl>

The purpose of this test is to check the ability of the model to provide the output in NetCDF format. This test is a copy of the Carrier and Greenspan test presented in this report as well. The output of this test is provided in both the binary and the NetCDF format. The two formats are compared in the graph presented in Figure 4.51.
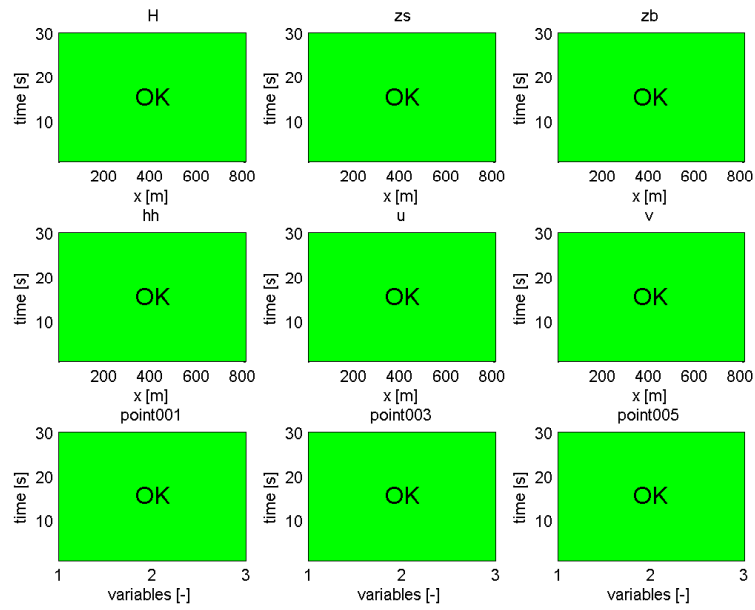
Figure 4.51: Comparison between Fortran and NetCDF output in dimensions x and time. Green dots represent a match, while red dots represent a mismatch.

Chapter 5

Default settings

This chapter contains a comparison of most of the figures and tables that can also be found in the previous chapter with the figures and tables that are based on the model results obtained when using the default settings of the XBeach model. These results give an indication for what kind of cases the default settings of the XBeach model are sufficient and for what kind of cases adjustments of the default settings are needed. The figures and tables resulting from the default settings are shown on the left side while the original figures and tables are shown on the right side.

5.1   Carrier and Greenspan
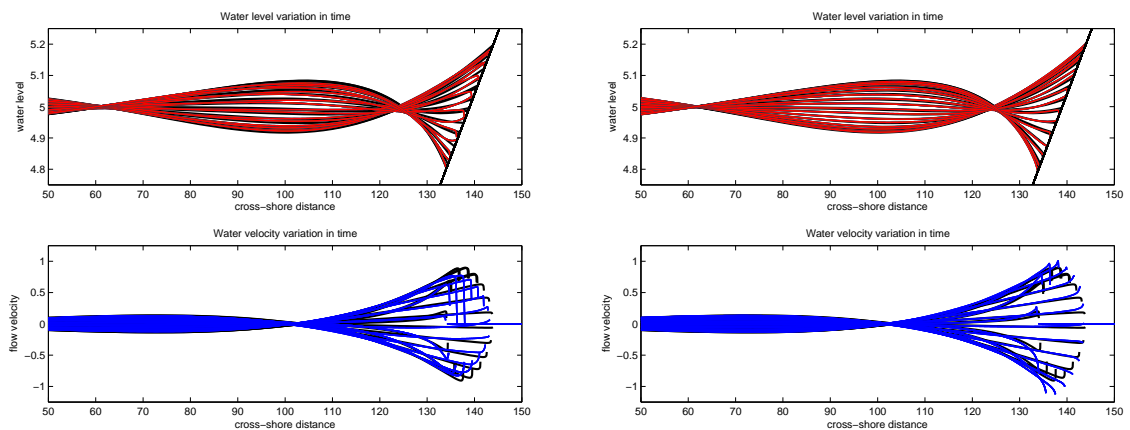
Figure 5.1

5.2 Long wave propagation
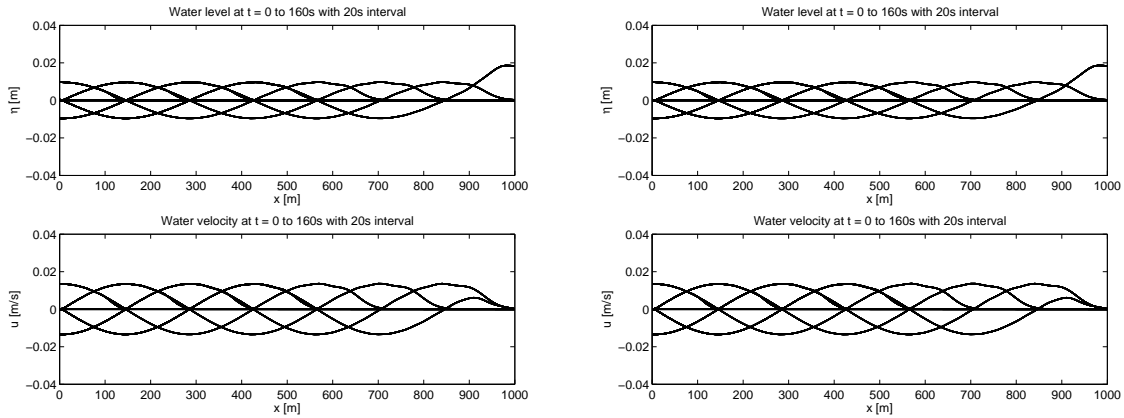
Figure 5.2
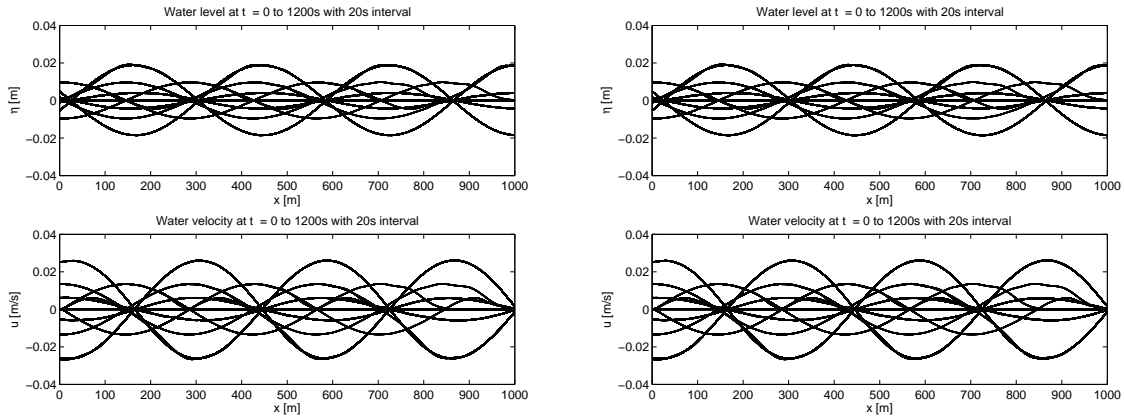
Figure 5.3

5.3 Boers 1C
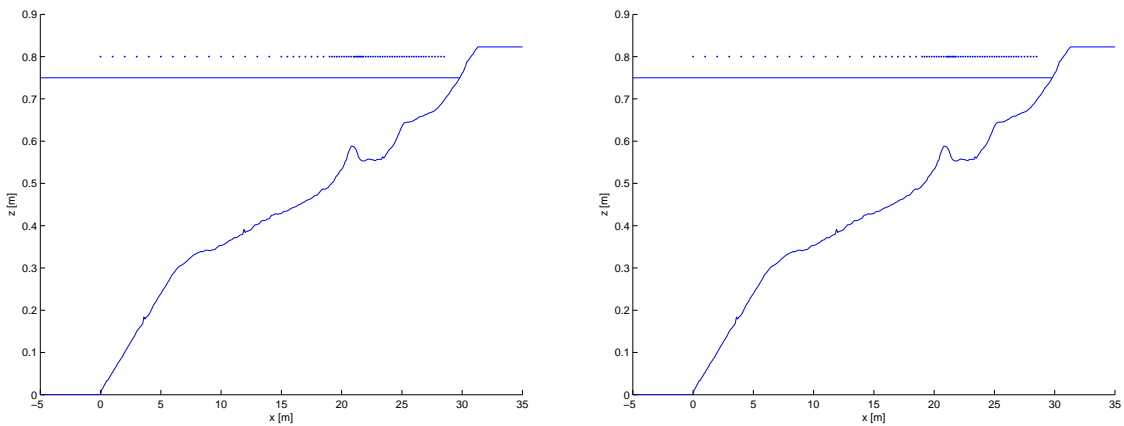
Figure 5.4
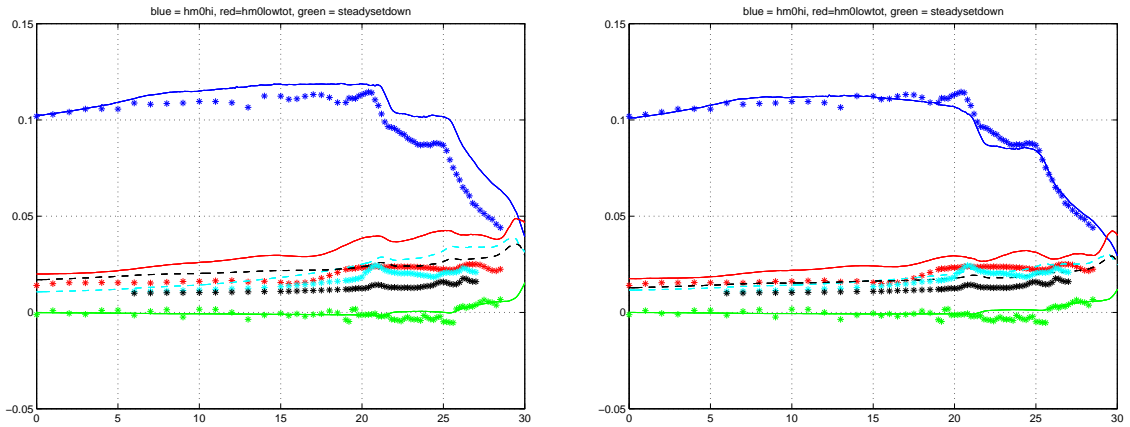
Figure 5.5

5.4   Zelt case 1
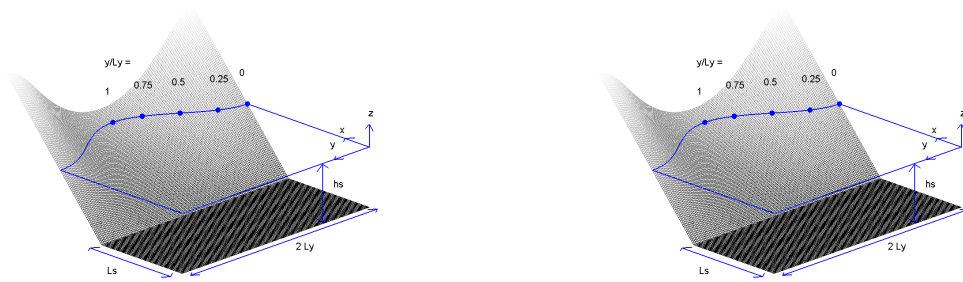
Figure 5.6
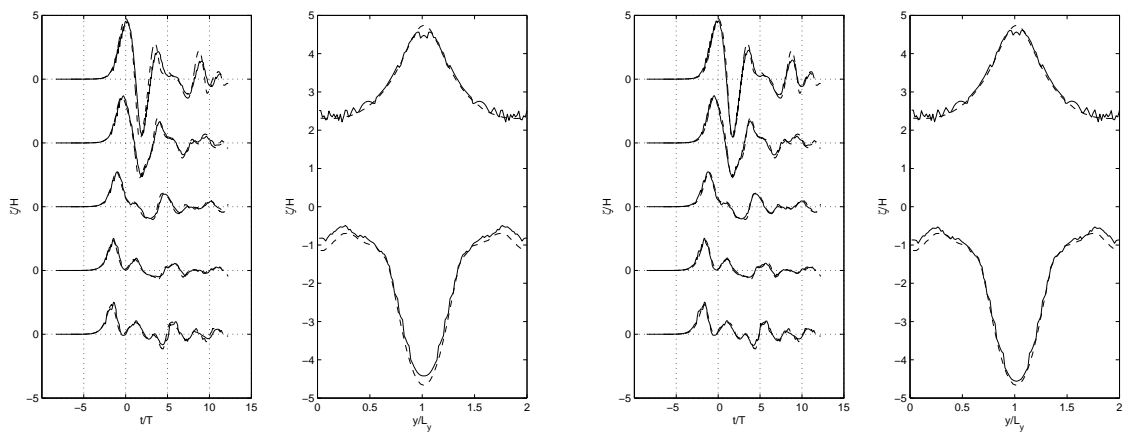
Figure 5.7

Table 5.1: Error statistics Zelt Case 1

	R^2	Sci	Rel. bias	BSS		R^2	Sci	Rel. bias	BSS
Timeseries (min)	0.04	0.17	-0.14	-5.03 Timeseries (min)	0.07	0.16	-0.15	-5.09
Timeseries (max)	0.98	2.23	0.03	0.97 Timeseries (max)	0.99	2.24	0.03	0.97
Max. runup	0.98	0.03	0.01	0.99 Max. runup	0.98	0.03	0.02	0.99

5.5 Delilah
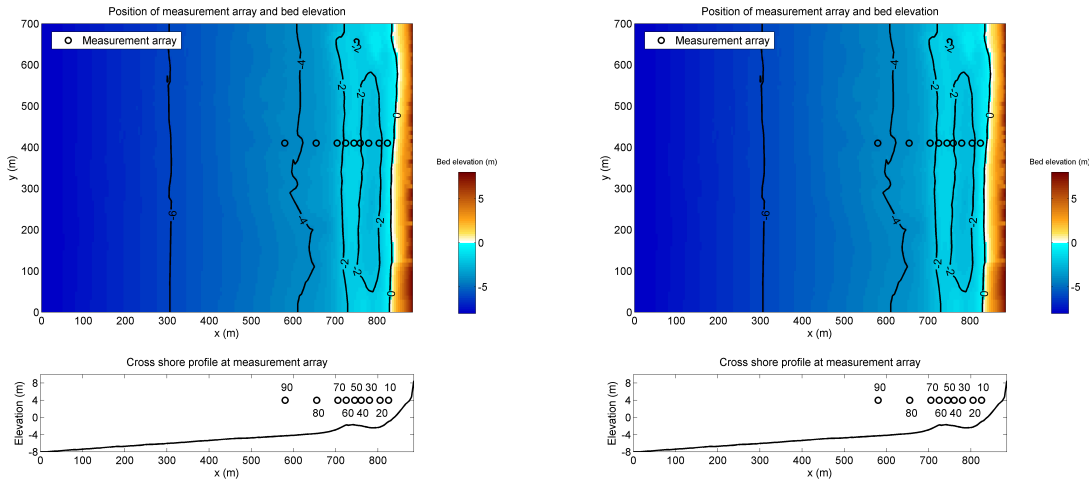
Figure 5.8: DELILAH field experiment 1990. Top panel: Plan view of the model location and measurement gauge array (circles). Bottom panel: Cross shore profile at the location of the measurement gauge array (circles) and measurement gauge names.
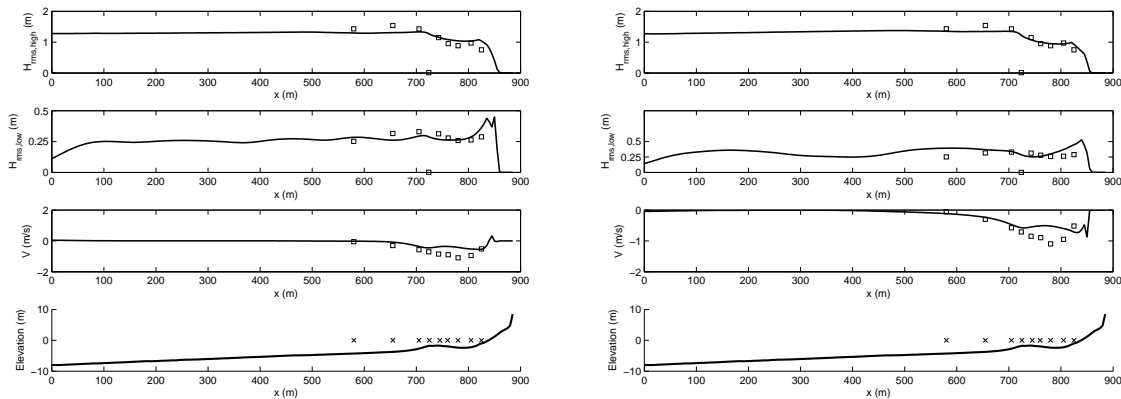
Figure 5.9: DELILAH field experiment 1990. First panel: Time-averaged measured (squares) and modelled (line) RMS-wave height of the short waves. Second panel: Time-averaged measured (squares) and modeled (line) RMS-wave height of the infragravity waves. Third panel: Time-averaged measured (squares) and modeled (line) longshore velocity. Fourth panel: Cross shore profile at the location of the measurement gauge array with the positions of the gauges (crosses).

Table 5.2: Error statistics Delilah

	R^2	Sci	Rel. bias	BSS		R^2	Sci	Rel. bias	BSS
$H_{rms,HI}$	0.85	0.14	0.02	0.66	$H_{rms,HI}$	0.85	0.09	-0.02	0.85
$H_{rms,LO}$	0.02	0.14	-0.01	-1.26	$H_{rms,LO}$	-0.14	0.31	0.19	-5.94
v	0.46	0.52	0.44	0.28	v	0.37	0.40	0.28	0.17
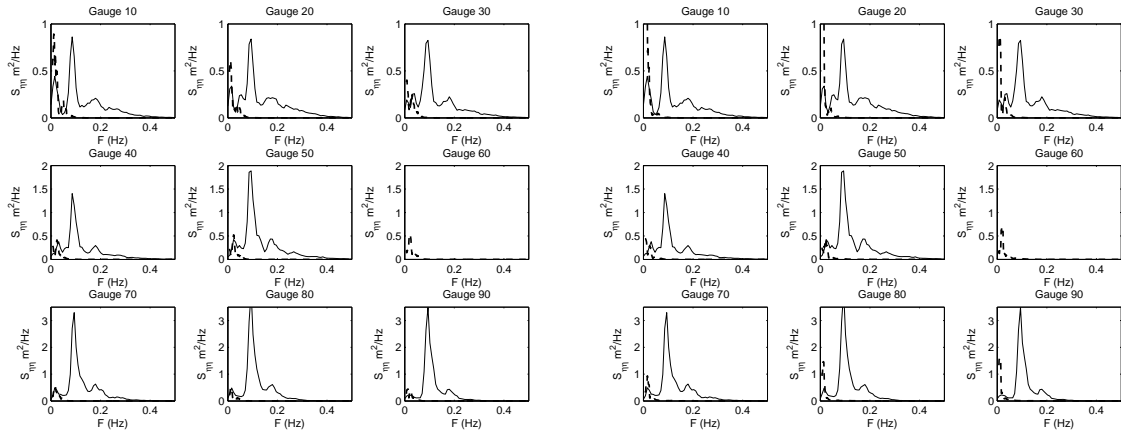
Figure 5.10: DELILAH field experiment 1990: Measured (solid line) and modelled (dashed line) surface elevation spectra for nine locations in the primary cross shore array. Gauge 90 is the most seaward.

5.6   Deltaflume M1263 part III test 1

Table 5.3: Brier skill scores (time)

| t [s]	BSS	t [s]	BSS
360	-0.78	360	0.71
1080	0.64	1080	0.88
3600	0.94	3600	0.87
10800	0.79	10800	0.82
21600	0.88	21600	0.87
36000	0.91	36000	0.88
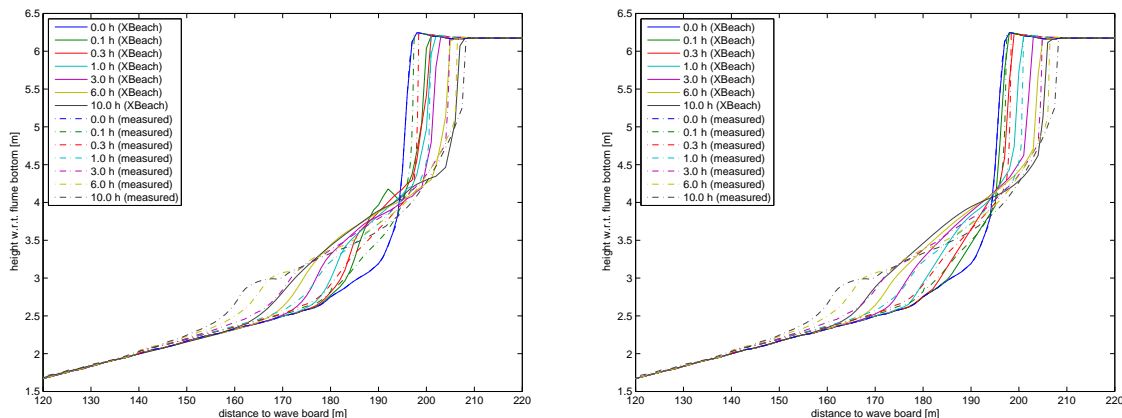
Figure 5.11: Comparison between measured and modelled profiles

5.7 Deltaflume M1263 part III test 2

Table 5.4: Brier skill scores (time)

t [s]	BSS		t [s]	BSS
360	-0.97		360	0.83
1080	0.30		1080	0.88
3600	0.89		3600	0.90
10800	0.91		10800	0.90
21600	0.94		21600	0.91
36000	0.95		36000	0.93
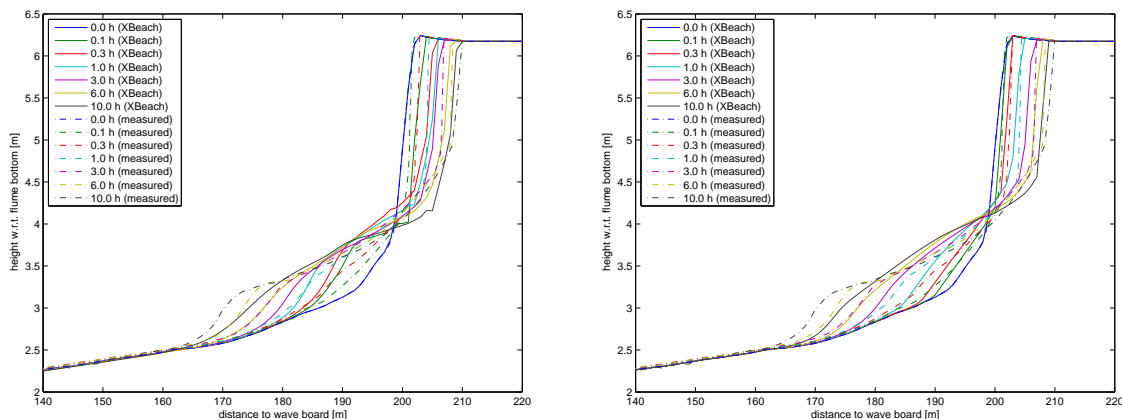
Figure 5.12: Comparison between measured and modelled profiles

5.8 Deltaflume M1263 part III test 3

Table 5.5: Brier skill scores (time)

t [s]	BSS		t [s]	BSS
6480	0.72		6480	0.90
14400	0.46		14400	0.91
69480	0.54		69480	0.79
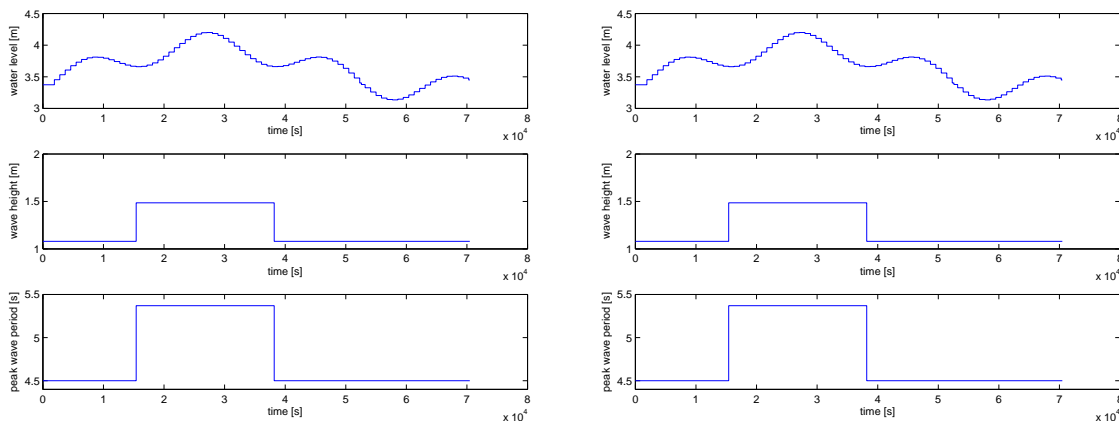
Figure 5.13: Hydraulic boundary conditions as function of time
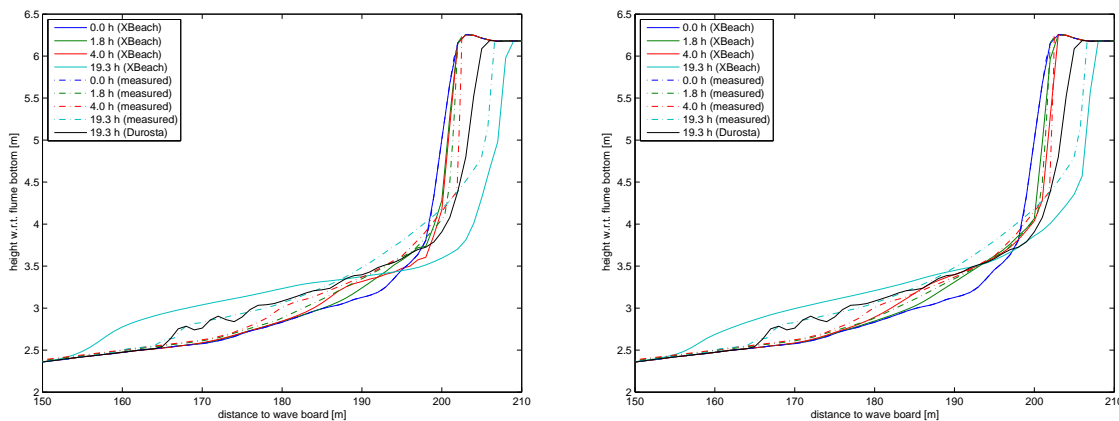
Figure 5.14: Comparison between measured and modelled profiles

5.9 Deltaflume M1263 part III test 4

Table 5.6: Brier skill scores (time)

t [s]	BSS		t [s]	BSS
18360	0.30		18360	0.76
61200	0.71		61200	0.80
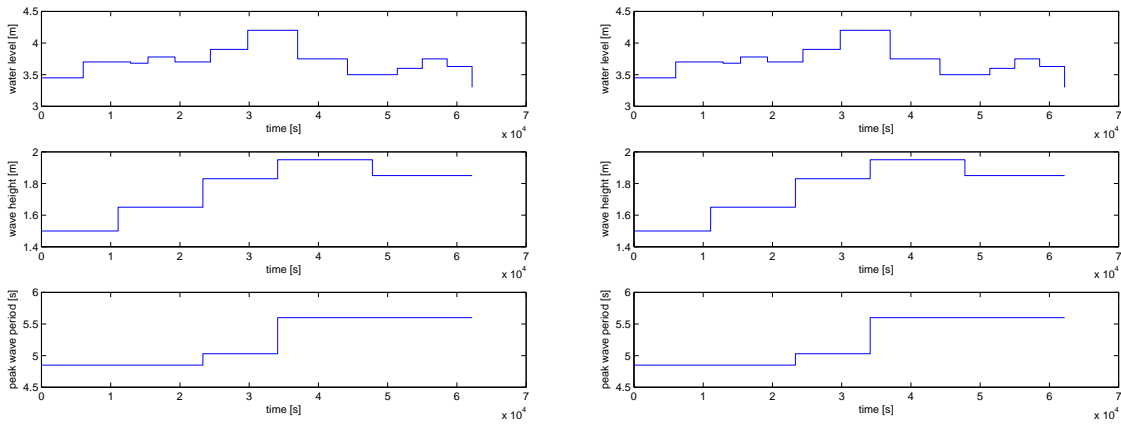
Figure 5.15: Hydraulic boundary conditions as function of time
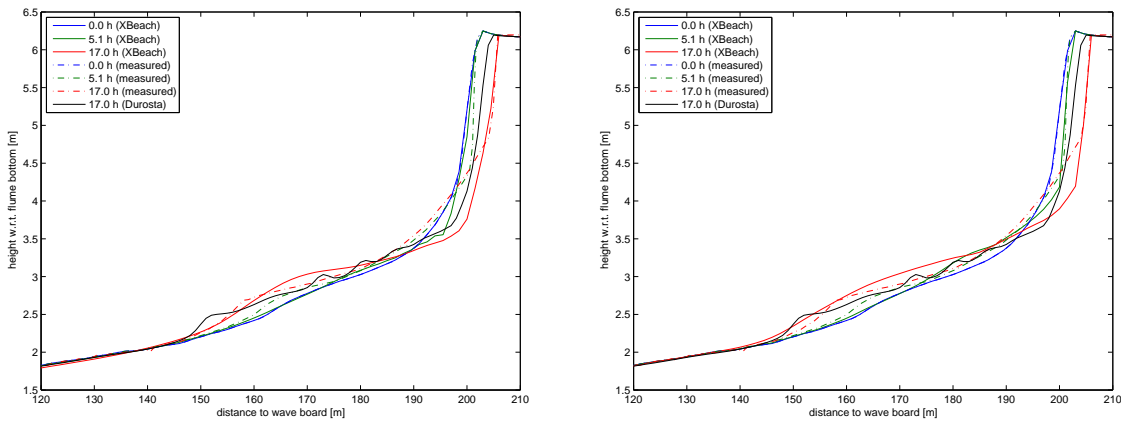
Figure 5.16: Comparison between measured and modelled profiles

5.10   Deltaflume M1263 part III test 5

Table 5.7: Brier skill scores (time)

t [s]	BSS
10800	0.95
21600	0.86

t [s]	BSS
10800	0.83
21600	0.97
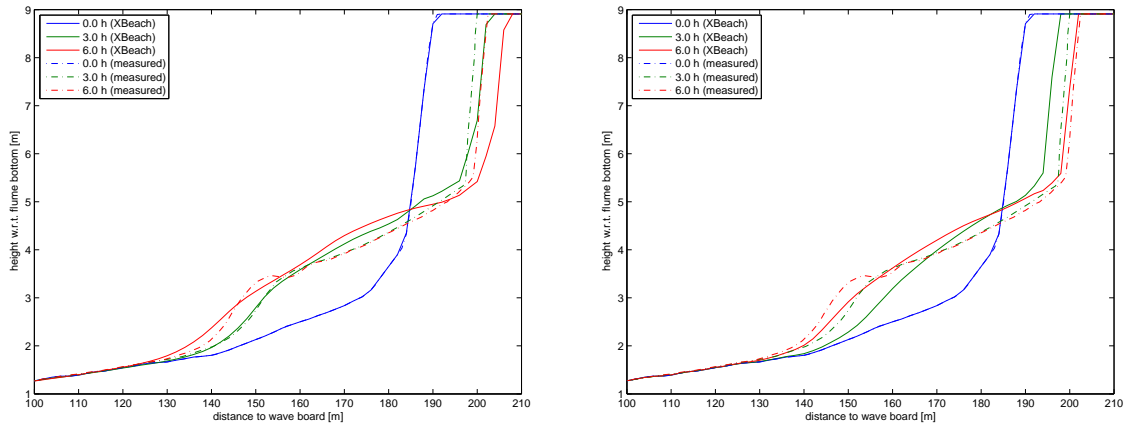
Figure 5.17: Comparison between measured and modelled profiles

5.11   DeltaflumeH298 T1

5.11.1   Results

Table 5.8

	R^2	SCI	Rel. Bias	BSS		R^2	SCI	Rel. Bias	BSS
sedero	0.8621	0.5662	-0.1213	0.6910	sedero	0.8156	0.6131	-0.2111	0.6653
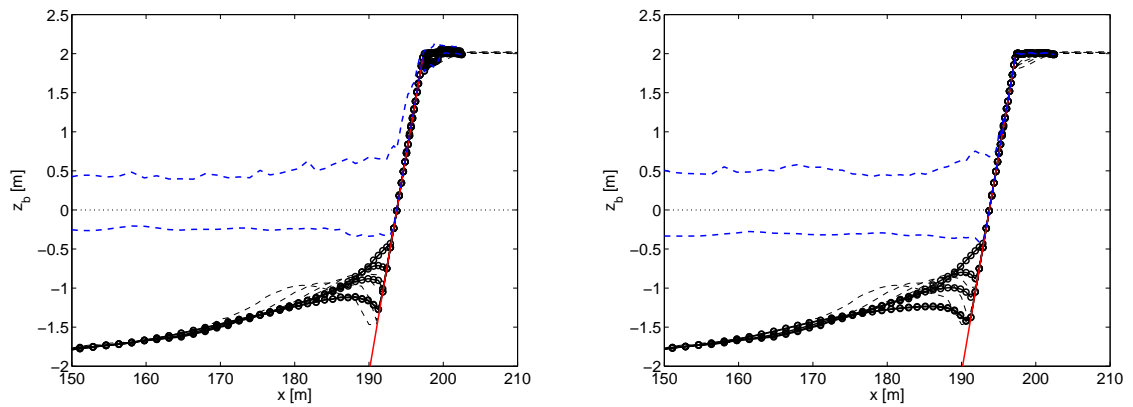
Figure 5.18
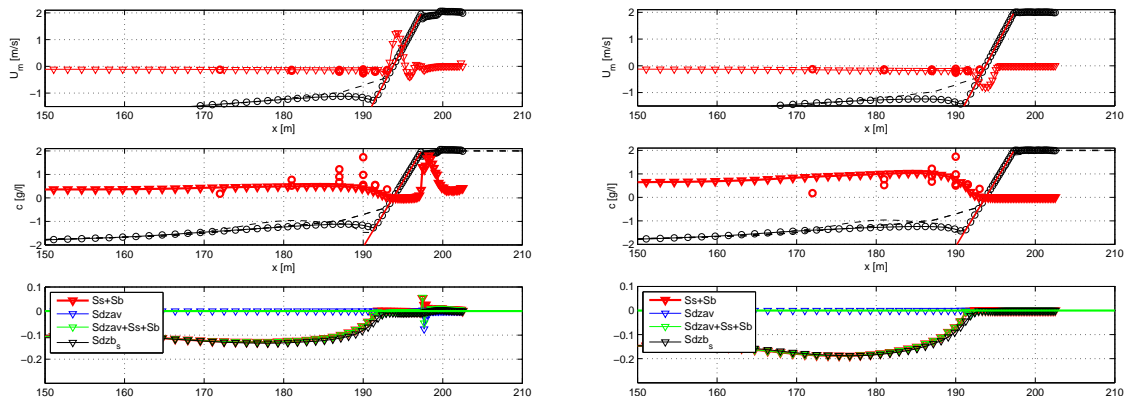
Figure 5.19

5.12 DeltaflumeH298 T3

5.12.1 Results

Table 5.9

	R^2	SCI	Rel. Bias	BSS		R^2	SCI	Rel. Bias	BSS
sedero	0.9547	0.8230	0.1508	0.3435	sedero	0.5211	0.8872	0.0208	0.2110
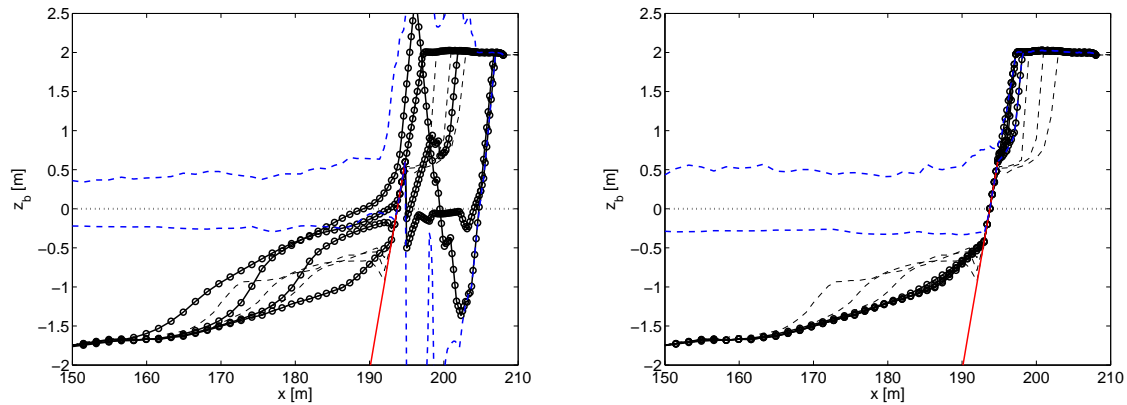
Figure 5.20
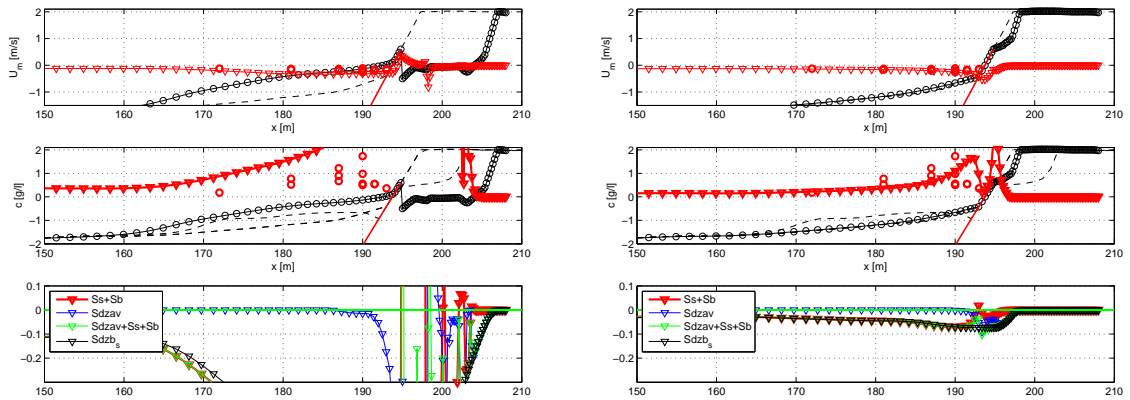
Figure 5.21

5.13   Deltaflume LIP 11D 2E
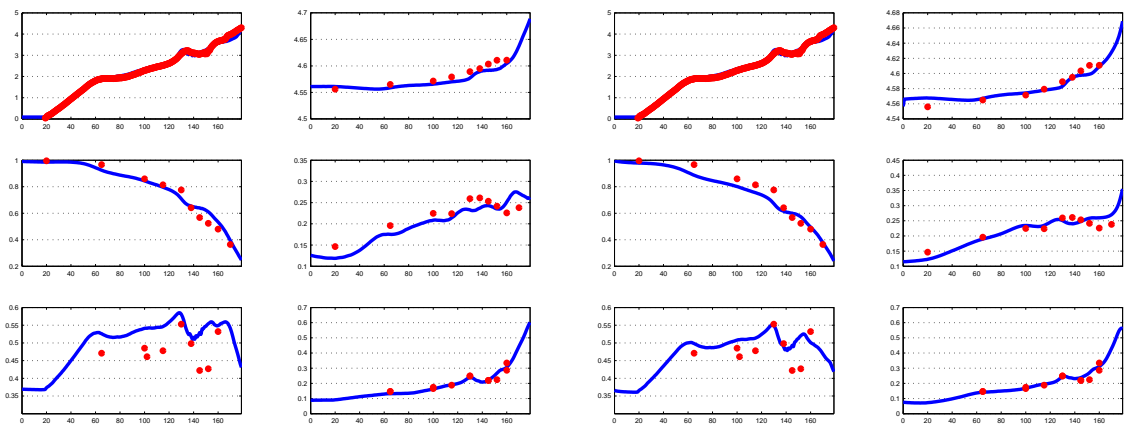
Figure 5.22: Computed and observed hydrodynamic parameters for test 2E of the LIP11D experiment. Top left: bed level and mean water level. Top right: measured (dots) and computed mean water level with first-order steering (drawn line) as function of the cross-shore distance. Middle left: same for HF wave height; middle right: same for LF wave height; bottom left: same for HF orbital velocity; bottom right: same for LF orbital velocity.
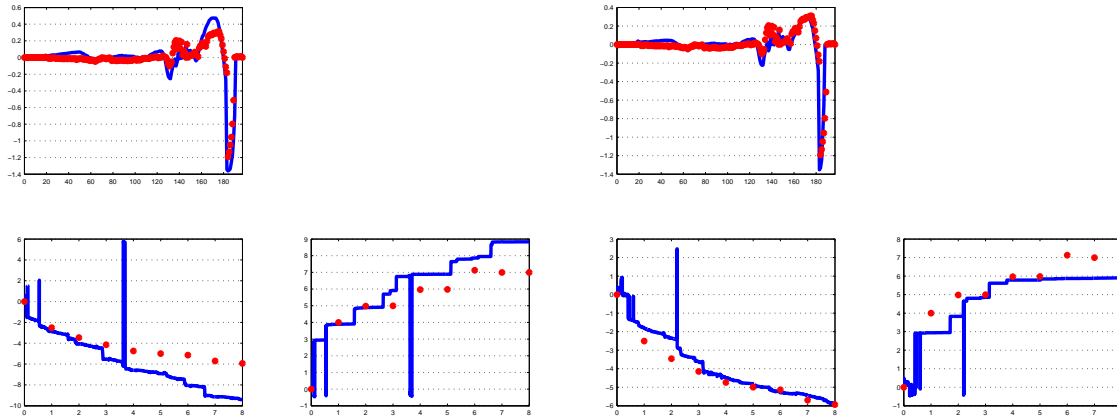
Figure 5.23: Computed and observed sedimentation and erosion after 8 hrs (top panel); erosion volume as function of time (bottom left) and dune retreat (bottom right) as function of time for test 2E of the LIP11D experiment, (Arcilla et al, 1993). All results with first-order steering.
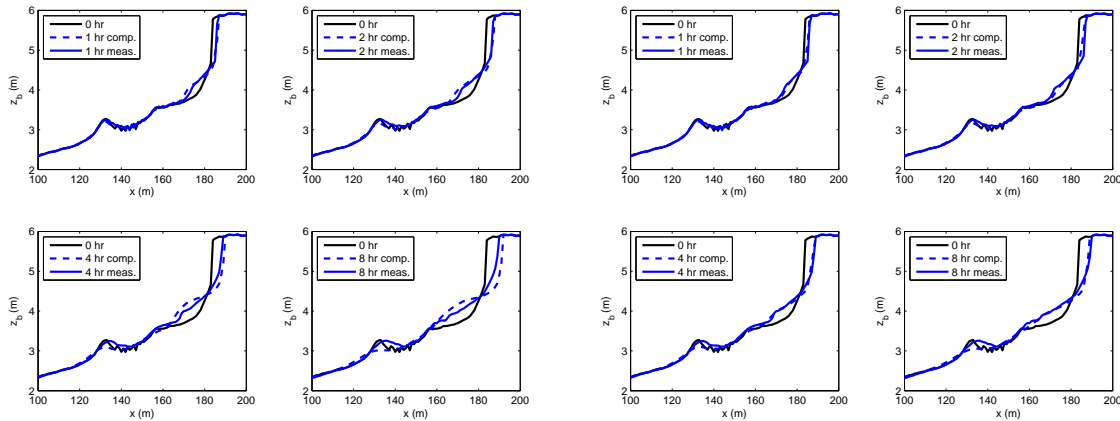
Figure 5.24: Measured and modelled bed level after 1, 2, 4 and 8 hours of wave action, for a water level of 4.56 m above the flume bottom.

Table 5.10: Error statistics Deltaflume LIP 11D 2E

	R^2	Sci	Rel. bias	BSS		R^2	Sci	Rel. bias	BSS
$SEDERO$	0.91	0.63	-0.15	0.63	$SEDERO$	0.80	0.63	-0.14	0.63
ETA	0.86	0.00	-0.00	0.91	ETA	0.86	0.00	-0.00	0.89
VOL	0.86	0.49	-0.42	-0.08	VOL	0.86	0.11	0.08	0.88
R	0.85	0.19	0.15	0.59	R	0.79	0.15	-0.13	0.81
$URMS$	0.42	0.15	0.13	0.22	$URMS$	0.37	0.10	0.06	0.17
$URMS_{LO}$	0.87	0.08	-0.01	0.90	$URMS_{LO}$	0.87	0.08	0.03	0.89

5.14   Deltaflume 2006 T01

5.14.1   Results
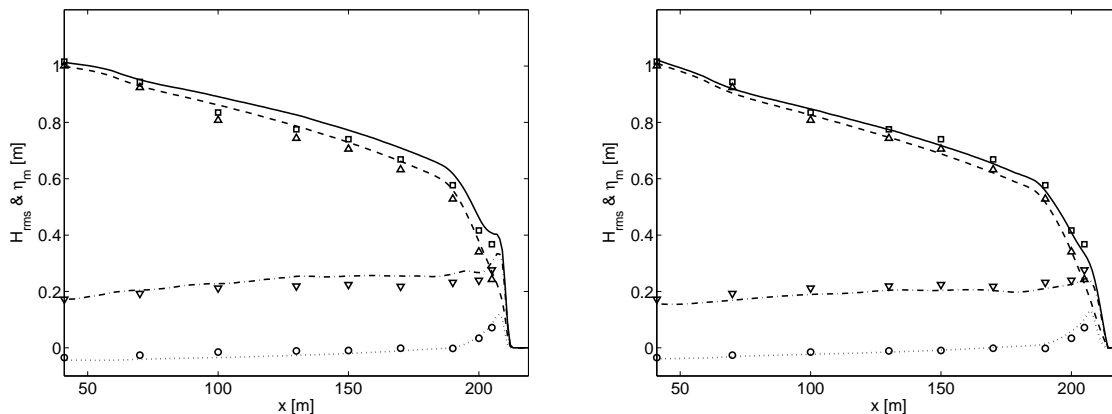
Figure 5.25: Simulated wave setup (dotted line) and transformation of the total (solid line), short (dashed line) and long (dashed-dotted line) wave height compared with measurements of the wave setup (circles) and the total (squares), short (upward triangles) and long (downward triangles) wave height.
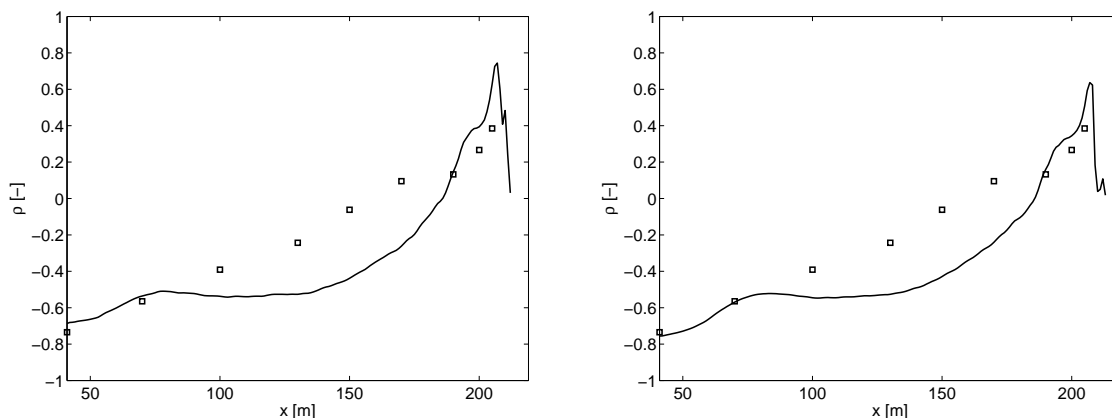

Figure 5.26: Simulated correlation ρ between the short wave variance and long wave water surface elevations (solid line) compared with the measured correlation (squares) as function of cross-shore position.
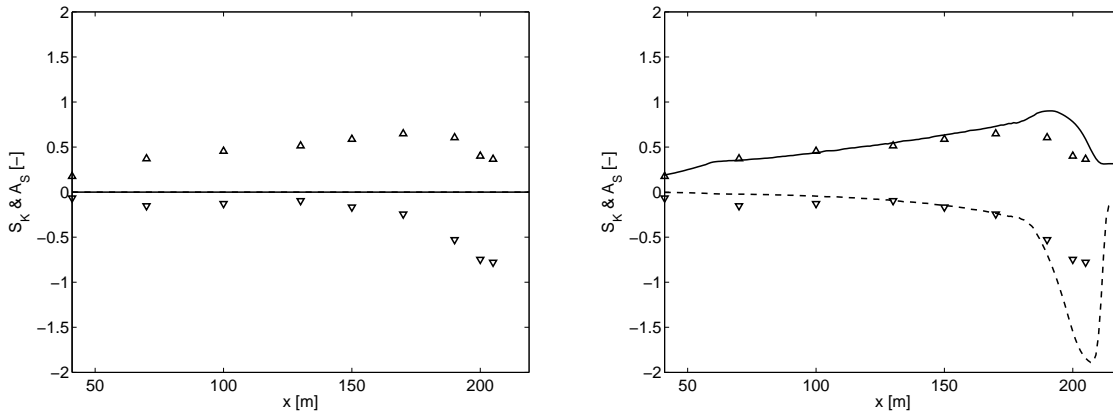
Figure 5.27: *Simulated wave skewness S_K (solid line) and asymmetry A_S (dashed line) compared with measured skewness (upward triangles) and asymmetry (downward triangles) as function of cross-shore position.*
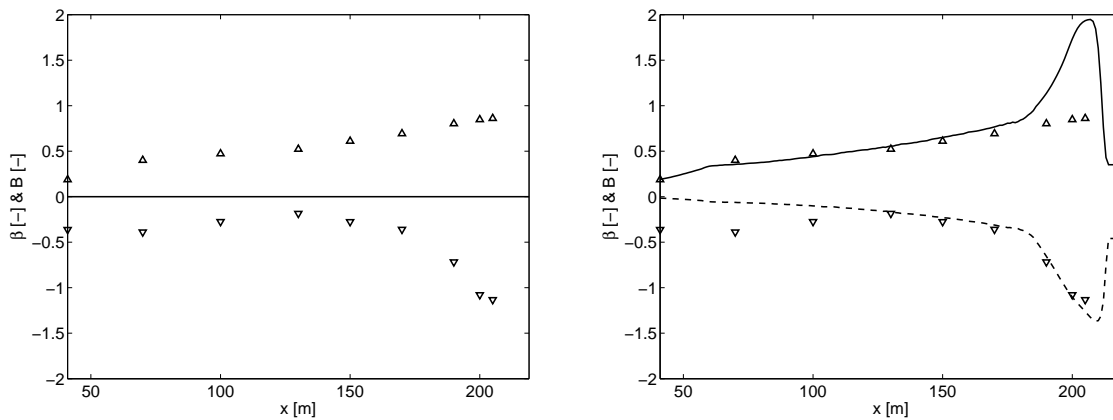
Figure 5.28: *Simulated wave nonlinearity B (solid line) and phase β (dashed line) compared with measured nonlinearity (upward triangles) and phase (down-ward triangles) as function of cross-shore position.*
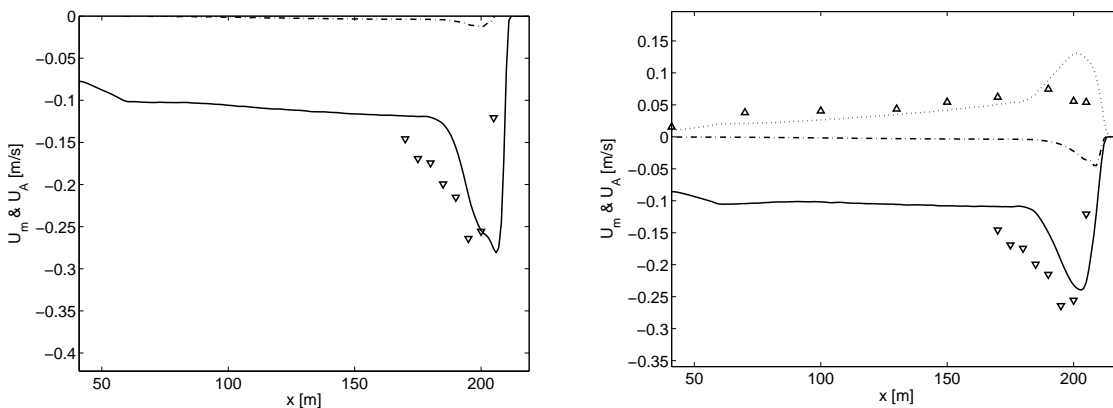
Figure 5.29: *Simulated test and depth averaged flow Um due to short and long waves (solid line) and long waves only (dashed line) as function of the cross-shore position. The dotted line corresponds to the wave averaged sediment advection velocity u_A due to nonlinear short waves. Markers correspond to measured undertow flow velocities due to short and long waves (downward triangles) and the sediment advection velocity due to nonlinear waves (upward triangles).*
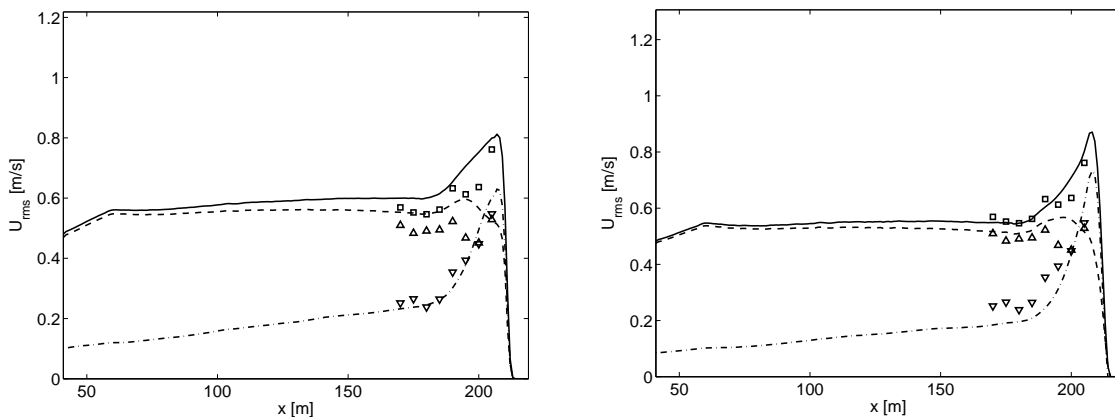
Figure 5.30: Transformation of the simulated total (solid line), short (dashed line) and long (dashed-dotted line) wave orbital flow compared with the meas-ured total (squares), short (upward triangles) and long (downward triangles) wave orbital flow as function of cross-shore position.
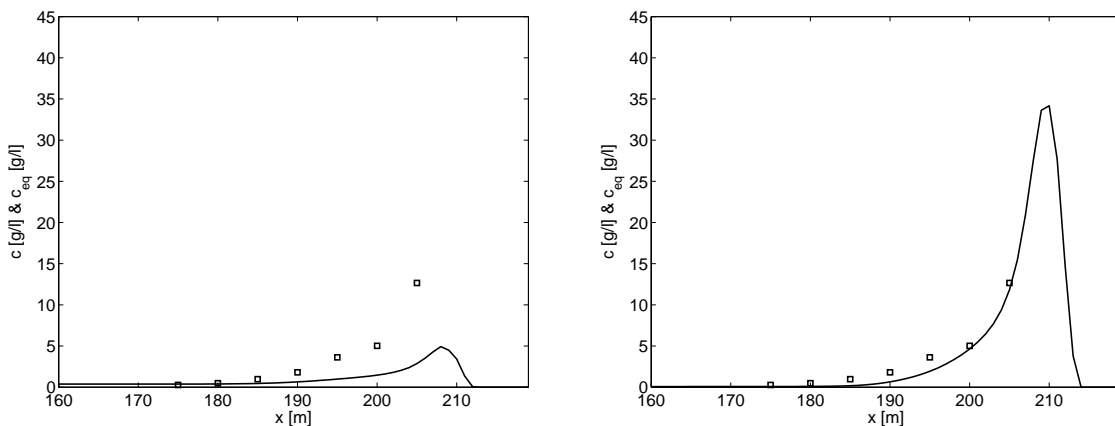

Figure 5.31: Simulated test and depth averaged sediment concentration (solid line) compared with the sediment concentrations obtained from suction tubes (squares).
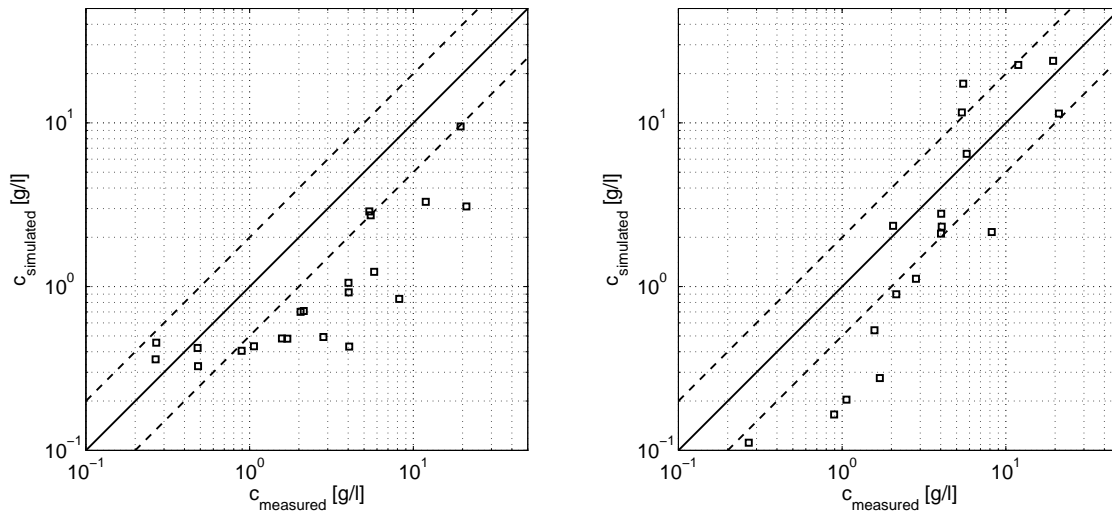
Figure 5.32: Scatter plot of simulated time and depth averaged sediment concentrations compared with vertically integrated suction tube measurements. The solid line corresponds to a perfect match between measurements and simulations whereas simulation results between the dashed lines are within a factor two with the measurements.
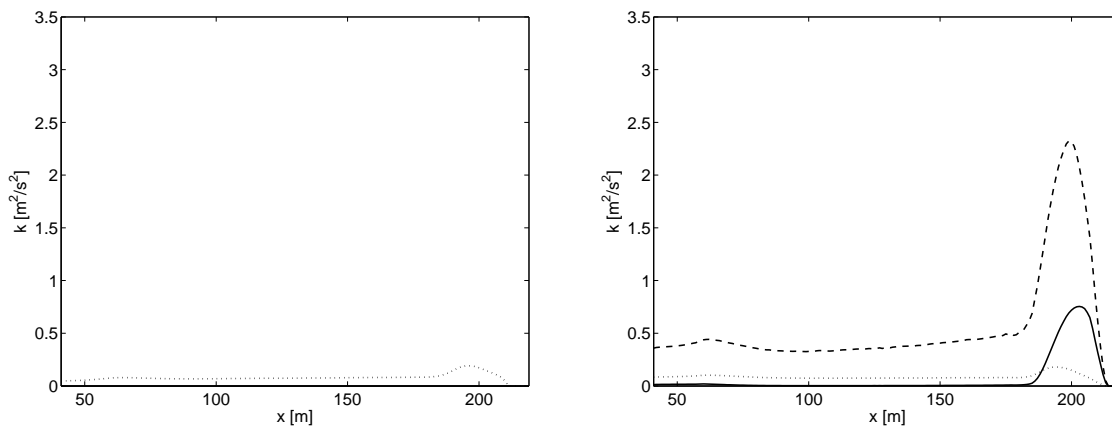

Figure 5.33: Simulated wave averaged turbulence energy (dotted line), bore averaged turbulence energy (dashed line) and near-bed bore averaged turbulence energy (solid line) as function of cross-shore position.
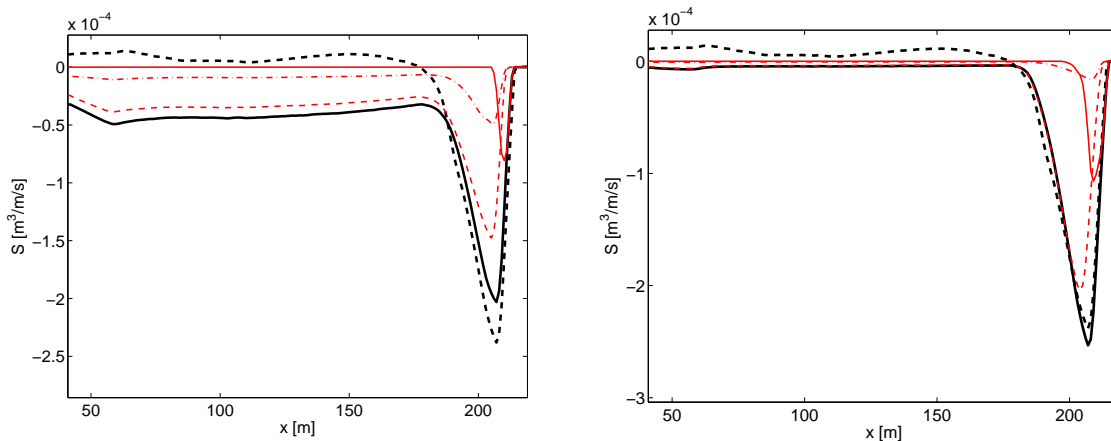
Figure 5.34: Measured (thick dashed line) and simulated (thick solid line) test av-eraged sediment transport from bed level changes. The simulated transport is separated in a transport due to avalanching (dashed-dotted line) and a transport related to the hydrody-namics (dotted line).
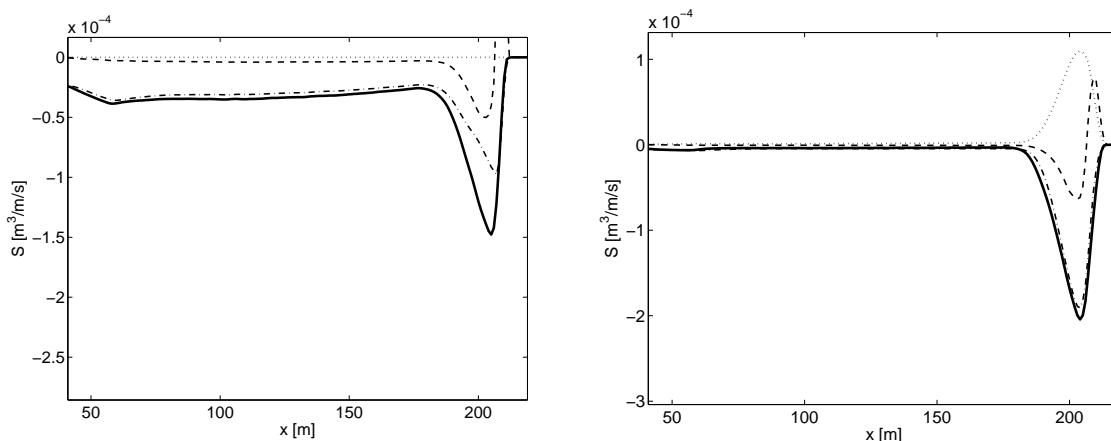

Figure 5.35: Simulated test averaged sediment transport related to the hydrodynamics (solid line) divided into wave asymmetry related sediment transport (dotted line), long wave related sediment transport (dashed line) and sediment transport associated with the short wave undertow (dashed-dotted line).
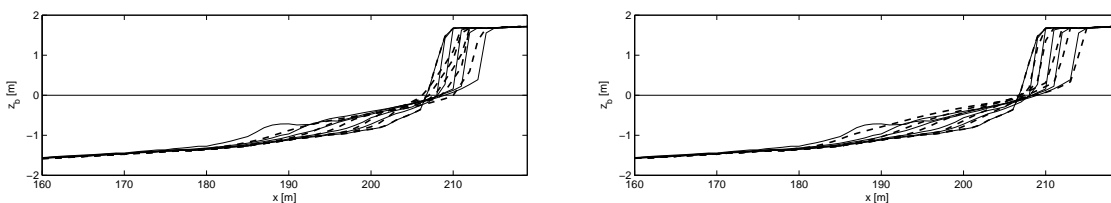

Figure 5.36: Simulated profile evolution (dashed lines) compared with measured profile evolu-tion (solid lines) after t = 0.0, 0.1, 0.3, 1.0, 2.04 and 6.0 hours.
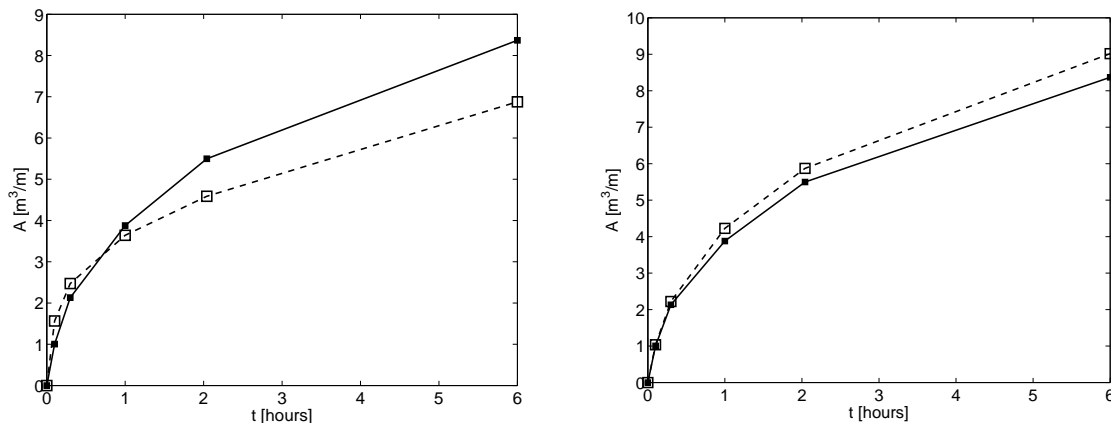
Figure 5.37: Simulated dune erosion volume above still water level (dashed line with open squares) compared with the measured dune erosion volume (solid lines with closed squares) as function of time.

Table 5.11

	R^2	SCI	Rel. Bias	BSS		R^2	SCI	Rel. Bias	BSS
$H_{rms,hf}$	0.9978	0.0461	0.0393	0.9950	$H_{rms,hf}$	0.9987	0.0193	-0.0070	0.9972
$H_{rms,lf}$	0.9722	0.1199	0.1080	0.8224	$H_{rms,lf}$	0.9821	0.0927	-0.0893	0.9605
ρ	0.8860	0.5833	-0.2038	0.6663	ρ	0.9147	0.5319	-0.2717	0.7664
S_k	NaN	1.0000	-0.9562	0.0000	S_k	0.7559	0.3756	0.2408	0.0303
A_s	NaN	1.0000	0.7698	0.0000	A_s	0.9751	1.0740	-0.4556	-1.3220
β	NaN	NaN	NaN	NaN	β	0.9599	0.2820	0.1527	0.8050
B	NaN	1.0000	-0.9420	0.0000	B	0.8938	0.7510	0.4119	-2.4984
$U_{rms,hf}$	-0.4493	0.1542	0.1334	-1.4070	$U_{rms,hf}$	-0.4834	0.1114	0.0775	-1.5743
$U_{rms,lf}$	0.9787	0.0946	-0.0026	0.8930	$U_{rms,lf}$	0.9660	0.1914	-0.1294	0.7623
U_m	0.1991	0.3631	0.1001	-1.1554	U_m	0.3175	0.3422	0.1864	-0.4566
C_m	0.9967	0.9999	-0.7563	0.0002	C_m	0.9950	0.9997	-0.7562	0.0008
sedero	0.9524	0.3207	-0.0623	0.9010	sedero	0.9836	0.1894	-0.0182	0.9645
A	0.9986	0.1711	-0.0707	0.9128	A	0.9999	0.0756	0.0607	0.9927

5.15   T01 Zebra
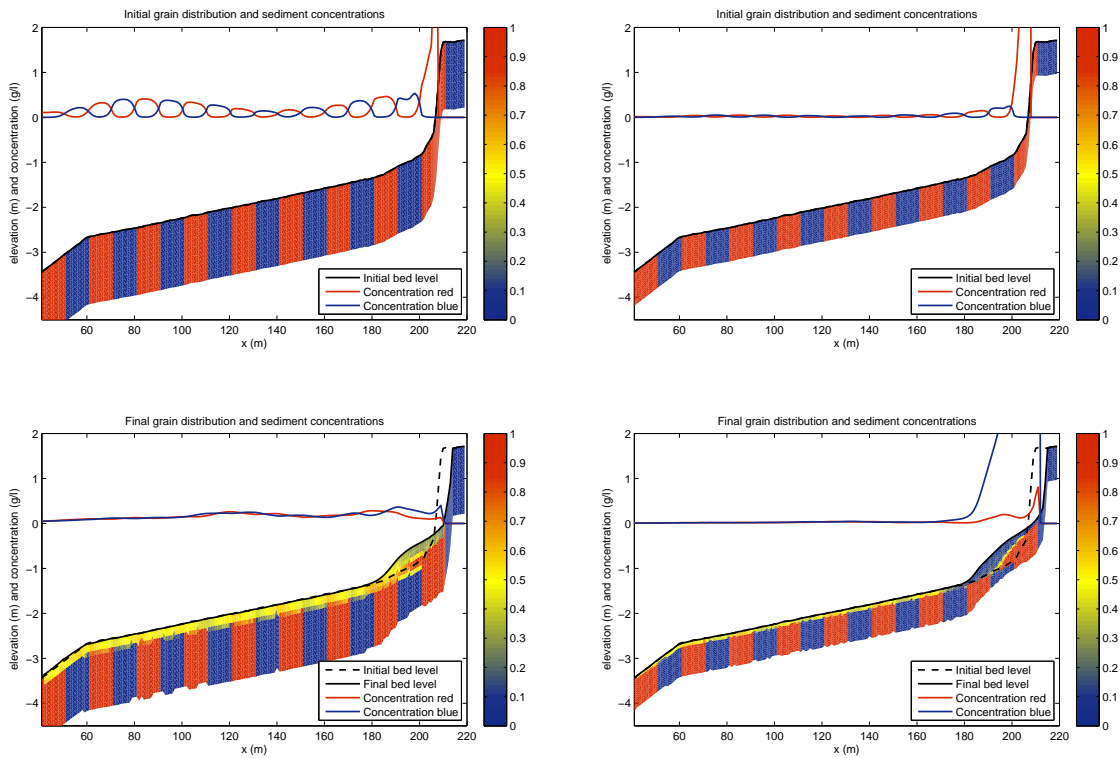
Figure 5.38
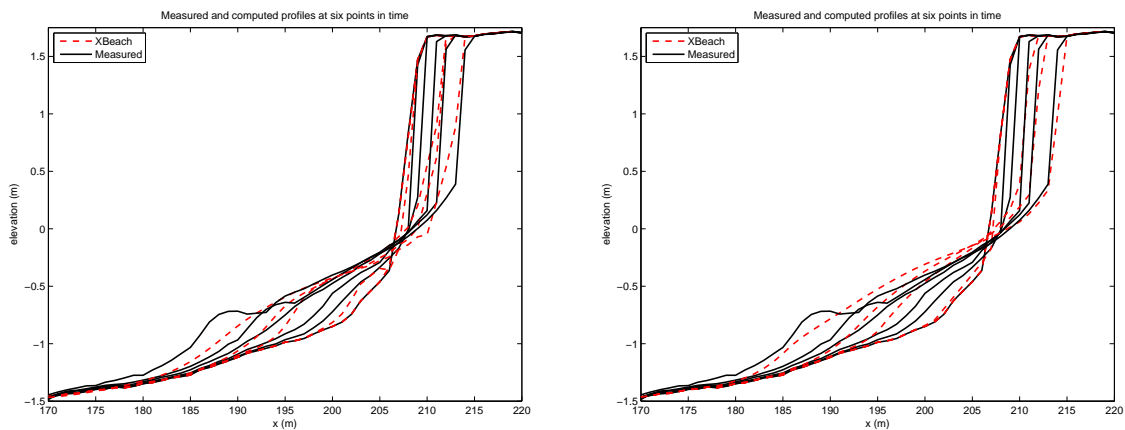
Figure 5.39

Table 5.12

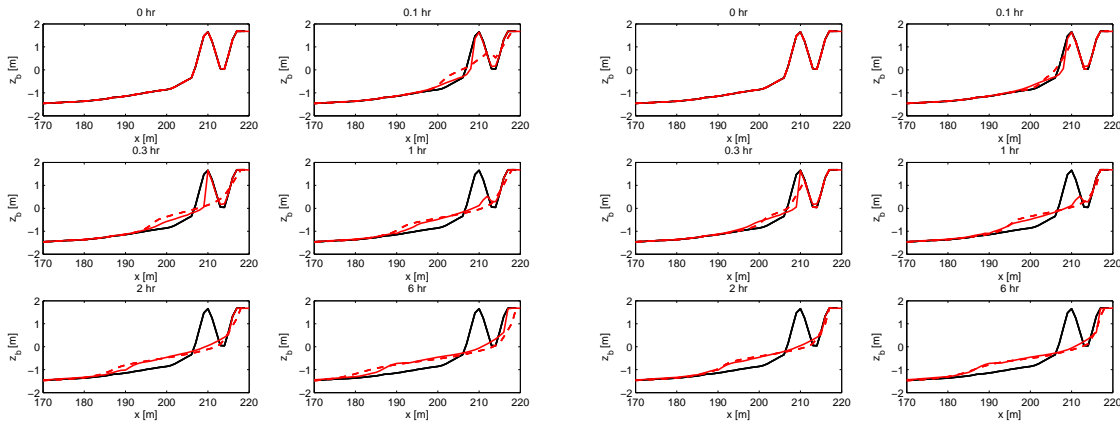|	R	SCI	Rel. Bias	BSS (S)	BSS (NRE)		α SCI	β Rel. Bias	BSS (S)	BS
$t = 360s$	0.9973	0.0750	-0.0248	0.9943	= 360s 0.9944	0.9972 0.9945	54 0.0003 255	0.0007	0.9942	0.9
$t = 1080s$	0.9796	0.2011	-0.0236	0.9589	= 1080s 0.9594	0.9780 0.9526	105 0.0057 331	0.0006	0.9500	0.9
$t = 3600s$	0.9877	0.1468	-0.0295	0.9755	= 3600s 0.9784	0.9965 0.9758	26 0.0002 69	0.0010	0.9928	0.9
$t = 7344s$	0.9949	0.1052	-0.0238	0.9871	= 7344s 0.9889	0.9945 0.9898	77 0.0028 214	0.0007	0.9888	0.9
$t = 21600s$	0.9882	0.1716	-0.0364	0.9596	= 21600s 0.9703	0.9821 0.9765	84 0.0170 131	0.0018	0.9641	0.9

5.16 Deltaflume 2006 T04

Figure 5.40: Deltaflume 2006 test T04. Measured (drawn lines) and modelled (dashed lines) profile after 0, 0.1, 0.3, 1, 2 and 6 hours of wave action.
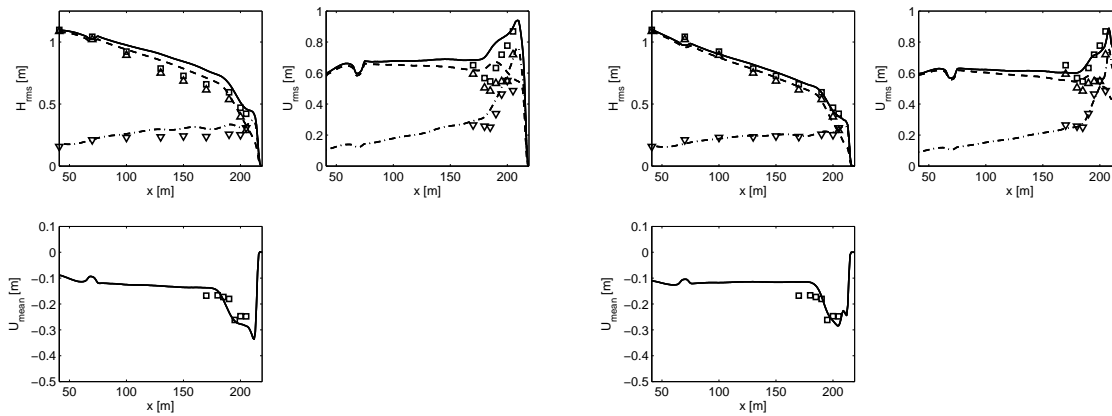

Figure 5.41: Deltaflume 2006 test T04. Upper left panel: Measured (markers) and simulated (lines) LF (downward triangles / dashed-dotted line), HF (upward triangles / dashed line) and total (squares / solid line) wave height. Upper right panel: Measured (markers) and simulated (lines) orbital flow velocity. Lower left panel: Measured (squares) and simulated (solid line) time and depth averaged flow velocity.
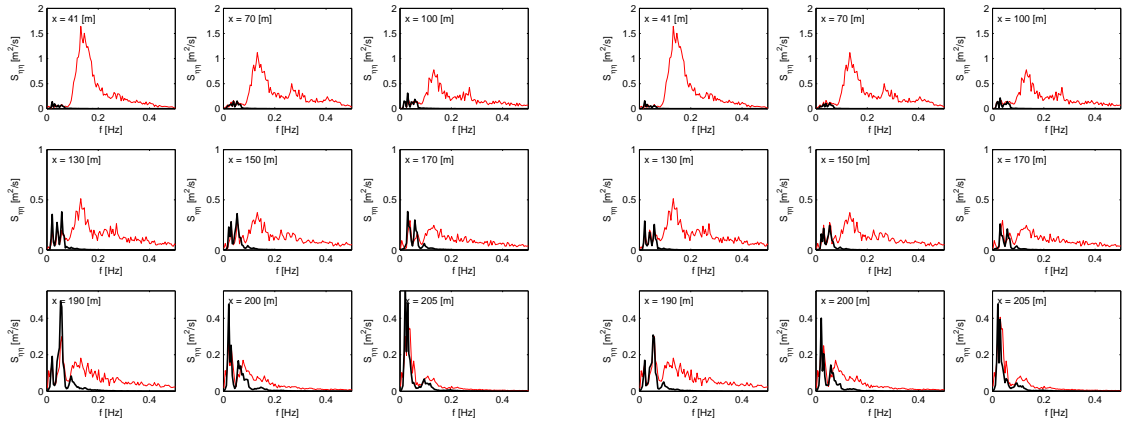
Figure 5.42: Measured wave spectra including both incident waves and long waves (thin line) compared with simulated long wave spectra (thick line) at different cross-shore positions (see upper left corner of sub-panels). Measured and simulated spectra are computed over the whole test duration.
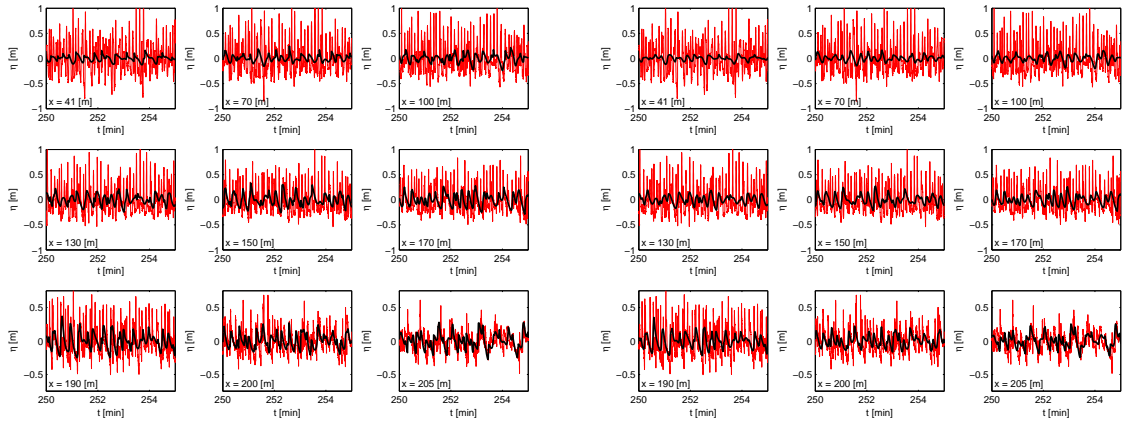

Figure 5.43: Measured water surface elevations including both incident and long waves (thin line) compared with simulated long wave water surface elevations (thick line) at different cross shore positions (see lower left corner of sub-panels) after 4.17 wave hours.
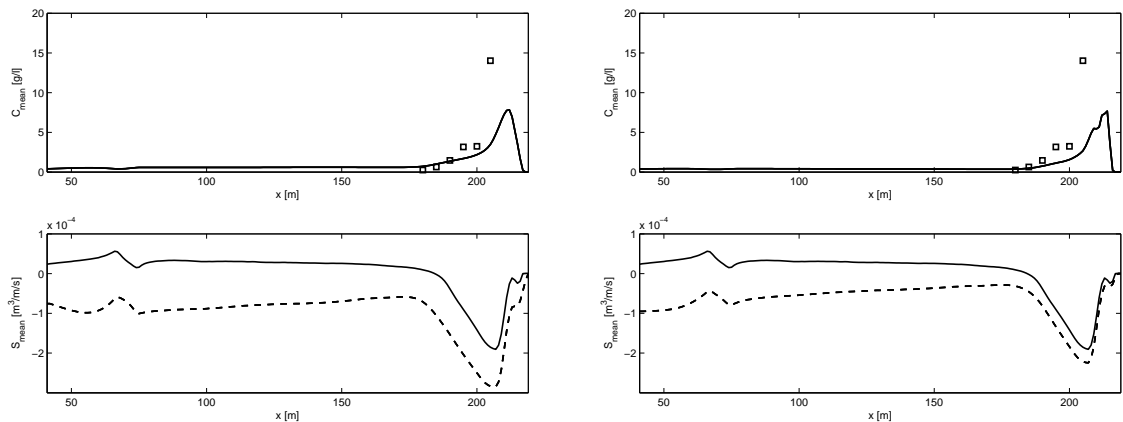

Figure 5.44: Deltaflume 2006. Test T04. Top panel: observed depth-averaged concentrations (squares) vs. model result. Bottom panel: total sediment transport observed from profile evolution (drawn line) vs. model result (dashed line).

Table 5.13: Error statistics Deltaflume 2006 T04

|	R^2	Sci	Rel. bias	BSS		R^2	Sci	Rel. bias	BSS
H_{rms}	0.87	0.10	0.08	0.96	H_{rms}	0.88	0.04	-0.01	0.98
$H_{rms,HI}$	0.88	0.08	0.06	0.97	$H_{rms,HI}$	0.88	0.04	-0.01	0.99
$H_{rms,LO}$	0.77	0.21	0.18	0.54	$H_{rms,LO}$	0.82	0.07	0.01	0.82
U_{rms}	0.72	0.18	0.15	0.67	U_{rms}	0.79	0.08	-0.00	0.77
$U_{rms,HI}$	-0.68	0.21	0.12	-0.90	$U_{rms,HI}$	-0.57	0.16	-0.02	-0.58
$U_{rms,LO}$	0.78	0.26	0.21	0.76	$U_{rms,LO}$	0.79	0.13	0.02	0.81
U_m	0.77	0.14	-0.06	0.54	U_m	0.80	0.18	0.09	0.36
Sed/Ero	0.96	0.25	-0.08	0.94	Sed/Ero	0.97	0.14	-0.07	0.98

5.17   Zwin T01

5.17.1   Results
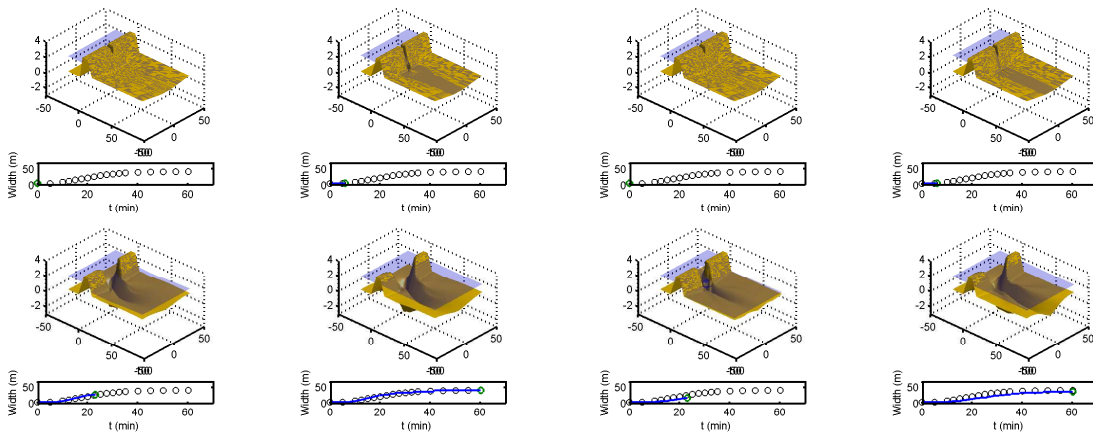
Figure 5.45: Sequence of 3D visualizations of the breach during the Zwin test (Visser, 1998). Bed level, water level and development of breach width (dots: observation, line: model).
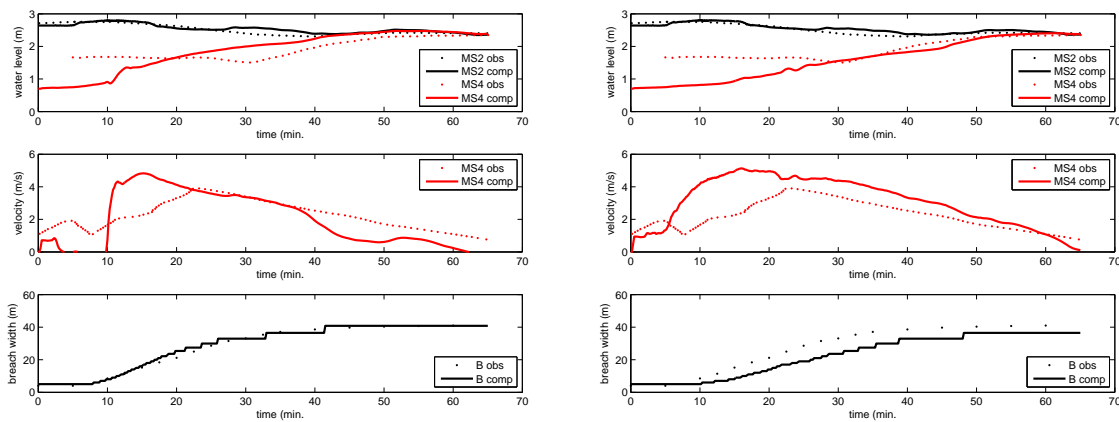

Figure 5.46: Zwin test (Visser, 1998). Observed (drawn lines) and modelled (dashed lines) time series of water level (top panel and velocity (middle panel). Bottom panel: development of breach width, observations (dots) vs. model (drawn line).
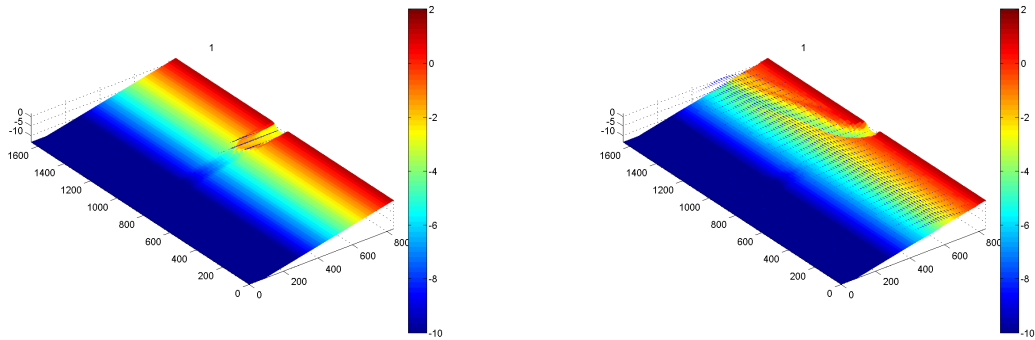
5.18   River Outflow

Figure 5.47

5.19   Assateague Island

Table 5.14: Hydrodynamic boundary conditions XBeach simulations

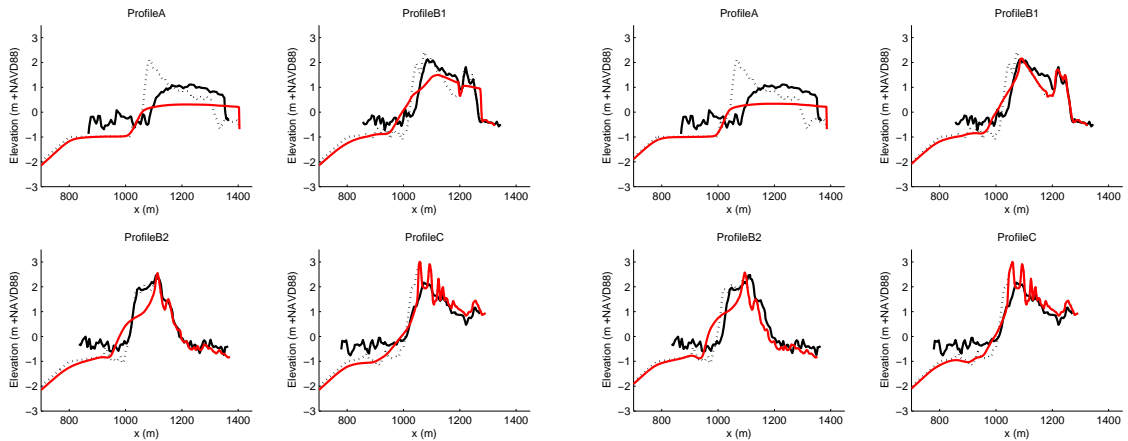|	Storm 1	Storm 2		Storm 1	Storm 2
Surge level [m +NAVD]	0.8	1.0	Surge level [m +NAVD]	0.8	1.0
H_s [m]	4.1	3.9	H_s [m]	4.1	3.9
T_p [s]	8.5	8.5	T_p [s]	8.5	8.5

Figure 5.48: Pre-storm profiles (black dotted line), measured post-storm profiles (black solid line) and modelled post-storm profiles (red solid line). Upper left panel: profile A. Upper right panel: profile B1. Lower left panel: profile B2. Lower right panel: profile C. The seaward side is on the left in all panels. Note that the measured post-storm profiles contain only the sea surface and emerged topography and no submerged topography.